

Pressure-activated, colour-changing and
flexible material for aiding lymphedema
patients in performing the MLD massage

- *An explorative design study*

By Loulou Koudstaal

Pressure-activated, colour-changing and flexible material for aiding lymphedema patients in performing the MLD massage

An explorative design study

By

L.F.J. Koudstaal

in partial fulfilment of the requirements for the degree of

Master of Science
in Mechanical Engineering

at the Delft University of Technology,
to be defended publicly on Friday November 3, 2023 at 10:00 AM

Student number:	4445627
Project duration:	September 6, 2022-November 3, 2023
Supervisors:	Ir. F. Trauzettel TU Delft Dr. Ir. A. Sakes TU Delft
Thesis committee:	Dr. Ir. A. Sakes TU Delft Dr. Ir. J. Jovanova TU Delft Ir. K. Lussenburg TU Delft

An electronic version of this thesis is available at <http://repository.tudelft.nl/>.

Preface

In my younger (and older) days, I used to gaze at the fish in Blijdorp's Oceanium, to find the most special ones with the most magical colours eventually exclaiming: "Look, that one has both purple and yellow and blue and also has silver stripes!". I only took a step back when that eight-legged giant tissue-like thing, an octopus, headed my way, not realizing what I was missing out on. Little did I know that this creature, as I later learned from nature documentaries, possessed incredible intelligence and the ability to change colours at will, a natural magician.

When I heard about the research opportunity within the BITE (Bio-Inspired Technology) group at TU Delft to mimic the colour-changing mechanism of the octopus, I was immediately drawn to it. No one in the group had ventured into this field, allowing me to explore the broader world of biological colour changes before zooming in on the octopus. The meaningful application I found - helping lymphedema patients in regaining control over their treatment and time, added the extra touch, making it a piece I was eager to study.

In the grand symphony of my academic journey, we have arrived at this moment, reaching the final notes. Each note was pressed with care. Initially, there is the process of figuring out how this piece is structured, what challenges lie ahead. Sometimes, I got stuck, but I persevered and restarted. The journey had its crescendos and diminuendos, with dynamics that required multitasking as though I had eight arms and eight separate brains, tackling various compositions simultaneously. Improvisations and guidance from mentors who co-played the duet components with me, were required. As I steadily clarified my thoughts and made sense of the complexities, the piece evolved from *accelerando* to *allegro con spirito*, and a harmonious melody took the overtone. Now, we find ourselves in a serene *calando*, as we reach the conclusion. It has been a grand and magical piece.

Despite the long trek, I remained fascinated by the project. Even after gaining a clear understanding of the octopus's colour-changing mechanism, for me, it is still the closest thing to magic. I am inspired, and I hope you will be too after reading this thesis report. Enjoy!

Loulou Koudstaal
Delft, October 2023

Acknowledgements

Throughout this journey, I received invaluable support from many people. First, my appreciation goes to Fabian Trauzettel. I value the encouragement, the structure you brought into this project through the weekly meetings, and the fact that a discussion about whether the thesis or other things, was always possible regardless of the time. I also want to express my sincerest thank you to Aimée Sakes. Your inspiration and guidance were instrumental in navigating the project's early challenges. Even when you were almost full-term pregnant, you took the time for me. I would also like to extend my gratitude to Vera Kortman, Jette Bloemberg, and Esther de Kater for being friends and counsellors at the same time. Whether it was a coffee break after a meeting to unwind, a talk in the 3D print room, or keeping an eye on my prints, or doing my favourite ballet fit classes together, you were there. Last but not least, I extend heartfelt thanks to my family, friends, and Christiaan for their support.

“And if you believe in the Cinderella moment, the twelve o’clock, in that place, in the midnight hour, it is where Picasso meets Einstein. Art meets science.” – Neri Oxman

Contents

Preface	i
Acknowledgements	ii
1. Introduction	1
1.1. Lymphedema and MLD	1
1.2. MLD treatment options.....	2
1.3. PTET construct	2
1.4. Inspiration from biological colour change.....	2
1.5. Goal of the study.....	3
1.6. Study layout.....	3
2. State of the art	3
2.1. Mechanochromics.....	3
2.2. Flexible optical pressure sensors	4
2.3. Biomimetic colour change	4
3. Theoretical analysis	5
3.1. MLD massage.....	5
3.2. Blood flow and vein dynamics during reactive hyperemia	5
3.3. Cephalopod’s colour change.....	6
3.4. Basics of stress and strain	7
4. List of requirements	8
4.1. Demands	8
4.1.1. Performance.....	8
4.1.2. Dimensions	9
4.1.3. Materials	9
4.2. Wishes.....	9
4.3. Concept directions	10
5. Iterative design process	10
5.1. Layered design.....	10
5.2. The middle layer: colour change	10
5.2.1. Magnetics.....	11
5.2.2. Fluid mechanics	11
5.2.3. Solid mechanics	11
5.3. The top layer: pressure distribution and minimising friction.....	13

5.4.	The bottom layer: friction generation	13
5.5.	Final design.....	13
5.5.1.	Bio-inspired working mechanism.....	13
5.5.2.	Prototype design and manufacturing.....	13
5.5.3.	Compatibility to the requirements	14
6.	Evaluation.....	15
6.1.	Goal of the experiment	15
6.2.	Experimental setup	15
6.3.	Experimental design	15
6.3.1.	Experimental variables	15
6.3.2.	Experimental procedure.....	17
6.3.3.	Data preparation.....	17
6.4.	Hypotheses.....	18
6.5.	Results	21
6.5.1.	General data analysis	21
6.5.2.	Sample 1 vs others.....	24
6.5.3.	Sample 7 vs others.....	24
6.6.	Interpretation of results.....	24
7.	Discussion	25
7.1.	Main findings.....	25
7.1.1.	Design.....	25
7.1.2.	Performance.....	26
7.1.3.	Evaluation hypotheses	27
7.2.	Limitations.....	27
7.3.	Design recommendations.....	27
7.4.	Experimental recommendations	28
7.5.	Application fields.....	28
8.	Conclusion	29
Appendix.....		31
A.	Prior experiments.....	31
A.1.	Use of FSR's.....	31
A.2.	Experimental trial	35
A.2.1.	Design.....	35
A.2.2.	Improvement points	38
B.	Final experiment construction parts.....	38
C.	Robotic garments.....	40
D.	State of the art flexible optical pressure sensors.....	41

E. Matlab codes.....	43
E.1. Analysis of a sample.....	43
E.2. Mean forces and mean areas plotted against the indent.....	53
E.3. Coloured area size means and force means.....	55
E.4. Calculating the deviation of the sensor.....	57
E.5. Measurement pixel.....	58
E.6. Creating colour change visualisation.....	59
E.7. Stiffness hypotheses.....	63
F. Figures, snapshots and binary images for each first trial of a sample.....	65
F.1. Sample 1.....	65
F.2. Sample 2.....	66
F.3. Sample 3.....	68
F.4. Sample 4.....	69
F.5. Sample 5.....	70
F.6. Sample 6.....	71
F.7. Sample 7.....	72
F.8. Sample 8.....	73
F.9. Sample 9.....	74
F.10. Sample 10.....	75
F.11. Sample 11.....	76
F.12. Sample 12.....	77
G. Summarizing images.....	78
H. Tables.....	81
References.....	82

Pressure-activated, colour-changing and flexible material for aiding lymphedema patients in performing the MLD massage

An explorative design study

Loulou Koudstaal

Abstract

The MLD massage is a key component of a lymphedema patient's treatment. Currently, research is ongoing manifesting a transition from system care to self-care by designing robotic sleeves that are able to perform an effective and safe MLD massage enabling the patient to gain a sense of empowerment and ownership over their treatment and time. This research presents an innovative approach towards the MLD treatment by introducing an intermediate step: the bio-inspired design of the patient training education tool (PTET), a tool which aids the patient in performing the MLD massage safely and efficiently by themselves. The PTET is a pliable and slim sheet that easily adapts to the contours of the limb. Exerting manual pressure onto this sheet induces a colour change at a specific pressure threshold, giving the lymphedema patients a visual sign they have reached the required amount of pressure for this type of massage. The mechanism of colour change is inspired by the cephalopod's dispersion and aggregation of its chromatophores. This study presents the design and validation of the working mechanism of a bio-inspired flexible colour-changing sheet, and first insights into the adaptability of the design variables and their relation to the threshold pressure, threshold indent and degree of colour change.

Keywords

Colour change – mechanism – bio-inspired design – pressure-activated – soft robotics – lymphedema – MLD massage

1. Introduction

1.1. Lymphedema and MLD

Lymphedema is a chronic condition characterized by the accumulation of lymphatic fluid in the tissues, and affects 250 million people globally [5, 6]. It occurs when the lymphatic system is impaired due to damage, or an obstruction. Most common reason for impairment is the removal or damage of lymph nodes during surgical procedures, such as lymph node dissection, radiation therapy for cancer treatment or having a mastectomy [7]. As a result fluid, which composes of residues and toxins for disposal and nutrition, leaks from the capillaries into the interstitial spaces [5]. Symptoms of lymphedema are pain, discomfort, reduced motion, fatigue, and body image issues [5, 8]. In severe cases it results in permanent skin damage, infections, skin cancer or amputation [6, 9].

A treatment for lymphedema, to manage and reduce these symptoms, involves two phases: reduction therapy and maintenance therapy [8]. Manual Lymph

Drainage (MLD) forms in both phases a key component. MLD massage addresses the impaired lymphatic flow by manually redirecting the accumulated fluid to healthy lymphatic pathways, and thereby transport it back into the cardiovascular system [5, 9-11]. A combination of dragging and squeezing motion, which are respectively the shear and normal force, encourages the opening of healthy lymph nodes and promotes the transportation of lymph fluid [6]. This is visualized in [Figure 1](#). The most challenging part of performing MLD massage is that excessive pressure can cause increased swelling and damage to the sensitive skin and remaining lymph nodes, impeding the effectiveness of the treatment and potentially causing further complications. Although, insufficient

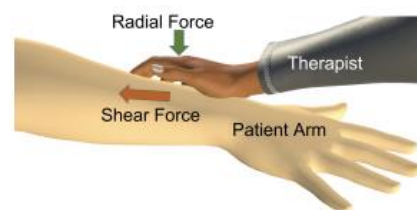


Figure 1. Visualized radial compression force and shear force during an MLD massage [2].

pressure is not stimulating the lymphatic flow. Therefore this therapy is performed by a trained therapist to ensure safety and efficacy. The MLD treatment is time-intensive for both the therapist and patient due to its consistency of 4-5 times a week, 20-40 minutes per treatment. Refraining from MLD means the condition can take on dire forms with a high risk of complications [2, 12]. The large number of lymphedema patients needing MLD, the time-consuming nature of MLD, and the necessity of careful implementation by a therapist, calls for an innovative take on this type of therapy.

1.2. MLD treatment options

Conventional treatments to perform lymph drainage are pneumatic stationary pumps and in-clinic sessions [10]. These pumps aid lymph drainage. However, there is a problematic trade-off between wearability, effectiveness, and costs of these devices. Current research is focusing on eliminating this trade-off and often focusses on the use of robotic sleeves for MLD, but it often remains the case that compromise must be made between size, noise level and effectiveness. However, these at-home treatments with robotic sleeves that are able to exhibit the MLD massage, would be beneficial in terms of time efficiency, increased patient capacity, and continuity of care. Some of these garments are elaborated on in [Appendix C](#). A difficulty within these garments is found in the application of the shear force element of the MLD massage. Furthermore, these garments are often bulky and noisy due to pressurized air, which doesn't make it comfortable to wear. These robotic sleeves are of considerable cost, which makes them a product tailored to a more select patient group [2, 5, 6, 9, 13-15]. Additionally, an obstacle in the design of a robotic sleeve is the non-uniformity of the limb diameter and their inability to massage the entire length of the limb in one cycle. Ultimately, these garments can be vulnerable to bacterial growth and difficult to clean, thereby posing an increased risk of infection [2, 5, 8, 9, 15, 16].

The robotic sleeves are indicative of the transition within the treatment of lymphedema from system care to self-care. This step is of great importance for the patient to gain a sense of empowerment and ownership over their treatment and time, and as alleviated workload for the healthcare system. However, this step cannot be undertaken due to the mentioned flaws within the robotic designs. Hence, an intermediate step that involves an innovative approach to self-care treatment of lymphedema, is needed [8].

This research addresses the design research for a Patient Training Education Tool (PTET), which facilitates safe and efficient self-administered MLD massages by patients. The PTET offers a portable and cost-effective alternative to robotic sleeves while providing patients control over their treatment and time. A training tool would add value during the intermediate and final stages towards self-management of lymphedema as it will be an extra dimension to the patient's treatment making it more versatile.

1.3. PTET construct

The challenge of an MLD massage lies in striking a delicate balance between applying adequate pressure to ensure successful reabsorption of lymph fluid into healthy lymph nodes, and avoiding too strong or soft pressure preventing adverse complications or ineffective treatment. Assigning the MLD massage to a lay person necessitates therefore an intuitively operable device, such as one equipped with optical sensors [17-19]. A promising solution is a pressure-responsive sheet that provides visual feedback by changing colour at specific threshold pressure that coincides with the 30-60mmHg required for MLD. However, this threshold pressure varies among patients, and more so across distinct skin areas. Hence, an adaptable and modular design is imperative. Drawing inspiration from the colour-changing cephalopod, this research introduces the PTET as a flexible, and slim sheet that easily conforms to the contours of the underlying surface and changes colour upon pressure during the MLD massage. This sheet could serve as a tool for pressure mapping, giving lymphedema patients the assurance they can administer the MLD massage themselves in a safe and efficient manner.

1.4. Inspiration from biological colour change

In human-made surroundings colour change serves as a practical or aesthetic purpose. There are thermochromic materials that change colour at a critical temperature (T_C), which are seen in battery testers [20, 21]. Or mechanochromics, which proceed an optical change based on mechanical stimulation, and can be used in anticounterfeiting devices [22]. There are photochromic lenses that adapt their tint based on exposure to ultraviolet light [23]. In electronic displays liquid crystals exhibit vibrant colour changes when electrically stimulated [20]. Currently, scientific research focuses on colour changing working mechanisms in nature, as these outperform man-made colour change systems in terms of speed and variety.

Organisms use colour changes as a means of communication with species, temperature regulation, or camouflage [3]. Masters of camouflage are the chameleon and the cephalopod [3, 24-27]. Also certain fish species, foxes and hares are able to adjust their skin pigments to blend in or communicate [28]. While these animals all make use of pigmentary colouration, birds make use of structural colouration in their plumage, such as the purple sunbird and the bird of paradise, to attract mates during courtship rituals [29, 30]. In addition to its pigmentary colouration, the cephalopod possesses reflective platelets, i.e. structural elements, which create a 1D photonic crystal. This type of crystal produces many bright colours as a result of different light interactions and changing the spacing of the platelets [3, 24].

Remarkably, among the diverse array of natural colour-changing phenomena, human skin represents a unique case where pressure is the stimulus of colour change. It remains rare to find pressure-induced colour change in nature. When the skin is subjected to pressure it may exhibit a change in hue, e.g. bruising or blood displacement. Due to cardiovascular activities and the light-absorptive properties of haemoglobin interacting with the optics of the skin, colour change is observed [31]. This is a distinctive illustration of how pressure can influence the dynamic visual characteristics of a living organism.

1.5. Goal of the study

This study uses the knowledge of these colour change mechanisms as a source of inspiration for the design of a training education tool for lymphedema patients. This tool will function as an alternative approach to the MLD massage with benefits of being portable (i.e. lightweight and small), easily washable, and cost-effective such that it always remains an extra dimension to the lymphedema patient's treatment.

The goal of our study is to develop and test a bio-inspired patient training education tool (PTET), a pliable and slim sheet that shows colour variation at an assigned threshold pressure, which will assist a patient in the self-care component of their treatment, and thus functions as an aid in performing an effective and safe MLD massage on the limbs.

This is an exploratory research that starts with a state-of-the-art research and a theoretical analysis on the relevant subjects. This analysis is followed by several design concepts and iterations, which results in a final design and experimental validation.

1.6. Study layout

This study is subdivided into eight chapters. First, the state of the art of commercially available smart materials with a focus on mechanochromics, flexible optical pressure sensors, and biomimetic colour changes is given. A theoretical analysis that provides elaborated information on the MLD massage, vein dynamics of the skin during colour change, and biomimetic colour change materials, is also presented. [Chapter 4](#) lists the requirements of the PTET. Hereafter the concept directions are stated. [Chapter 5](#) elaborates on the process of achieving the stated requirements in a design. Hereafter, the experiment will be explained, which will show validation of the working of the PTET. In the [Chapter 7](#) and [Chapter 8](#) findings will be discussed and a conclusion will be drawn.

2. State of the art

In the study of colour-changing materials instigated by pressure, multiple references in literature are used refrained from their synonyms. Not all research call their colour-changing material immediately a sensor, as they present a mechanism, and therefore name their mechanism a colour-changing material. In this study both the sensors, and the presented mechanisms are included, with the requirement that the material is flexible and directly responding to its mechanical stimuli.

2.1. Mechanochromics

One viable option to achieve colour change is the use of smart materials. Many smart materials are already successfully commercialized. However, researchers aim to realise innovations by stimulating proactive use of smart materials in product design, such to improve the benefit of the user instead of using these materials for commercial exploitation [32].

Chromogenics, a class of smart materials that undergo reversible colour changes in response to external stimuli, are attracting significant attention because of their various range of applications [20, 33]. Regarding the scope of this research, we focus on the functional analysis of one of the chromogenic types: mechanochromics.

In mechanochromic materials optical variations in transparency, fluorescence and colour take place in response to mechanical stress or deformation [32]. This trigger causes variations in the form of a molecular structure change, an interference with the intermolecular exchange process, or a development

within the physical structure photonic and morphological wise [22, 33]. This type of material could be of great use in an electronic skin, smart screens, bionic actuators, encryption and anticounterfeiting devices. Different flexible and stretchable mechanochromic polymers and composites take the form of rubber, hydrogel, fiber or foam. Most mechanochromics are easy to process, compatible, and have a tunable mechanical stiffness. A challenge in mechanochromic material design is to retrieve the exact changes in molecular structure and chemical bonds during the loading process. The force stimulus that is needed to achieve a colour change is for a lot of applications too high. Various materials need a tensile strain of 300% to show visual optical changes. Attention should be paid towards a valid structural designability, facile procedures, recoverability, force sensitivity and distinguishable optical variation, while designing a mechanochromic material [22].

2.2. Flexible optical pressure sensors

The state-of-the-art of flexible sensors responsive to mechanical stimuli primary centers around the domains of healthcare, robotics and biomedicine. These areas demand high sensitivity, accuracy, reproducibility, mechanical flexibility and low cost. Existing sensing mechanisms make use of piezoelectric, pyroelectric, piezoresistive, triboelectric, magnetoelectric, and electroluminescence effects. In some cases these effects are combined with chemical and biological sensors. The electrical sensors are continuing to be at the forefront of wearable devices and soft robotics when it comes to measuring the deformation of materials. Developments within this industry lie within the multifunctionality of sensing systems (i.e. systems capable of concurrently measuring multiple parameters while also exhibiting the capacity to change shape and colour for example), and in having an optical sensor readout instead of the physical sensors as an alternative [34, 35].

Colorimetric sensors are a type of optical sensors that show distinguishable colour change due to a change in what is measured. This colouration can be observed by the naked eye when the optical change occur in the visible range (400-800nm). The colorimetric sensors are designed to be used by individuals with minimum qualifications, because measurements can be done non-invasively and the systems are intuitively to operate [18, 19]. Photonic crystals, liquid crystals, or mechanochromic effects are currently used to achieve a colour change within a material. A lot of research has been done into creating structural colouration as a

result of mechanical stimuli using these described elements [19, 36-42]. An overview of this research is given in [Appendix D](#). All make use of the interaction with light and their changing shape while undergoing a mechanical stimulus. A different reflected peak wavelength will result in a different perceived colour. However, it is challenging for these material elements to be integrated into wearables and robotic applications [34]. The processes to create or integrate these materials require intricate equipment and meticulous procedural steps [37-39]. The focus has been on making the sensors more bendable and flexible in order to make them more comfortable and therefore wearable. A general approach to achieve this is reducing the sensor's thickness. Another approach is using polymeric materials with a low modulus and high stretchability [17]. However, it is found to be challenging to have a short recovery time, a small threshold stress, a small thickness and not having to compromise on reproducibility or recovery time [37, 39, 40, 43].

2.3. Biomimetic colour change

Biological colour changes are the source of inspiration in material designs in the fields of among others soft robotics, camouflage systems, sensors, artificial prosthetics, and human-machine interfaces, because they occur in soft skins, are rapidly adaptable, and can change to a myriad of hues and patterns. Research into mimicking colour change reveals material designs that operate mechanically, electrically or chemically, where the stimulus spans several possibilities: temperature (IR light), humidity, presence of certain chemicals, stretch, and (pneumatic) pressure [13, 42, 44-49].

Inspired by animals in nature, such as chameleons, frogs, and cephalopods, a research team developed an innovative design that is able to change colour in response to an applied external strain. This material employs Quantum Light-Emitting Diodes (QLEDs), which have drawn substantial interest in the field of lighting technologies because of their capability to emit varying wavelengths based on the size of Quantum Dots (QDs). The architecture of the material is as follows: a cathode, hole transport layers, emission layers, electron transport layers, an anode, and a thin film of piezoelectric material. Within the emission layers there are different sizes of QDs involved to obtain different colours. An interesting aspect of this design resides in the implementation of piezoelectric material. This layer serves as an external strain sensor. The applied external strain induces a variation in the electric potential, resulting in the generation of a

certain size of QDs and therefore subsequently an emission of diverse colours: red, yellow, or green [13]. Chou et al. [44] was inspired by the chameleon and designed a stretchable electronic skin, whereby the colour changing aspect is controlled by external pressure along with the duration of pressure. The design structure contains a highly sensitive pressure sensor with a layer of spray-coated single-wall carbon nanotubes, and a stretchable electrochromic device. This structure causes again a different voltage output depending on the amount of pressure, which modifies the colour of the skin. Another design refrained from electrical circuits, was a flexible sheet of silicone with embedded pneu-nets: an independent network of microfluidic channels that are pneumatically driven. By filling and flushing coloured aqueous solutions into the networks colour change can be controlled [46].

Within the state-of-the-art into colour-changing materials and sensors, no design has been found that focuses on a reversible colour-changing material with external applied pressure as control stimulus and is refraining from electrical or chemical components. This identifies the development of a bio-inspired colour-changing skin, that responds to applied pressure without the use of electrical or chemical elements, as a promising design gap. Here, an attempt to demonstrate an interactive colour-changing device that responds to applied pressure, while using a cost-effective and mechanical method, which promises to open new possibilities for the development of next-generation MLD massage education tools with visual response and more.

3. Theoretical analysis

3.1. MLD massage

The blood vessel system is a closed circulation system, which circulates blood by the pumping force of the heart. Blood flows automatically from higher blood pressure areas to lower blood pressure areas. In contrast with this blood vessel system, the lymphatic system is a one-way channel originating in the initial lymphatics and from there scattered across different tissues of the body. This results in a higher internal pressure downstream than upstream due to passive transport of lymph fluid. To prevent stagnation also active transport is implemented. A smooth vessel in the lymph vessel wall produces rhythmic spontaneous contraction to pump the lymph fluid upstream. Valves in the channel prevent regurgitation. When one suffers from lymphedema this system does not work anymore due to

damage of the vessels and nodes or due to their removal [50]. Excessive fluids accumulates in the interstitial spaces. This fluid needs to be redirected to the remaining healthy lymph nodes [5, 6].

Emile Vodder from Copenhagen presented the first method of manual lymph drainage in Paris in 1936. The Vodder technique made use of different hand movements each for treatment of a different area of the body: the pump, scoop, rotary, stationery circle, and the thumb circle. All with a pressure of 30mmHg. Later Leduc, Casley-Smith, and the Földi method were presented, but all were variations of the Vodder technique. Some main principles of the MLD are: (1) Do not use oils to be able to stretch the skin and enhance different interstitial pressures, (2) Slow and repetitive movement with pauses in between to allow the skin to return to its initial position, (3) An MLD sequence moves always proximally or centrally towards functioning lymph nodes, (4) Aim is to initiate lymph drainage without increasing capillary filtration and hyperaemia [54].

As previously delineated, executing an MLD massage demands a judicious and measured approach. Excessive pressure can precipitate detrimental consequences, such as the compromise of integumentary structures or damaging healthy lymph nodes. Conversely, insufficient pressure is not effective. Therefore, the application of pressure adheres to a range. Recommended pressures during the MLD varies, but most research describe light pressures between 30mmHg (~ 4 kPa) and 60 mmHg (~ 8 kPa) as the most effective range, but there is no information on how this pressure was measured [15, 51-54]. Others have translated the numbers in research to more specific parameters: to a maximum shear force of about 1.5 N, a stroke displacement of around 30 mm, and a compression loading of 5 N [6]. Some tissue fluid tends to be sluggish, and to get these in motion as well, the pressure time should be at least 1 second long [52]. Desired is that it is a reminiscence of the physiological lymphangion's contractile activity, which is around 10 pressures per minute [53]. Furthermore it is also advised to elevate the limb between 30° and 45° [54, 55].

3.2. Blood flow and vein dynamics during reactive hyperemia

Human skin represents a unique case where pressure is the stimulus of colour change. This phenomenon's blood flow and vein dynamics can be understood by

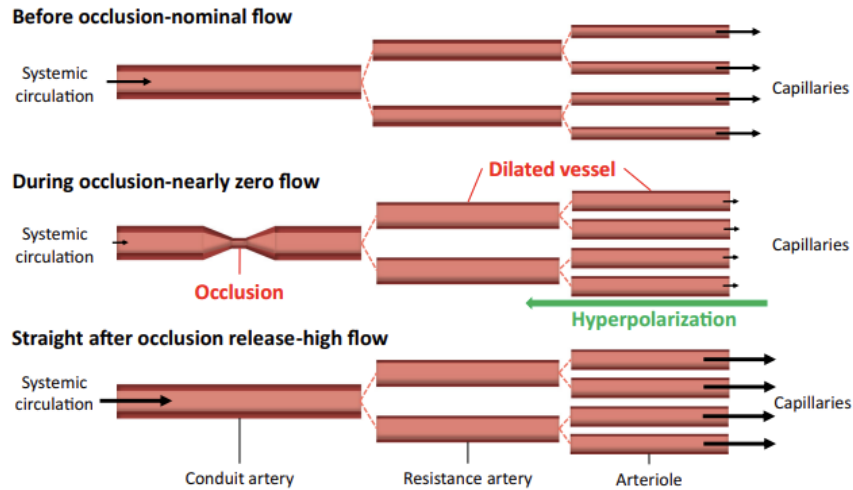


Figure 2. The state of the microvasculature before, during and after occlusion. The bigger the arrow, the higher the magnitude of flow [4].

evaluating reactive hyperemia. Reactive hyperemia, a non-invasive technique whereby the magnitude of limb reperfusion is measured after a short period of ischemia by arterial occlusion, is a standard method to assess the microvascular reactivity. Understanding the microvascular functions and its regulations is of importance in diagnostics, progress monitoring and therapeutical approaches in case of diseases whereby the (micro)vascular system malfunctions. The microcirculation is responsible for the delivery of oxygen and nutrients to the body's organ tissues, and for removing waste. Multiple cardiovascular diseases can be early diagnosed by checking the microvascular health. This system organizes the blood flow and pressure to comply with the metabolic demands. Their direct control consists of adapting the diameter of the microvessels, i.e. operate a vaso-dilation or vaso-constriction, which is changing the hydrodynamic resistance, their indirect control. Reactive hyperemia represents the initial increase in flow and an instant restoration of flow. An occlusion of a conduit artery is followed by a reduction of pressure, which is propagated to the arterioles. Due to an impaired oxygen flow, the vessels dilate to correct the error until the occlusion is resolved, resulting in an increased blood flow, see Figure 2. During this process, the ischemia is observed on top of the skin as blanching, while the increased blood flow appears as a blushing colour. This colouration is therefore one example of a biological colour change followed by manual pressure. Note that the level of colouration differs per individual. In addition the haemodynamic features (viscosity and density of the blood), the geometric properties (diameter and length of the vessel), and the structural properties (stiffness) are all factors that influence the physiological process of active hyperemia [4].

3.3. Cephalopod's colour change

The cephalopod's mechanism to change colour is a physiological mechanism where the chromatophores, the cells with pigment, are dispersed and aggregated to obtain colour. These chromatophores are divided over three stacked layers. Each layer corresponds to brown, red or yellow pigment colours. Radially located muscles cause the pigment containing cells to expand or retract with a ratio of up to 1:500. In expanded state, the cells are disc formed, and are able to absorb its corresponding wavelengths from the incident light. In retracted state these cells are hairpin-shaped, and absorption is not possible, resulting in the transmission of incoming light. Deeper into the skin, underneath the pigment layers, are light-reflecting layers, which constituents are iridophores and leucophores. These are non-pigmentary, structural colouration cell types,

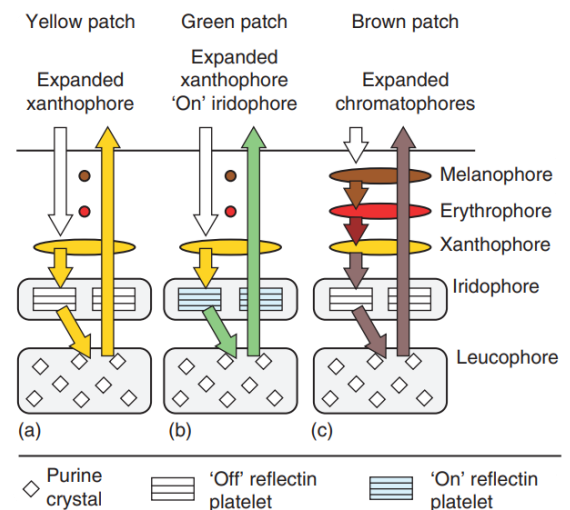


Figure 3. Cephalopod colouration given schematically. The melanophores, erythrophores and xanthophores form the three pigment layers. Deeper in the skin are the iridophore and leucophore layers, which refract light that is transmitted by the pigment layers [3].

which reflect the unabsorbed incident light [3, 24, 27]. Iridophores can be turned “on” or “off” by controlling the space between their reflectin platelets. By changing this space, the refraction index changes, which causes a change in the refracted wavelength and therefore a change in colour [3, 24]. In [Figure 3](#), the layers that facilitate colour change in the cephalopod are shown schematically.

3.4. Basics of stress and strain

Examining instances of active hyperemia and the chromatic changes observed in the cephalopods, it becomes apparent that physiological elements undergo dilation or constriction processes to render colours either perceptible or imperceptible. Taking into account the PTET, that will undergo a colour change as a result of external pressure onto its top surface, an understanding of the fundamental principles governing stress and strain within materials is of paramount significance. It provides understanding of how a given material would undergo dilation or constriction subjected to compressive forces.

The behaviour of a body under stress differs per material due to different material properties. Stress is an external or internal applied and distributed force onto the surface of a body [1]. In [Figure 4](#) an isolated section is given of a body where forces and reaction forces are shown. The force distribution at Q will have a normal component and tangential component. These components could be tensile or compressive and shear stresses, respectively. The infinitesimal area that is surrounding Q lies in the yz-plane ($\Delta A_x = \Delta y \Delta z$), which designates the force component in the x-direction to be the normal force. The average distributed force per unit area, i.e. the average stress, in the x direction is calculated using [Equation 1](#).

$$\overline{\sigma_{xx}} = \frac{\Delta F_{xx}}{\Delta A_x} \quad (1)$$

Stresses are also generated by the forces ΔF_{xy} and ΔF_{xz} , which are tangential and therefore shear stresses. See [Equation 2 and 3](#).

$$\tau_{xy} = \frac{dF_{xy}}{dA_x}, \quad (2), \quad \tau_{xz} = \frac{dF_{xz}}{dA_x} \quad (3)$$

Stress can instigate elastic or plastic deformation. Refraining from being elastic or plastic, the increased length is called the normal strain. Stress and strain’s relationship is described using the Young’s modulus in [Equation 4](#).

$$stress = Y * strain \quad (4)$$

Implementing the formula’s for stress and strain, results in [Equation 5](#):

$$\frac{F}{A} = Y * \frac{\Delta L}{L_0} \quad (5)$$

Using Hooke’s law:

$$F = k * \Delta L \quad (6)$$

we can determine the stiffness (k):

$$k = \frac{Y * A}{L_0} \quad (7)$$

Young’s modulus is a fixed material property, and is also known as the modulus of elasticity. The Young’s modulus is commonly used for rigid materials, as it provides not enough information about how soft and flexible a material like silicone is for example. For these types of material Shore Hardness (on the Durometer hardness scale) is used to be able to state something about the material’s resistance to indentation [56]. Poisson’s ratio is another material property that explains something about a material’s mechanical behaviour and is used for both soft and rigid materials. The mechanical response of transverse strain to uniaxial stretching is given by the Poisson’s ratio in [Equation 8](#).

$$\nu = -\left(\frac{\epsilon_2}{\epsilon_1}\right) \quad (8)$$

Here, ϵ_2 and ϵ_1 are respectively the transverse and axial strain. Most commonly a material is characterized by a positive Poisson’s ratio, because most materials reduce laterally when being stretched. However, there are materials that behave the opposite, and exhibit a negative Poisson’s ratio. These type of materials are

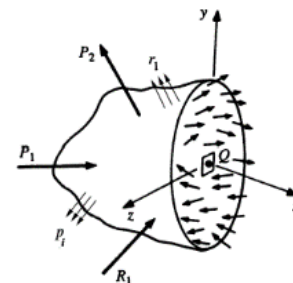


Figure 4. An isolated section of a body where concentrated force (P_i), surface force distribution (p_i), possible reaction forces (R_i) and reaction surface force distribution are visualized. There is a force distribution at Q [1].

called auxetics. Their width and length increase when being stretched. The opposite is true when they are being pressed [57].

4. List of requirements

This chapter defines and describes the design requirements for the patient training education tool. Table I summarizes these design requirements. The requirements are split into demands and wishes. The demands are essential for the use and functioning of the PTET. The wishes center on envisioning a prospective design that could potentially serve as an enhanced PTET or, alternatively, assume a distinct functional role.

4.1. Demands

4.1.1. Performance

1. *Manual actuation.* The PTET serves the purpose of facilitating the Manual Lymphatic Drainage massage. The input of this pad is manual pressure, subsequently resulting in a colour change.
2. *Threshold pressure.* Recommended pressures during the MLD lie between 30mmHg (~ 4 kPa) and 60 mmHg (~ 8 kPa). At least the minimum pressure must be achieved, the threshold force is therefore stated at 30mmHg, which is equal to $\sim 0.004\text{N/mm}^2$. However, it is important to note that no explicit methodology has been provided for the measurement of this value. Consequently, the precise required pressure exerted on the skin, and hence, on the surface of the PTET, remains unknown.
3. *Colour change.* The functionality of this tool lies in its displayed colours. This tool should display two different colours visible to the naked eye under two different conditions, i.e. under no pressure or threshold pressure. Within the used HSV-colour model, each dimension (hue, saturation and value brightness) ranges from 0 to 1. In the context of transitioning from blue to red, this necessitates an increase in the H-value. To achieve a perceptible alteration in colour, the minimum increment is set on 0.1. Next to a hue change, the colour changed area should be visible adjacent to the point of pressure.

4. *Response time.* For the optimal performance of the product and, consequently, the outcomes of the MLD massage, it is imperative that the colour change occurs instantaneous. If incorrect pressure is applied, adverse effect could happen. Therefore, it becomes essential for the patient to observe instant whether or not they are applying the correct amount of pressure. Human visual perception typically requires 13 ms.
5. *Reversibility.* The colour change, in consideration of product recyclability, should not be permanent. Multiple strokes are typically administered during a massage session. Hence, it is of paramount importance that the colour change is readily reversible. To ensure reversibility, it is imperative to establish a permissible duration for which the colour may persist, as well as to define a duration within which the colour must revert to its initial state. See requirement 6 and 7.
6. *Colouration persistence.* As long as the pressure persists equal to or exceeds the threshold pressure, the associated colour should likewise persist. Consequently, this colour change should be visible adjacent to the point of pressure. In the event that this condition is not met, the colour must endure for a minimum of 1 second following the release of pressure, allowing the naked eye sufficient time to observe the colour change. The persistence of the changed colour should not exceed a maximum duration of 2 seconds to allow fast repeatable use of the product.
7. *Relaxation time.* In compliance with the stipulated reversibility requirement, the material must revert to its initial colour. A requisite of a 2-second relaxation time is necessary to ensure seamless continuity of the MLD massage. This is essential to prevent any delays in usability when commencing a new stroke during the MLD massage.
8. *Flexible.* The colour-changing material must be a comfortable fit. The material should therefore be flexible and adaptable to multiple shapes. It must be able to bent, twist, and bend without breaking.

9. *Friction generation.* While performing the MLD massage, the PTET must remain in place. There should be a non-slip design between this material sheet and the skin such that friction is generated when pressure is applied from the top of the sheet.
10. *Handling.* It is recommended to keep the limb elevated at an angle between 30° and 45° during the MLD massage. The design should still be operable at this angle.

4.1.2. Dimensions

11. *Thickness:* Only a few articles described the thickness of their final and total design of their colour-changing sensor, which lie between 0.9-4mm with Zhuang being the outlier, 23mm (Yuan et al., 2017) (Yokota et al., 2021) (Zhang et al., 2018) (Zhang et al., 2020) (Zhuang et al., 2022). This study focuses on keeping the sheet under 5mm, such that the applied force could be easily transported to the skin and to keep the product portable.
12. *Scalability.* For the sake of using this material for lymphedema patients, the colour-changing material must be scalable to at least the area size of an average leg.

4.1.3. Materials

13. *Durability.* For cost and environmental reasons, it is important for the product to last many cycles. The material should have a high fatigue resistance. Its colour changing mechanism and the characteristics of the material should withstand many cycles to achieve a long lifetime.
14. *Hygienic.* The material is placed on very sensitive skin, which is prone to bacteria. Hence, the product must be completely hygienic and therefore washable.
15. *Skin safe:* The material used should have an OECD TG 439 certification, which means certified to be skin safe.

4.2. Wishes

16. *Gradient colour change.* It is desirable that, when the material is conceptualized as a mesh,

that different degrees of pressure show different degrees of colourations. This phenomenon could result into gradient colour change, as the application of pressure at a specific point results in higher force concentration at that precise point, creating a gradient or slope.

17. *Active colour change.* In the animal kingdom, passive and active colour changes exist. Passive means that the colour-changing object, the observer or light changes position, causing the colour to change due to a different angle of incidence. Active colour change means that everything stays fixed, and a colour change is cause by a combination of an external stimulus and mechanism in place.
18. *Easy manufacturing.* The objective for the PTET is to ensure widespread accessibility. To maintain a low price, manufacturing should be simple and fast. For the prototype it is desired to work with the 3D-printer.
19. *Power consumption.* Xie et al. put it as a requirement for a robotic e-skin to have ultra-low power consumption [34]. The design should not be reliable on power use, therefore to have low power consumption.
20. *More than two colours.* The PTET must be able to not only indicate the minimum amount of pressure that is needed for the MLD massage but also, desirably, the upper threshold pressure. Even more favourable would be to involve multiple colours to indicate where one is within the pressure range.
21. *Soft.* It is discussed that the material must be flexible. However, it is desired for the sheet to be soft, i.e. that it falls under gravity. Soft material means the material is malleable, which suits perfectly for this product that needs itself to form around many limbs.

TABLE I. Overview of the design requirements and wishes

Description	Value
<i>Demands</i>	
1. Manual actuation	-
2. Threshold pressure	$\sim 0.004\text{N/mm}^2$
3. Colour change	$\Delta h \geq 0.1$
4. Response time	13ms
5. Reversibility	-
6. Colouration persistence	As long as pressure persists
7. Relaxation time	≤ 2 sec.
8. Flexible	-
9. Friction generation	High
10. Handling	$30^\circ - 45^\circ$
11. Thickness	Very thin
12. Scalability	-
13. Durability	High fatigue resistance
14. Hygienic	-
15. Skin safe	OECD TG 439
<i>Wishes</i>	
16. Gradient colour change	-
17. Active colour change	-
18. Easy manufacturing	-
19. Power consumption	Low
20. Multiple colours	> 1
21. Soft	-

4.3. Concept directions

The theoretical analysis of the MLD massage, models of active hyperemia and colour-changing octopus skin, and understanding of pressure, results in four concept directions that consists of exerting pressure upon a chromatic element to transform pigment into an imperceptible or perceptible state. Inducing a transformation to the imperceptible state necessitates the utilization of either liquids (inspired by the vein model of active hyperemia), magnetics or auxetics. Conversely, changing a material to the perceptible state requires a solid and elastic material that expands upon pressure. It is essential to take into account that the final

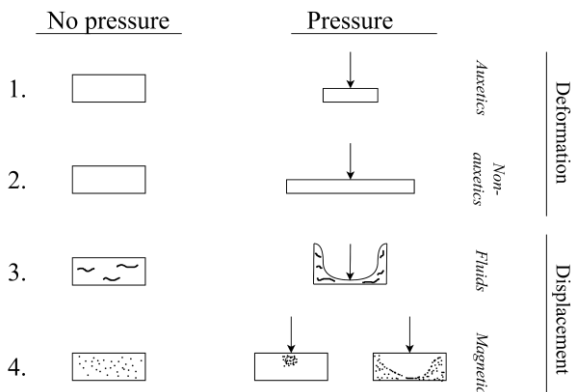


Figure 5. Concept directions.

design must maintain a soft texture. Both concept directions are schematically visualised in [Figure 5](#). Consideration is being given to whether such systems could be placed in a sheet that still retains its flexibility, desirable its softness. Thereby should it generate friction on the bottom to ensure sticking onto the skin.

5. Iterative design process

5.1. Layered design

Many research focus on a layered design approach [13, 42, 44, 45, 48]. This is also evident in natural colour change mechanisms exhibited by cephalopods, chameleons, crab spiders, as well as the multilayer structural colouration observed in beetles, fishes, and avian species. This study draws inspiration from these biological systems, thus adopting an analogous approach, characterized by a layered design. The PTET is divided into three functional layers, see [Figure 6](#). The bottom layer is there to generate friction when pressure is applied from the top. The middle layer contains a colour changing mechanism, and causes colour change, its main function. The top layer needs to be smooth for the user to operate the system, and at the same time make sure that pressure is distributed such that the colour change can be observed adjacent to the point of pressure. Note that the bottom layer for friction generation could be integrated in the middle layer of the colour changing mechanism. An iterative approach is followed to arrive at a final design. Each layer in this design ensures the fulfilment of one or more requirements stated in [Chapter 4](#). For each design a proof of concept is built to analyse its main function colour change until a satisfactory result is achieved.

5.2. The middle layer: colour change

[Section 4.3](#) discusses four concept directions for this study's main function 'colour change', each with a different use of material: auxetics, non-auxetics, fluids and magnetics. This chapter comprises of concepts that have built on these concept directions.

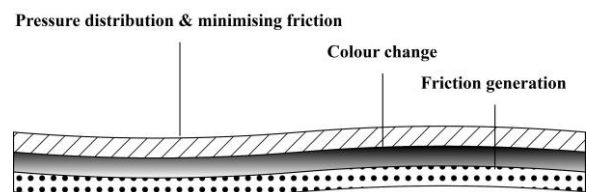


Figure 6. A proposed layered design with each of their functions.

5.2.1. Magnetics

Inspired by a children’s toy, the “Magna Doodle”, a flexible magnetic drawing board is considered. The toy is filled with thick, opaque white liquid, which contains black magnetic particles. A magnetic pencil is used to attract the magnetic particles. These particles keep floating due to the liquid being thick and heavy. A magnetic slider underneath the board is used to bring these particles downwards again. This drawing board is inherently rigid. Retrieving the requirement that the sheet should be flexible necessitates the development of a flexible board. The objective here is to design a flexible magnetic drawing board, and attract the magnetic particles when a specific normal pressure value is applied. This design makes use of encapsulated fluid and magnetics. The application of pressure leads to an indentation, which causes magnetic particles located at the board’s base to approximate the magnetic stylus at a specific pressure.

The first prototype consisted of polypropylene sheets as casing, white oil paint, linseed oil and iron filings for the liquid mix, and neodymium magnets used as the magnetic pencil. Three major problems were encountered. First, the white mixture stuck to the polypropylene covering its “window” through which the iron filings would be visible. As a result no colour change could be observed. Second, the seal was too weak at various locations causing leaks. Third, after a while the iron filings started to rust. These problems ask for another opaque mix and different cover material.

The second prototype consisted of a casing made from silicone (Ecoflex 00-20). The silicone’s structure consisted out of many holes filled with pure linseed oil and iron particles. Because the liquid wasn’t opaque anymore, there has been experimented with different hole shapes making sure the magnetic filings weren’t visible when they were located at the base of the sheet. Attached to the bottom was a flexible magnet layer which attracted back the iron filings instant after showing up at the top. See [Figure 7](#) for this layered design. Eventually, this design proved to be infeasible due to the silicone absorbing the oil in approximately 7 days. As a result, the magnetic particles became

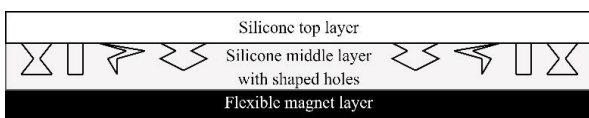


Figure 7. The layered design of a flexible magnetic drawing board. The bottom magnetic layer attracts the magnetic particles continuously that are placed in the holes of the middle layer.

immobilized within the holes, leading to substantial friction. This made the attraction of the magnetic particles to the bottom even harder as no flexible magnet layer was found that was strong enough. Next to this, this design necessitated neodymium magnets as pressure stylus. These magnets could be attached to the hand with gloves, but the requirement of manual actuation is not met properly.

5.2.2. Fluid mechanics

The human skin is a unique case in nature where pressure causes colour change. This concept therefore has a design that simulates the mechanism of blood vessels, especially the short period of ischemia due to arterial occlusion, which has been described in [Section 3.2](#).

Several Voronoi relief patterns were created in Rhino, which eventually formed the 3D-printed malls for silicone (Ecoflex 00-20). See [Figure 8](#). The Voronoi lines gave some appearance of blood vessel structure. There is experimented with the shape of the blood vessels and their width. A (half) square shape, a (half) round shape, and diameters ranging from 0.4mm to 1.6mm were created. Again, the challenge ultimately proved to be creating a leak-proof space for the coloured aqueous solutions. Thereby, it is difficult to ascertain the optimal viscosity necessary for determining the precise pressure threshold at which the liquid emerges from beneath its point of pressure application. Moreover, the issue persists, as the liquid exclusively relocates beneath the area of contact rather than dispersing adjacently. Consequently, the trifecta of leakage, viscosity optimization, and localized colour change, leaves us not choosing this design.

5.2.3. Solid mechanics

The preceding concepts posed notable challenges attributed to their reliance on liquid-based systems, and therefore the necessity of encapsulated fluids. The prerequisite to use the sheet at an inclination ranging

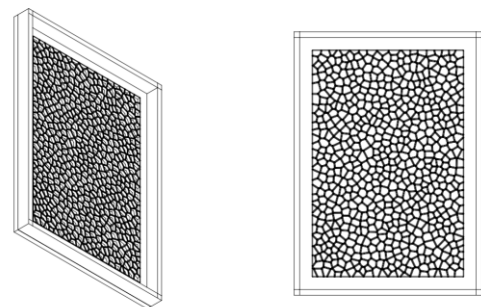


Figure 8. Drawings from a Voronoi pattern as relief in a box serving as a mall for silicone.

from 30° to 45° is in addition harder to achieve using these fluid-based systems. This section, in contrast, highlights the explored concepts with solid materials.

5.2.3.1. Auxetics

The idea of selectively concealing specific colour regions under mechanical stress while allowing the revelation of other colour regions, can be achieved using auxetic materials. These materials have a negative Poisson ratio, i.e. when you stretch them longitudinally, they doesn't become thinner, as in the case of rubbers and most materials, but actually widens in lateral direction [58].

Chiral, bichiral, trichal, snap and star auxetic structures were printed varying their material. TPU worked best. Yet the available materials did not have the desired flexibility. Thereby, it would be difficult to provide certain area boxed with a different colour than others. This concept was not pursued any further.

5.2.3.2. Non-auxetics

Next to 3D print materials, this study makes use of silicones. This study uses Ecoflex in its design as this is an often used silicone rubber in soft robotics, energy harvesters, and stretch-based sensors [59]. Thereby, hardened Ecoflex 00-20 is skin safe and certified. Three designs were created.

The first design comprises a stratified arrangement of multiple discs, wherein the uppermost tier consists out of discs filled with silicone with a yellow colour, and the bottom tier consists of discs filled with silicone with a red colour. By exerting pressure the yellow disc tier moves downwards towards the red disc tier, resulting in a colour transition to orange. This design posed a challenge in creating a sturdy 3D-printed mall that could be used repeatedly, while also keeping the total sheet thin. The implementation of discs with a rod in the middle, employing a double-bellow configuration, made the structure fragile. During the removal of cured silicone, the rods often broke off due to their slender diameter.

A second design consisted of hexagon-shaped cavities next to each other, forming a honeycomb structure, also made from Ecoflex 00-20. The silicone structure consisted out of three layers. Two same coloured outer layers and a different coloured middle layer. When pressing the structure from top the middle layer is pushed outwards of its hexagon shape, showing the colour of this middle layer next to the pressure point. For this design also certain issues arise. The colour of

the intermediate layer remains observable when the design is observed under an angle. Furthermore, the act of indentation induces the formation of a vacuum in the pressed cavities beneath the pressure surface.

A third design employed the existing Voronoi structure. The crux of this design is in the filling up of the mall. At first, a thin silicone layer of one colour is created up until the height of the relief. Following the curing of this primary silicone layer, a subsequent layer of silicone, distinguished by a different colour, is poured in. This methodology resulted in a structure that consists out of "islands" and "rivers" both exhibiting another colour. The thinner the rivers or higher the islands, respectively the more concentrated is the colour of the islands or the less visible is the colour of the rivers. By making a sliding movement over the islands, the rivers' colour becomes shortly visible. After several attempts, and also experimenting with an iridescent underlayer, this concept also proved not to work optimally.

A fourth design followed up on the one described above. Instead of a Voronoi pattern, a mesh was created. See [Figure 9](#). This design involved casting of a separate layer that has a low pigment concentration, imparting a subtle blue hue. The relief side of this silicone layer is placed on top of a red silicone layer. Due to the inherently diminished pigment in the blue layer, it becomes almost transparent when subjected to compression, thereby revealing the underlying red layer. Interestingly here, the concept uses the second concept direction described in [Section 4.3](#). However, instead of a broader presentation of pigmentation, the emphasis is placed on reducing pigment concentration vertically, thereby achieving a state of translucency. There is chosen to continue with this design, because it is the most promising in terms of the described requirements.

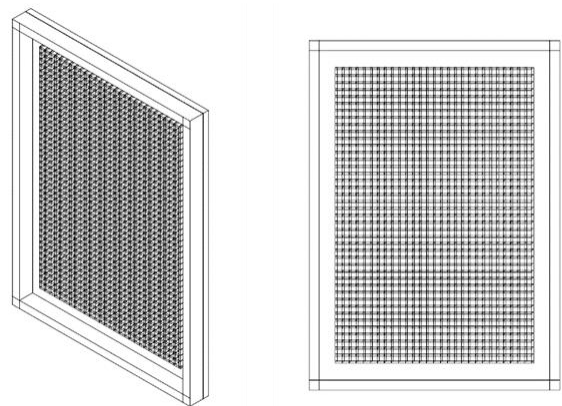


Figure 9. Mesh relief in a box serving as a mall for silicone.

5.3. The top layer: pressure distribution and minimising friction

In the final design, the silicone that forms the top layer is rough, causing a lot of friction when being rubbed by an object or hand. Hence, a reduction in friction becomes imperative. Furthermore, in the final concept, the colour change only occurs to the immediate vicinity of the pressure point, making it imperceptible to the naked eye. Distributing the force over an area that is larger than the surface area of the pressure point, will make sure the colour would also become visible adjacent to the point of pressure.

To achieve these requirements, a novel top layer is added, comprising a specific type of plastic material. Adding the plastic causes the PTET to be flexible instead of soft. The wish to keep this material soft outweighs its requirements for visible colour change and minimised friction of the top layer. There are choices between the amount of flexibility in this top layer. Opting for a less flexible plastic will distribute the applied force over a larger area creating a larger area of colour change. Opting for a very flexible plastic would preserve the PTET sheet's inherent softness, albeit potentially compromising the distribution of the force and therefore colouration.

5.4. The bottom layer: friction generation

As the counterpart of the top layer, the underlayer has to serve as a source of friction. In its current state, the red silicone layer inherently facilitates this frictional attribute. However, additional structural enhancements could be made to augment the frictional characteristics.

5.5. Final design

5.5.1. Bio-inspired working mechanism

The cephalopod's colour change mechanism consist of two reflecting layers and three layer containing different chromatophores, i.e. cells with pigment. These cells are able to expand or retract with a ratio of up to 1:500 through radially located muscle contraction or relaxation. In expanded state, the cells are disc-shaped absorbing corresponding wavelengths from incident light, and in retracted state the cells are hairpin shaped, preventing absorption and therefore transmission of the incoming light [3, 24, 27].

This final design comprises multiple unit cells distributed across the surface, each incorporating a colour-changing mechanism, inspired by the

chromatophore cells of the cephalopod. We also adhered to the recommendation proposed by Luo et al. [17] to use polymeric materials. It is intrinsic to polymeric materials to expand under normal applied pressure. Hence, achieving a smaller coloured unit cell, is unattainable. Similar to the cephalopod, that disperses its chromatophores using radial muscles, in our design a rod-shaped unit cell may undergo expansion due to internal radial forces in response to external transverse compressive loading, thereby selectively reflecting, absorbing, and emitting particular wavelengths, resulting in a perceivable colour change. The challenging aspect in this context resides in attaining a 1:500 ratio, whereby, upon the aggregation of unit cells, their collective colour becomes imperceptible. However, this study uses an innovative approach which entails the deliberate prevention of colour absorption, ensuring the transmission of all wavelengths. This is achieved through unit cells composed of polymeric materials with an initially low pigment concentration. Upon expansion instigated by external applied pressure, these cells exhibit a near absence of pigment in the vertical direction, thereby yielding a state of nearly complete transparency or translucency. See [Figure 10](#).

5.5.2. Prototype design and manufacturing

Through the application of external pressure from top, the bulges experience a compression in the interstitial space, resulting in an expansion of their horizontal volume. The bulges have no recourse but to disperse, leading to a reduction in pigment concentration per unit volume. Given the initially low pigment concentration, resulting effect may display an extremely light blue colour, bordering transparency, when viewing the design from above. Employing a flexible plastic upper layer also reduces the interstitial space next to the point of pressure, compelling the bulges to disperse in that region as well. As the bulges disperse and permit optical transparency, the underlying layer, which is coloured red, becomes visible. This colour change

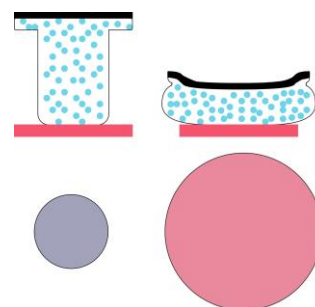


Figure 10. The colour change mechanism of a single unit cell from side and top view, under no load and under a compressive load.

occurs not only at the point of pressure but is therefore also observable adjacent to this point. At a certain force the bulges seem like they are merged into each other forming an almost transparent layer at the area underneath the pressure point. This transformation is visualized in [Figure 11](#).

The red bottom layer is made of Ecoflex 00-20 and aquarel. A small box is designed in Rhino, which is 3D-printed using a the Prusa i3 MK3S & MK3S+. The silicone mix consists out of 20 grams part A, 20 grams part B, 4 grams of red aquarel paint, and 6 grams of orange aquarel paint. This mix will fill 4 to 5 boxes of $46 \times 66 \times 2 \text{mm}^3$. The blue bumpy layer is also made of Ecoflex 00-20 and aquarel. Again a small box is created, but this time a relief on the bottom is created in the form of a mesh. Its grooves can vary in width. [Figure 9](#) shows a drawing of this box. This mall is filled with a concentration of 12 grams (6 grams part A + 6 grams part B) Ecoflex 00-20 and 0.002g of blue pigment (aquarel paint). There has been experimented with different concentrations. Between this red and blue silicone layers there is an option to add an interlayer of LDPE 0.05mm in between. Consequently, the blue layer has a higher degree of separation from the red layer, thereby enhancing the blue perceived hue when viewed from top in the initial state. There is hypothesised, because of the interstitial space being smaller, the pressed state where the blue layer is almost transparent is reached faster, i.e. at a smaller indent. The samples that are created are $46 \times 66 \text{mm}^2$. There will be experimented with different types of plastic material as top layer. These transparent plastics are placed on top of a 1:1 drawing of the 3D models of the trays created in Rhino. With a marker the outline of the sample is drawn onto the plastic. The correct sizes are cut.

Summarizing, the final design consisted out of 3 to 4 stacked layers depending on the presence of an interlayer: (1) a transparent flexible plastic top layer of 0.20 or 0.075mm, (2) a structured bulged blue silicone layer with a low initial concentration of blue pigment

of 2.5mm thick plus bulge height, (3) a transparent LDPE 0.05 interlayer (optional), and (4) a red silicone layer with a thickness off 2mm. To glue these layers together, pigment-free Ecoflex 00-20 is used. A thin layer is applied to all surfaces except the blue layer. No silicone is applied directly onto the bulges to prevent the grooves from being bricked up. Only to the edge of this side of the blue layer some thin layer of silicone-glue is applied.

5.5.3. Compatibility to the requirements

Comparing the presented design to the presented performance requirements, shows us that the following requirements are met: manual actuation, colour change, reversibility, flexible, friction generation, 30° - 45° handling, thickness below 5mm, scalability, hygienic as it is washable, skin safe. Also some wishes are met: gradient colour change, active colour change, easy manufacturing and zero power consumption. Other requirements, such as the threshold force, the response time of 13 ms, colouration persistence of 1 second, recovering time of 2 seconds and durability cannot be evaluated yet.

Given the overarching objective of this study, which is centered around the development of a responsive sheet sensitive to a specific pressure threshold, the principal emphasis of this experiment is to elucidate the precise pressure levels and degrees of indentation necessary to elicit a distinctive change in colouration. The indentation aspect is of significance in ascertaining the extent to which applied pressure can be transferred to the skin. Notable, it is conceivable that a greater applied force with a shallower indentation may transmit a lesser magnitude of force than a comparatively smaller applied force exerted with a deeper indentation. Additionally, the response time and if the recovering time is below the stated 2 seconds will also be examined. Each sample will undergo a three iterations of the experiment, examining whether or not the object can at least be used three times.

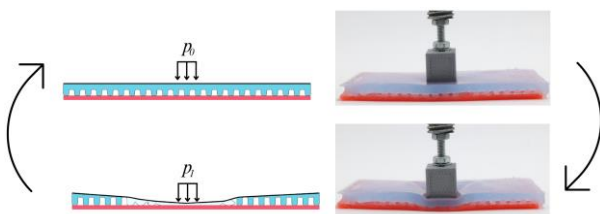


Figure 11. A schematic and prototype cross-sectional view of pressed and released states ($p_1 > p_0$) presented in a cycle to show the working principle and reproducibility of the design.

6. Evaluation

6.1. Goal of the experiment

The objective of the experiment within this study is twofold: (1) validate the colour-changing design of the PTET and (2) evaluate the correlation between pressure levels, indentation levels and the degree of colour change, while also assessing the impact of selected variables on this relationship. In both experiments was the degree of colour-change, i.e. the change in H-value within the HSV colour model in combination with the changed area size, the performance measure.

6.2. Experimental setup

Figure 12 shows the setup that was used to perform the experiments. The experiments were performed with a constant amount of light, such that the colour change could not be attributed to different amount of lights in the room. Illumination was exclusively provided by a Puluz light box (Model PU5025B) emitting 26 LM (lumens of light). Within this box, a white plate was placed, which was positioned on the left-hand side adjacent to the fixed stage. Simultaneously, another white plate was strategically placed on the right side to optimize reflective properties essential for the film recording. To stabilize the camera, a tripod was securely positioned on the Thorlabs platform, with each of its legs secured in designated holes. Attached to this tripod was a camera (Canon EOS M100), providing a slight angular perspective onto the fixed stage, whereon the sample was placed within the pre-marked boundaries. It is noteworthy that achieving a completely perpendicular alignment was unfeasible due to the presence of an L-bracket affixed to the

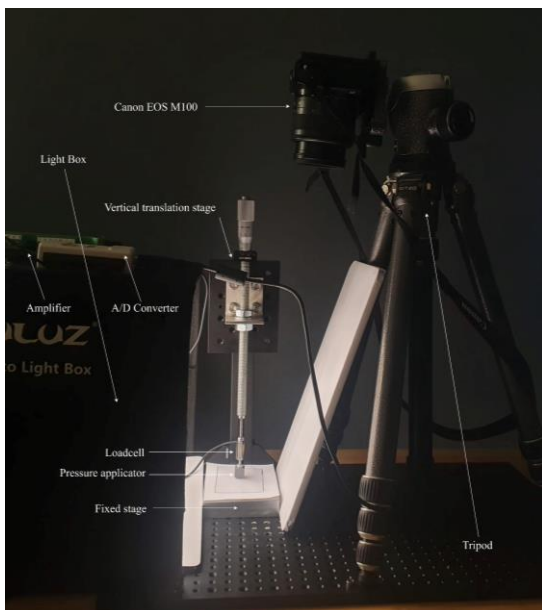


Figure 12. Overview of the experimental setup

vertical translation stage, which posed a line-of-sight obstruction within the experimental configuration. A trade-off had to be made between having footage taken at a minimum angle, or placing the loadcell next to the bracket so that there is a moment on the steel arm that is then twisted into the threaded rod. There was chosen for the first option, as the latter would make it unnecessary cumbersome to take into account the moments under which the load cell would be acting. The load cell that was used is an S-beam junior load cell (FUTEK, model FLLSB200), and was calibrated to measure forces between 0 and 50N. It was connected to an analogue signal conditioner (CPJ RAIL, SCAIME) and a data acquisition unit set at sampling rate of 10Hz (NI USB-6008, National Instruments Corporation). The loadcell was located between two components. On one side, it was attached via an M3 threaded rod to the pressure applicator. This applicator was a 3D-printed block of PLA with dimensions $10 \times 10 \times 10 \text{mm}^3$. On the other side, it was attached via an M3 threaded rod to an M10 threaded rod, which in turn was attached to the L-bracket. This L-bracket itself has been laser-cut from a 3mm steel plate. It was then bent into a 90-degree angle. The L-bracket was fixed to the vertical translation stage of Thorlabs, which could take precise steps of 0.01mm. In [Appendix A](#) and [Appendix B](#), the process of establishing this experimental setup is elucidated, and further details are provided regarding the fabrication of certain parts.

6.3. Experimental design

6.3.1. Experimental variables

Within the design space of the given design, several variables can be altered to hypothetically modify: (1) The pressure required to achieve a colour change, i.e. the threshold pressure. Threshold pressure is defined as the pressure applied at the incremental step, which results a 15mm^2 increment compared to the lowest coloured area value observed prior to this, or when the area is expanded by a factor 5 in cases with minimal area change. (2) The amount of colouration in terms of area, hue and saturation according to the HSV colour model. (3) The colour changed area increase in percentage. A pixel is classified as a colour-changed pixel and is accordingly incorporated into this area if, within the HSV colour model, the hue (H) value ≥ 0.851 and the saturation (S) value ≥ 0.466 . (4) The indentation that is required to achieve a colour change (i.e. threshold indentation). (5) Response time. (6) Recovery time. For this study we focus on finding a relation between different designs and the first four measures: threshold pressure, delta of hue change (i.e.

ΔH -value), percentage increase in colouration, and threshold indentation. The variables that we are altering are: (a) the bulge size (area mm^2), (b) groove width (mm), (c) bulge height (mm), (d) upper layer flexibility, and (e) the presence of interlayer. These variables were deduced from some prior experiments, which is elaborated on in [Appendix A.2](#).

These chosen variables each have two values: a minimum value and a maximum value. There are 12 samples. Sample 1 contains the mix of values of the variables that are expected to result in a lower threshold pressure for visual colour change. Sample 2 until Sample 6 alternate 1 variable compared to Sample 1. Sample 7 contains the mix of values of the variables that are expected to result in a higher threshold pressure for visual colour change. Sample 8 until Sample 12 switch off idem 1 variable per time to its other outer value. The first 6 samples can correlate a difference in bulge area, groove width, bulge height, upper layer flexibility, and the presence of an interlayer, to a positive or negative effect on the threshold pressure and threshold indent coupled with the degree of colour change. Due to the potential influence of multiple factors, i.e. variables, within the design, it was decided to conduct a second set of experiments, approaching the analysis from a different perspective. These second set of 6 samples can also establish a connection between a variable and variations in threshold pressure and threshold indent in conjunction with the degree of colour change. If the discrepancies identified in the first six samples and the second six samples correspond, it can be inferred that this variable indeed exerts either a positive or negative influence on the threshold pressure. It is hypothesized that these results include contradictions, as one variable may have a more significant impact than another, thereby undermining the effect of another variable.

It is important to underscore that the mould to create the textured blue silicone layer is generated in Rhino 7 using Grasshopper. The inherent limitations of this design concern the potential for undamaged removal of the silicone material. The inclusion of tall grooves, which result in elevated cavities, in combination with the presence of thin squares (a small bulge area), may lead to challenges in ensuring complete silicone coverage, primarily due to heightened viscosity of the silicone, or not being able to remove the silicone undamaged from the mall. Optimal parameters, encompassing the maximum bulge height, minimum bulge size, and minimum groove dimensions, is therefore chosen through an iterative approach of trial and error.

Summarizing, the experiment consist of 12 samples that contain different variables as shown in [Table II](#). The maximum and minimum bulge sizes are respectively $2 \times 2 mm^2$ and $1 \times 1 mm^2$. The maximum and minimum groove widths are respectively $2 mm$ and $1.4 mm$. The maximum and minimum bulge heights are respectively $0.8 mm$ and $0.4 mm$. The most flexible top layer is made from PolyPropylene of $0.075 mm$ (PP0.075), and the less flexible top layer is made from PolyVinylChloride of $0.20 mm$ (PVC0.20). Lastly, the samples differ in having an interlayer, which is made from Low Density PolyEthylene of $0.05 mm$ (LDPE0.05). In [Figure 13](#) these 12 samples are shown.

TABLE II. The samples and their variable values

Sample	Variables				
	Bulge area [mm^2]	Groove width [mm]	Bulge height [mm]	Upper layer	LDPE 0.05 interlayer
1	2x2	2	0.4	PVC0.20	No
2	1x1	2	0.4	PVC0.20	No
3	2x2	1.4	0.4	PVC0.20	No
4	2x2	2	0.8	PVC0.20	No
5	2x2	2	0.4	PP0.075	No
6	2x2	2	0.4	PVC0.20	Yes
7	1x1	1.4	0.8	PP0.075	Yes
8	2x2	1.4	0.8	PP0.075	Yes
9	1x1	2	0.8	PP0.075	Yes
10	1x1	1.4	0.4	PP0.075	Yes
11	1x1	1.4	0.8	PVC0.20	Yes
12	1x1	1.4	0.8	PP0.075	No



Figure 13. All prototypes of the 12 samples positioned next to each other.

6.3.2. Experimental procedure

Each sample is subjected to a tripartite testing process as follows. The sample is positioned within the demarcated boundaries on the paper. Subsequently, the paper is meticulously aligned with the fixed stage. This steps were taken to ensure that each sample is pressed at a consistent location on the surface. With the sample in place, the pressure applicator is set to its zero position. The Labview measurement system is activated but not yet saving the recording. The vertical stage is incrementally lowered until the pressure applicator gently makes contact with the surface, as indicated in Labview by a slight increase in force. The offset of the load cell is measured at 0.5953N; consequently, the initial positioning of the pressure applicator has to be marginally higher than this specified value. With all preparations complete, Labview data is saved, and the file is named: "Exp # - Try #." Data recording is initiated. Simultaneously, the camera recording is also commenced. A wooden spatula is employed to gently tap the pressure applicator to facilitate subsequent alignment between the video recording and data acquisition. Then, the stepwise indentation process is executed. The vertical stage is lowered by one-quarter millimeter, and the depth of the pressure applicator is verbally articulated while counting up to 3. This verbalization aids in future steps aligning the snapshots to the corresponding specific incremental steps. At the second step, a depth of half a millimeter is reached, followed by three-quarters of a millimeter at the third step, ultimately

extending to 3mm of indentation. Subsequently, the indentation is reduced in quarter-millimeter increments, with approximately 3 seconds for each step. Once the system returns to the zero point, the wooden spatula is employed once more to gently tap the pressure applicator. Subsequently, both data recordings, from Labview and the camera, are halted. This sequence represents the first trial for a given sample and is repeated three times per sample. All data is diligently stored and meticulously organized within folders. Additionally, a copy is generated and stored on a hard drive.

6.3.3. Data preparation

In preparation for data analysis, the acquired data will necessitate initial processing and entails the establishment of specific thresholds to define when the colour represents the altered colour. The data of the load cell was collected via Labview 2018 and analysed in Matlab R2023a. The videos taken by Canon EOS M100 are cropped in Movavi Video Editor Plus 2022, such that the edges of the samples are not visible anymore. As a consequence of the absence of bulges and the presence of smooth edges, a red colouration was visible from top view. These edges are of no relevance in the data analysis and therefore cropped out. The combination of pressure data and video resulted in a live snapshot cycle of a sample at each quarter-mm step, and a binary image cycle of these snapshots visualizing the colour changed area.

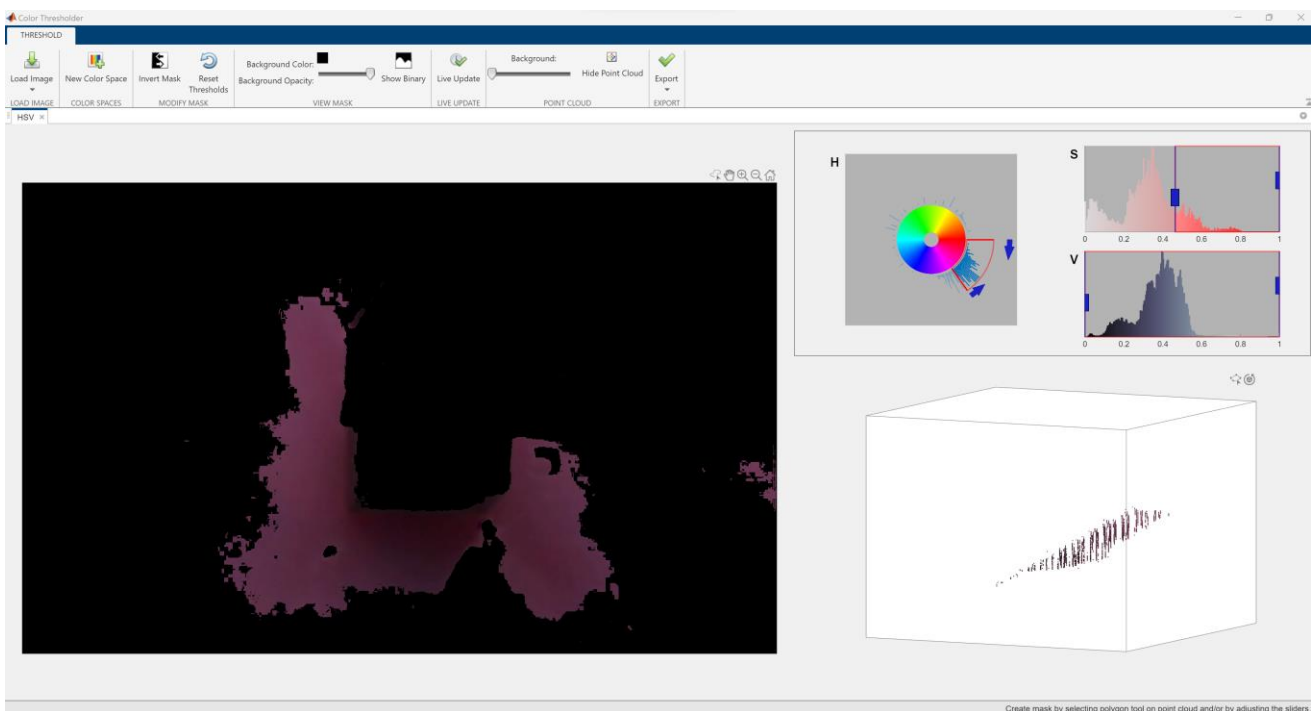


Figure 14. A screenshot of the Thresholder Application in Matlab R2023a, and a screenshot of a video of a sample at maximum indentation on which a mask is placed by adapting the region for the h and s values.

The criteria for the selection of pixels to be classified as colour-changed pixels necessitated a minimum saturation threshold of 0.466 and an H-value of 0.851. These threshold values were determined through the utilization of the Color Thresholder application integrated within the Matlab environment, see [Figure 14](#). This analytical process involved the examination of a snapshot at maximum indentation of a selected sample to ascertain the optimal parameter values for classification. The regions for the h- and s-values were adapted, but no delimitation was needed for the v-values, as is shown in [Figure 14](#).

6.4. Hypotheses

Several assumptions were made before the experiments were conducted. For instance, Sample 1 was configured with hypothetical values that ultimately result in a lower threshold pressure than the values assigned to Sample 7. An empirical experiment with a kitchen scale and pressure of a gentle touch of the hand, initial versions of the samples seemed to show that a higher threshold pressure was needed for a sample with smaller bulges. In addition the prior experiments elaborated on in [Appendix A.2](#) did not establish a clear relationship between increasing the bulge size and the threshold pressure. Therefore it was anticipated that increasing the bulge size would lead to a reduction in threshold pressure because the force would spread more quickly across the larger surface area, becoming more promptly visible alongside the pressure applicator, even if the intrinsic design of the smaller squared bulges requires less force to press in a similar indentation. It is expected that for this design with the smaller bulges, a higher indentation is needed to achieve a colour change, and therefore the threshold pressure is larger. However, regarding Hooke's law, an interesting perspective can be drawn.

In accordance with Hooke's law, the stiffness of a spring decreases as the cross-sectional diameter of the spring wire decreases. Also, when two springs are parallelly arranged, the required force for an equal displacement doubles compared to a single spring arrangement. Although silicone is an unpredictable material with a very high modulus of elasticity, that is not represented as Young's modulus but in Shore Hardness, we take the assumption for this intermediate experiment that the square bulges behave like springs and employ the same formula (see [Section 3.4](#)). Namely the modulus ultimately remains the same in all cases, because consistently the same type of silicone (Ecoflex 00-20) is used.

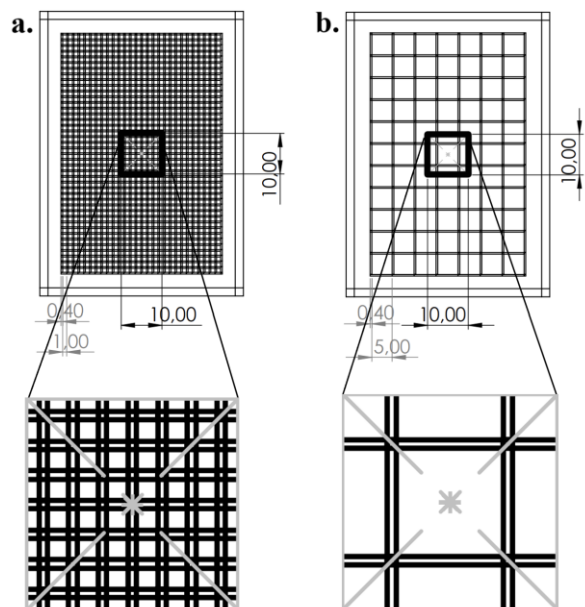


Figure 15. Solidworks drawings of two examples of a mold, where (a) represents the mould which results in a silicone patch with smaller bulges (1mm^2), and (b) represents the mould which results in a silicone patch with bigger bulges (25mm^2). In both drawings a pressure application area of $10 \times 10\text{mm}^2$ is indicated.

One could postulate that, in cases where a substantial increase in the quantity of smaller bulges occurs beneath a specific pressure surface area as compared to the situation involving larger bulges, and where this increase accelerates more quickly with a progressively enlarging pressure surface, there may be a point at which the cumulative stiffness of the smaller bulges becomes either equivalent to or surpasses that of the comparatively fewer large bulges. An intermediary experiment in Matlab R2023a is executed, wherein the total area is calculated against a progressively increasing pressure surface area, checking this hypothesis. See [Appendix E.7](#) for the Matlab code.

In this intermediary experiment, we juxtapose two mold designs, which results in two silicone sheets, one featuring smaller bulges with an area of 1mm^2 (A_a), and the other comprising bulges with an area of 25mm^2 (A_b). Both designs maintain an identical groove spacing of 0.4mm , as illustrated in [Figure 15](#). The depicted pressure surface in this figure measures 100mm^2 , positioned precisely at the center of the mold, and consequently, at the center of the final cured silicone specimen. We know the stiffness is calculated using [Equation 7](#). The Young's modulus and initial length is equal for both specimens, given that the same type of silicone is used and the initial height of the bulges are the same. This results in the following equation that demonstrates the relation between stiffness and area.

$$\frac{k_a}{A_a} = \frac{k_b}{A_b} \quad (9)$$

Next to this relation, the amount of bulges is also of interest. If the force direction is perpendicular to the surfaces between which the bulges, an accumulation of the stiffness of the bulges, results in the total stiffness. We noticed that underneath each pressure surface we could count the bulges of which their whole area gets squeezed (“whole bulges”), bulges that are squeezed over one length and cut off at a certain point (“half bulges”), and bulges that are only squeezed on one corner (“corner bulges”). Depending on the pressure area, the amount of each of these bulges is calculated, which results in the value of the total area, and therefore to the total stiffness.

For mould **a**, we take the length or width and divide this value by two, and subsequently subtract half of the groove size. A while loop in Matlab R2023a then calculates how many times a whole bulge and a groove fits in the remaining length ($count_a$). The counting quits when at a certain point the remaining length (x or y) is smaller than the whole length of the bulge size. The number of bulges is then counted as follows:

$$n_{total,a} = n_{whole,a} + n_{half,a} + n_{corner,a} \quad (10)$$

$$n_{total,a} = (count_a * 2)^2 + (count_a * 2) * 4 + 4 \quad (11)$$

The total area of the bulges is:

$$A_{total,a} = (count_a * 2)^2 * A_a + (count_a * 2) * 4 * x * \sqrt{A_a} + 4 * x^2 \quad (12)$$

A similar approach is done for mould **b**.

$$A_{total,b} = ((count_b * 2) + 1)^2 * A_b + ((count_b * 2) + 1) * 4 * y * \sqrt{A_b} + 4 * y^2 \quad (13)$$

Concluding information:

$$k_{total,a} = A_{total,a} * \left(\frac{Y}{L_0}\right) \quad (14)$$

$$k_{total,b} = A_{total,b} * \left(\frac{Y}{L_0}\right) \quad (15)$$

Plotting the width of the pressure area versus the stiffness, and versus the amount of bulges, results in respectively [Figure 16 and 17](#). Based on the obtained findings, it is apparent that the proliferation of smaller bulges has a steeper incline when compared to the design featuring larger bulges. Nevertheless, the rise in stiffness demonstrates a lesser incline in comparison to the stiffness of the larger bulges. Consequently, no point is found where the cumulative stiffness of the

smaller bulges becomes either equivalent to or surpasses that of the comparatively fewer large bulges. Ultimately, the observed increase in stiffness in this instance was attributed solely to the enlargement of the contact area. The smaller bulges contact area did not surpass the total contact area of the larger bulges. Such an outcome may occur if the groove width of the larger bulges is widened. A new test, wherein the groove width of Design b is modified to 1mm, yields [Figure 18 and 19](#). Another test, wherein the groove width of Design b is modified to 2mm, yields [Figure 20 and 21](#). By increasing the groove width of design b in comparison to the groove width of design a, the stiffness of design b can indeed become equal to, or even fall below, the stiffness of design b at a specific junctures.

The hypothesis has been corroborated. The expansion of the pressure surface area can induce alterations in the overall stiffness, and the stiffness of the smaller bulges may even surpass that of the larger bulges. However, this occurs exclusively when the groove spacing of the larger bulges has attained a certain magnitude, certainly greater than the groove spacing of the design featuring the smaller bulges. In addition, it is noteworthy that in this model the pressure area does exert a measure of non-linear influence on the stiffness, and this relation differs per design. Furthermore, the empirically observed lower threshold force for the larger bulges may still be attributed to the requirement for a reduced indentation compared to smaller bulges, even if the intrinsic design of the bigger bulges is stiffer. Next to this, it appears that a larger surface tension with a flexible material results in a slight indentation toward the centre, which aids in reducing the indentation and therefore reducing the required force. Another reason could be that due to the larger blocks in contact with the red layer, the red colour becomes visible right from the outset, resulting that only an increase in saturation will cause a visually colour change. This, in turn, contributes to a reduction in the threshold indentation.

Next to prior findings and therefore expectations that the widening of the groove results in lower contact area and therefore a lesser stiffness, it was expected that a wider groove would lead to a lower threshold pressure because the silicone is thinner in these areas, thus offering less overall resistance to indentation. The same reasoning can be applied to the height of a bulge. When there is more silicone along the vertical length to be compressed, i.e., a higher bulge, the threshold pressure will be higher because more silicone must be pushed aside before the underlying layer becomes visible.

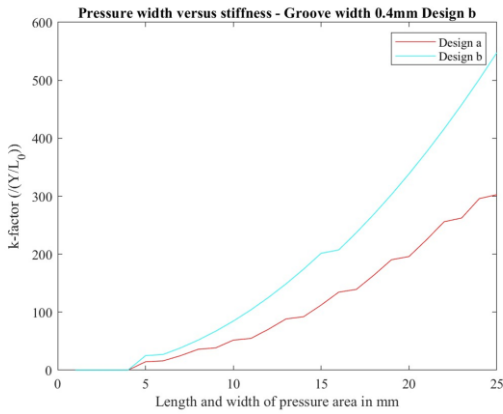


Figure 16. Demonstration of the increase in stiffness compared to the pressure area width increases, where the groove of design a and b are equal.

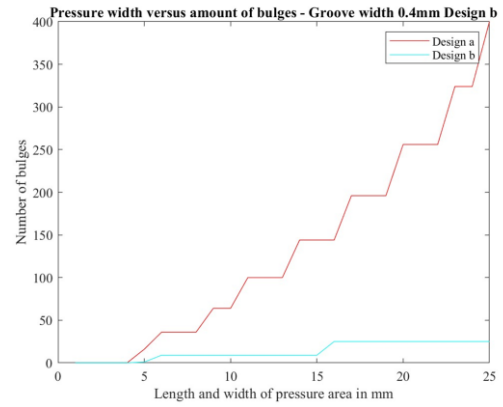


Figure 17. Demonstration of the increase in bulges when the pressure width length increases, where the groove of design a and b are equal.

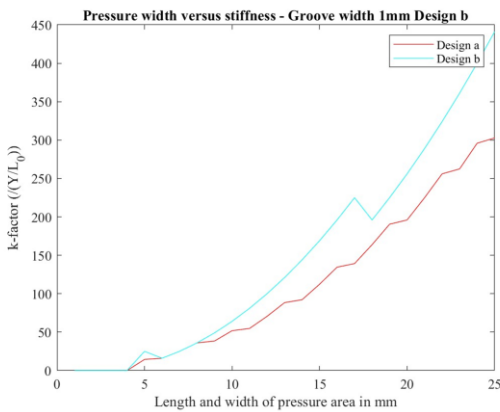


Figure 18. Demonstration of the increase in stiffness compared to the pressure area width increases, where the groove of design b = 1mm.

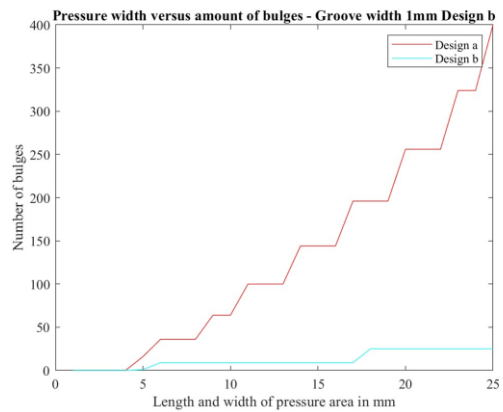


Figure 19. Demonstration of the increase in bulges when the pressure width length increases, where the groove of design b = 1mm.

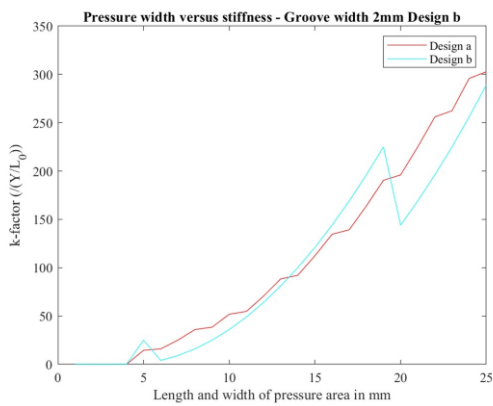


Figure 20. Demonstration of the increase in stiffness compared to the pressure area width increases, where the groove of design b = 2mm.

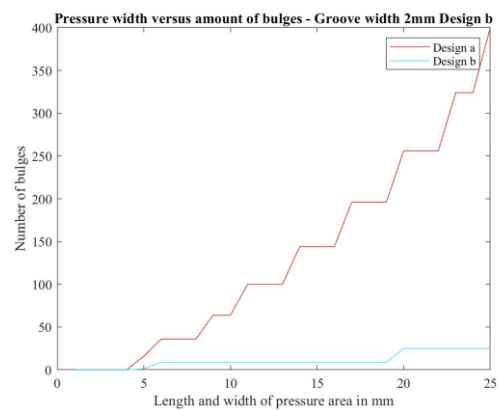


Figure 21. Demonstration of the increase in bulges when the pressure width length increases, where the groove of design b = 2mm.

Concerning the upper layer, it is believed that a less flexible upper layer corresponds to a lower threshold pressure. While the overall force progression during the experiment will naturally be lower with a more flexible upper layer compared to a more rigid one, colour change is expected to occur more rapidly with the more rigid upper layer. This is because the pressure is

distributed more evenly, and less indentation is required to achieve a greater area of colour change. In the case of a highly flexible layer, colour change is expected to occur primarily beneath the surface of the pressure applicator and may not be quickly observable adjacent to this applicator. It will only become somewhat visible with significant indentation.

Lastly, it is anticipated that a plastic intermediate layer will result in higher threshold pressure because this layer would provide slightly more resistance during compression.

Stating the hypotheses:

Lower threshold pressure and is obtained by:

- H1 – a larger bulge**
- H2 – a wider groove**
- H3 – a lower bulge**
- H4 – a less flexible top layer**
- H5 – having no interlayer**

Lower threshold indentation is obtained by:

- H6 – a larger bulge**
- H7 – a wider groove**
- H8 – a lower bulge**
- H9 – a less flexible top layer**
- H10 – having no interlayer**

More area growth is obtained by:

- H11 – a larger bulge**
- H12 – a wider groove**
- H13 – a lower bulge**
- H14 – a less flexible top layer**
- H15 – having an interlayer**

More ΔH is obtained by:

- H16 – a smaller bulge**
- H17 – a smaller groove**
- H18 – a higher bulge**
- H19 – a less flexible top layer**
- H20 – having an interlayer**

6.5. Results

6.5.1. General data analysis

The experiment yielded three stair graphs per sample, as each sample underwent a loading and unloading cycle thrice. See [Figure 22](#) for a representation of this progression. The Savitzky-Golay filter, a general filtering method in cases of experimental data that has noise and irregularities, is used to extract the important trend of the raw data. Using Matlab R2023a the mean applied force is computed at each incremental step and aligned with these indentation steps. This is accomplished by identifying the time indices corresponding to the cessation of the flatline phase, followed by the computation of the mean of the recorded force values over the prior three-second interval. This elucidated insights into the force progression per sample. Next to this, insights were gained when the force is plotted against the indentation and the red coloured area. See [Figure 23 and 24](#). Strikingly, hysteresis is observed in each of the 12 samples, one more pronounced than the other, signifying that the force during the forward phase of the cycle exceeds the force progression during the return phase. Comparing all hysteresis loops, it is identified that a more flexible top layer results in a greater hysteresis effect. Refer to [Appendix E.1](#) for the Matlab code in which a comprehensive analysis is conducted for a sample. Consult [Appendix G](#) for a total representation of the hysteresis loops.

Moreover, snapshots were extracted from the video recording at moments coinciding with these found incremental steps. Initially, through the utilization of

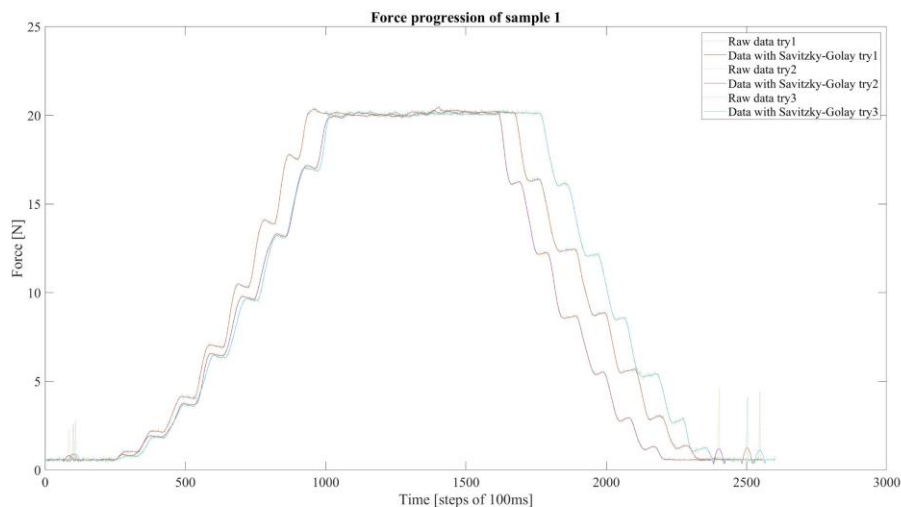


Figure 22. The force progression of sample 1 during loading and unloading of the sample. The three trials are presented with their raw data, and their data processed with the Savitzky-Golay filter.

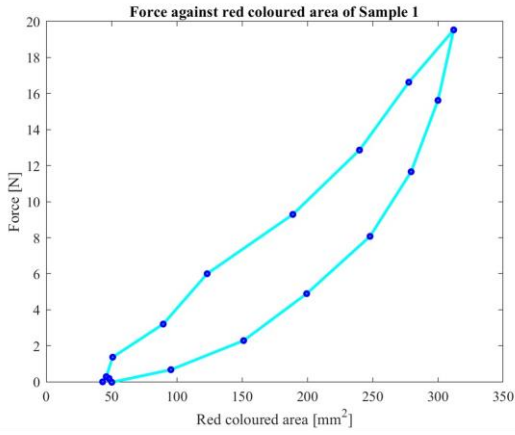


Figure 23. The force progression shown by the mean force at each incremental step of indentation versus the calculated mean red coloured area at each incremental step.

the recorded video data, force data, and the moment at which the wooden spatula made contact with the bottom of the pressure applicator, the video was synchronized with the force data to facilitate the precise extraction of screenshots at the appropriate indices. A mask was applied on these snapshots, identifying the pixels that did not classify as a colour-changed pixel, see Figure 26. A pixel is classified as a colour-changed pixel and is accordingly incorporated into the colour-changed area if, within the HSV colour model, the hue (H) value exceeds 0.851, and the saturation (S) value exceeds 0.466. In Figure 25 snapshots of sample 4 are juxtaposed with their accompanying binary images at initial state, threshold state, and maximum state, showing the defined area of colour change. An additional analysis was done delineating the colour progression of each sample from its initial state to maximum state, see Figure 27.

Threshold pressure is defined as the pressure applied at the incremental step that resulted a 15mm^2 increment

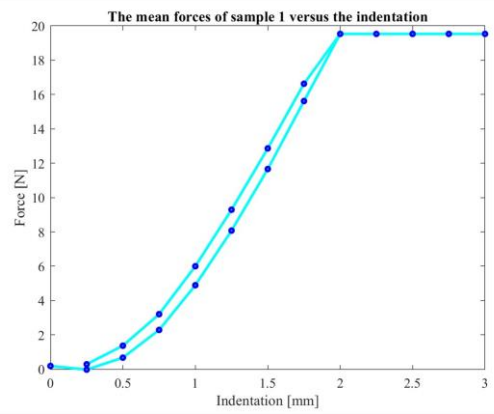


Figure 24. The force progression shown by the mean forces at each incremental step of indentation.

compared to the lowest coloured area value observed prior to this, or when the area is expanded by a factor 5 in cases with minimal area change. Table III summarizes the threshold pressures and the accompanying threshold indent. All samples attained their maximum state at a force between 18.59N and 19.83N, except for Sample 12, which reached its maximum at 15.81N. Table III also presents the maximum indentation values associated with these forces, along with the percentage of colour changed area compared to the area that was reached at the threshold pressure. This indicates an increase in applied pressure results in an increase of the transparent area, and therefore an increase in red coloured area.

Sample 1 until sample 6 provides information about the relationships between a variable and its influence on the performance measures: threshold pressure, threshold indent, growth, and ΔH . Sample 7 to sample 12 may validate, or contradict these insights.

TABLE III. Threshold and maximum values, percentage of increase in colour changed area compared to area at threshold pressure and the colour differences

Sample	Threshold and maximum values				Differences in HSV-values		
	Threshold pressure [N/mm ²]	Threshold indent [mm]	Maximum indent [mm]	Growth in percentage [%]	ΔH	ΔS	ΔV
1	$3.2059 \cdot 10^{-2}$	0.75	2.00	348.1	0.0709	0.2461	0.0816
2	$2.0694 \cdot 10^{-2}$	0.75	2.00	286.4	0.0891	0.2285	-0.1152
3	$6.3618 \cdot 10^{-2}$	1.25	2.25	471.94	0.1124	0.2601	-0.0930
4	$12.6135 \cdot 10^{-2}$	1.75	2.25	400.4	0.1858	0.3279	-0.0163
5	$5.1478 \cdot 10^{-2}$	1.25	2.75	136.8	0.0243	0.1402	0.1548
6	$4.6141 \cdot 10^{-2}$	1.00	2.00	159.41	0.0246	0.1468	0.1395
7	$4.1437 \cdot 10^{-2}$	1.25	2.50	384.4	0.1350	0.3538	-0.0197
8	$11.2165 \cdot 10^{-2}$	2.00	2.75	261.2	0.1241	0.3397	-0.221
9	$2.8887 \cdot 10^{-2}$	1.00	2.00	202.5	0.0435	0.2034	0.1319
10	$2.4811 \cdot 10^{-2}$	1.00	2.50	232.0	0.0623	0.2981	0.0945
11	$2.2321 \cdot 10^{-2}$	1.00	2.00	128.2	0.0092	0.1212	0.1545
12	$2.8571 \cdot 10^{-2}$	1.50	3.00	133.28	0.0010	0.1427	0.1348

The data analysis encompasses distinct steps, each with its own set of threshold criteria. Initially, a requirement is imposed on the hue (H) and saturation (S) values to correctly identify the shade of colour-changed red. Subsequently, a threshold is applied to the minimum increase in the area of this colour, ensuring that the alteration in size is perceptible and distinct from the initial state. Ultimately, a comparison is made between the colour at the outset and its transformed state. Should the hue change exceed 0.1, a visible colour change has transpired. This last step is taken because the initial starting colour may already closely align with the specified parameters for colour-changed red, and the eventual change, despite its minimal change in size, remains unnoticeable.

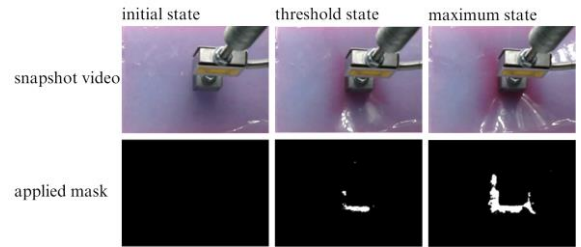


Figure 25. Snapshots at indicated states of sample 4 and the accompanying binary images. A mask was placed over the snapshot conforming to the minimum H- and S-value.



Figure 26. The snapshots at each incremental step is shown, in combination with their binary images of sample 1.

6.5.2. Sample 1 vs others

Sample 1 achieved an increase of 15mm^2 of colour changed area, i.e. pixels that had a minimum H-value of 0.851 and S-value of 0.466, at a pressure of $3.2059 \times 10^{-2} \text{ N/m}^2$. Its colour changed area from maximum indent, i.e. the indent at maximum force, compared to the state at threshold pressure, has grown with 348.1%. The required hue change of minimal a ΔH of 0.1, is not achieved, as this value is 0.0709. However, the colour change is merely noticeable visualized in [Figure 27](#).

Compared to Sample 1: Sample 2, with a decreased bulge area, required the lowest required threshold pressure. The coloured area growth decreased, and a small increase in H-value happened. Sample 3, with a thinner width, required a higher threshold force. The coloured area growth increased. The H-value also increased up until a point it is identified as a valid colour change. Sample 4, with a higher bulge height, required a very high threshold force. Increasing the bulge height resulted in a higher growth percentage, and a ΔH of 0.1858, which it makes the sample with the highest hue change, and therefore most discernible colour change. Sample 5, with a softer top layer, resulted in a higher required threshold pressure, a decrease in growth percentage, and an unrecognizable colour change. Sample 6, with an interlayer, exhibited a lower threshold pressure. It has a smaller growth percentage, and likewise Sample 5 an unrecognizable hue colour change.

6.5.3. Sample 7 vs others

Sample 7 achieved an increase of 15mm^2 of colour changed area, i.e. pixels that had a minimum H-value of 0.851 and S-value of 0.466, at a pressure of $4.1437 \times 10^{-2} \text{ N/m}^2$. Its colour changed area from maximum indent, i.e. the indent at maximum force, compared to the state at threshold pressure, has grown with 384.4%. The required hue change of minimal a ΔH of 0.1, is achieved, as this value is 0.1350.

Compared to Sample 7: Sample 8, which exhibited a larger bulge size, required a higher threshold force. A lower growth percentage was achieved, however the colour change was noticeable although the hue change is a bit smaller. Sample 9, with a larger groove, needed a lower threshold pressure for colour change. The larger groove resulted in a lower growth percentage, and unnoticeable hue difference. Sample 10, with a lower bulge height, required a lower threshold pressure. The lower bulge height resulted in a lower percentage growth of coloured area. Next to this, the

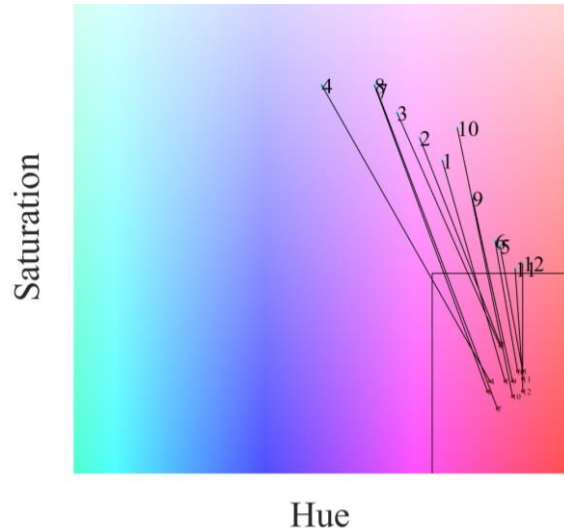


Figure 27. 2D HSV colour map wherein the initial colours and maximum achieved colour is indicated. The horizontal line indicates the minimum saturation of 0.466, and the vertical line indicates the minimum hue of 0.851.

hue change is less. Sample 11, with a less flexible top layer, resulted in a lower threshold pressure, but in a smaller coloured area growth. In addition, the colour change is unrecognizable. Sample 12, which has no interlayer, also has an unrecognizable colour change. The area growth is low in comparison, and a smaller required force was needed.

Next to this presented data, in [Appendix F](#) one will find the snapshots with corresponding binary images and a force-coloured area graph per sample. In [Appendix G](#) summarizing images are found in the form of force-indent, coloured area-indent, and HSV 2D colour map graphs.

6.6. Interpretation of results

Validated results are that a lower threshold pressure occurs, when the bulge area is smaller, the width of the groove is bigger, the bulge height is lower, the top layer is less flexible, and no interlayer is added.

TABLE IV. Summarized conclusions

		Performance measures			
		Lower Threshold pressure	Lower threshold indent	More area growth	Larger ΔH
Variables	Bulge size	↓	X	X	↓
	Groove width	↑	↑	↓	↓
	Bulge height	↓	↓	↑	↑
	Upper layer flexibility	↓	↓	X	X
	Interlayer	↓	X	X	X

Furthermore, the threshold indent can be lowered by having a wider groove, lowering the bulge height, or making the top layer less flexible. To achieve a higher growth percentage of the colour changed area compared to the threshold state, one could reduce the groove's width, or increase the bulge's height. To increase the difference in hue, reducing the bulge size and groove width, while increasing the bulge height, is recommended. An initially lower hue, i.e. a more initial blueish colour, can be achieved by samples exhibiting a smaller groove size, and a higher bulge. The influence of variables that aren't mentioned in these validated result show contradiction on that specific aspect. These validated results are summarized in [Table IV](#).

These results let us evaluate the hypotheses:

Lower threshold pressure and is obtained by:	
H1 – a larger bulge	<input checked="" type="checkbox"/>
H2 – a wider groove	<input checked="" type="checkbox"/>
H3 – a lower bulge	<input checked="" type="checkbox"/>
H4 – a less flexible top layer	<input checked="" type="checkbox"/>
H5 – having no interlayer	<input checked="" type="checkbox"/>
Lower threshold indentation is obtained by:	
H6 – a larger bulge	<input checked="" type="checkbox"/>
H7 – a wider groove	<input checked="" type="checkbox"/>
H8 – a lower bulge	<input checked="" type="checkbox"/>
H9 – a less flexible top layer	<input checked="" type="checkbox"/>
H10 – having no interlayer	<input checked="" type="checkbox"/>
More area growth is obtained by:	
H11 – a larger bulge	<input checked="" type="checkbox"/>
H12 – a wider groove	<input checked="" type="checkbox"/>
H13 – a lower bulge	<input checked="" type="checkbox"/>
H14 – a less flexible top layer	<input checked="" type="checkbox"/>
H15 – having an interlayer	<input checked="" type="checkbox"/>
More ΔH is obtained by:	
H16 – a smaller bulge	<input checked="" type="checkbox"/>
H17 – a smaller groove	<input checked="" type="checkbox"/>
H18 – a higher bulge	<input checked="" type="checkbox"/>
H19 – a less flexible top layer	<input checked="" type="checkbox"/>
H20 – having an interlayer	<input checked="" type="checkbox"/>

Taking our application into consideration led to the requisite of $\Delta H > 0.1$ to achieve a visually perceptible colour change. In addition it is imperative that the threshold pressure closely align with the required threshold pressure of 30mmHg. Subsequently, the sample should demonstrate a substantial growth percentage. Within our experiment, sample 7 emerges

as the sample that is most in compliance with these requirements.

In the context of the very small hue changes, a correlation has been observed in the diminished growth of colour changed area. This observation can likely be attributed to the initial state, which already encompasses a substantial number of pixels classifying as colour changed, which is therefore also the case in the threshold state. Consequently, the potential for growth is limited, and any change primarily happens in the brightness value due to increasing indentation causing a more vivid red colouring. This phenomenon is indeed substantiated by the data presented in [Table III](#).

7. Discussion

7.1. Main findings

7.1.1. Design

This exploratory design study resulted in a bio-inspired design of a pressure-activated flexible colour-changing sheet to be used as a Patient Training Education Tool (PTET) for individuals with lymphedema, and its first validations. The sheet changes colour upon applied pressure due to a low pigment concentration blue silicone sheet with bulges becoming almost transparent as a result of being indented. This transparency causes the red layer to become observable to the naked eye. The higher the applied pressure, the larger the transparent area, and therefore the larger the colour changed area. This is visualized in [Figure 26](#). It is seen that upon applied pressure the colour is changed next to the pressure applicator. The sheet exhibits a layered design, where each of the layers are responsible for a different function. The top layer's function is dividing the pressure over an area larger than the pressure applicator and making sure no large amounts of friction will be encountered when rubbing over the material. There is chosen for a flexible plastic layer (pvc0.20 or pp0.075) to achieve this. The primary function of the bottom layer is providing friction. The inherent property of silicone fulfils this function, facilitating friction when being subjected to lateral motion against a surface. The intermediate blue silicone layer is designed to attain transparency and conceal the underlying layer in unpressurized state. This optical effect is achieved through its structured composition, featuring heightened bulges and low pigment concentration. Beneath the blue layer may or may not be an interlayer attached, which could separate the blue silicone layer from the red layer. In summary, this study

introduces a sheet design that is able to change colour in response to applied pressure. Moreover, it provides supplementary insights into the impact of various variables, enabling the customization of the threshold force required for inducing a colour change, thereby accommodating diverse applications.

7.1.2. Performance

Within the design space of this colour-changing sheet, it has been empirically demonstrated that the threshold pressure, threshold indent, growth factor and ΔH can be effectively modified by adjusting the bulge area size, the groove's width, the height of the bulge, the flexibility of the top layer, or the inclusion of an intermediate layer between the blue and red. Note that the visibility of a colour change at higher forces often corresponds to a greater degree of indentation. In such cases, the silicone design may not necessarily entail increased resistance to compression; in fact, it can be more readily compressible, as could be evidenced by the trend of force versus indentation. However, a colour change becomes more apparent at a higher indentation. This phenomenon is exemplified when comparing samples featuring a highly flexible top layer to those with a less flexible top layer.

Some results contradict each other. For example, Sample 2 has a smaller growth in colour change, whereas Sample 7 has a larger growth, even though both of these are the sample with the smaller bulge compared to sample 1 and sample 8, respectively. This may be attributed to the wider groove and lower bulge height of sample 2, which result in a smaller growth, as has been validated in both sets. For sample 7, the opposite is true. Hence, it can be asserted that a variation in the value of one variable may exert a greater effect on a performance metric compared to another variable.

The requirement that stipulated a threshold pressure of 0.004N/mm^2 is, unfortunately, not attained. Sample 7, which emerged as the sample that performs the most optimal in compliance with the application requirements, has a threshold pressure of 0.04N/mm^2 . However, although a pressure threshold of 30 mmHg is mentioned in literature, research is missing on how this measurement is obtained and what the actual optimal pressure is per area of the arm. Such a unit of measurement is conventionally used as a unit for measuring blood pressure. These vascular structures are placed deeper beneath the skin. It is therefore important to be cautious when translating pressure values across different contexts. The application of force directly onto the external surface of the skin may

necessitate a considerably higher magnitude of force to effect a comparable pressure level.

Moreover, it is plausible that colour changes may occur at lower threshold forces than initially shown. This thought arises from the predefined threshold values for the S(0.466) and H(0.851), which must be met to classify as a region of changed colour. Consequently, instances of subtle colour changes at lower forces may go unnoticed. For instance, in the case of Sample 4 with a larger bulge size, a greater concentration of pigment exists along the vertical axis. This increased pigmentation causes the subtle colour changes that do happen to not be detected by the Matlab code in which the H- and S-values are defined.

Furthermore, hysteresis occurs during the experiments of the colour-changing sheet designs. This would complicate the process for the patient to accurately acquire the required force through the process of applying and releasing pressure. The hysteresis effect may result in a colour change even when an incorrect amount of pressure is applied. In cases where this hysteresis remains confined within the designated range of $30\text{-}60\text{mmHg}$, no significant issues should arise. It is plausible that hysteresis arises from the presence of air within the grooves, from the inertia of the silicone material or from the use of a very flexible top layer. It is found that the effect of hysteresis is greater when a more flexible top layer is used. This is probably due to the fact that the more flexible (almost soft) top layer conforms with the silicone, thus accommodating the silicone's inertia. When a stiffer top layer is employed, it surpasses the silicone's force of inertia more swiftly and returns to its original state more rapidly. Also, the presence of air may lead to an elevated force during compression, while the silicone's inertia, upon release, may delay the return to its initial position, thereby having a delayed effect on the measured force. To mitigate the hysteresis effect, one could opt for a firmer silicone material to reduce its inertia, or choose a less flexible top layer. This choice depends on whether one aims to raise or lower the threshold pressure, respectively.

Lastly, it is noteworthy from the force-indentation diagrams that no forces exceeding 20N are recorded. This observation is intriguing considering that, at the point where the sensor reaches approximately 20N , the total displacement of the pressure applicator has not yet transversed the full thickness of the sheet. For the lesser flexible top layers, the indentation at the point where it reaches approximately 20N is smaller. It is probable that, at this juncture, the pressure applicator imprinted the rigid plastic layer, marking its edges. As a result, the

resistance force of this layer is less pronounced, likely remaining around 20N because hypothetically at this force, this impression is fully realized, and there is no concave deformation of the plastic underneath the pressure applicator; instead, it presents a flat plastic layer. An alternative explanation may be that the sensor has limitations in measuring forces beyond 20N, notwithstanding the fact that, in this particular instance, the sensor was calibrated to measure forces up to 50N.

7.1.3. Evaluation hypotheses

Regarding the hypotheses 1 until 10, and hypotheses 16 until 20, all were accepted, except for the ones that showed contradictory results in the experiments of sample 1 until 6 versus the experiments of sample 7 until 12, and except for hypothesis 1 and 6. These latter two were rejected even both experiment sets validated the results. A larger bulge does increase the threshold pressure.

In hypotheses 11 to 15, three of them could not be substantiated due to contrasting results obtained from the two sets of experiments, each consisting of six samples. Hypothesis 12 posited that a wider groove would yield a larger coloured area growth. However, this was not observed, and consequently, this hypothesis has been refuted. One plausible explanation for the wider groove ultimately experiencing less coloured area growth than a narrower groove is that it has been established that a wider groove initially, and consequently in the case of the threshold force, contains more pixels that are integrated into the coloured area calculation. This is attributed to the fact that with a wider groove there is a larger area that contains less blue pigment vertically due to the broader grooves. Consequently, there is proportionally less room for growth when the design features a wider groove. Hypothesis 13 was also rejected. A similar explanation could be given to the fact that a larger bulge size experiences a larger area growth, i.e. there is less room for growth in the case of lower bulges due to a higher initial coloured area.

7.2. Limitations

In this study, a pressure-activated colour change is accompanied by a change in hue, saturation, brightness value, and thereby the magnitude of the area of colour change. By configuring the H-value and S-value to certain threshold values, some (subtle) colour changes are not included in the calculation of the area of colour change, and may therefore stay unnoticed in the lower force ranges. This study is limited to showing the size

of area of the colour that exceeds an H-value of 0.851 and an S-value of 0.466, relative to the applied force.

Furthermore, it should be acknowledged that this study exclusively examines vertically applied forces, a limitation that potentially compromises the applicability of this sheet as PTET. During MLD-massage, not only normal forces, but also shear forces are applied, with the therapist's hand concurrently imparting both compression and lateral motion to the skin. In instances where lower forces are applied to the colour-changing sheet, it is conceivable that colour-change occur within the confines of the pressure applicator's surface. However, when shear forces are also applied within a sliding motion, there exists the prospect that the colour change may become perceptible to the naked eye, provided that the recovery time for such changes is of sufficient duration to encompass the motion of the force-application area.

Another limitation of this study is the limited scope of values assigned to the variables for examination. Consequently, the present analysis shows only the identification whether a variable exerts an effect on the threshold force for colour change and the extent to which colour changes occur. However, the precise origin of this influence, such as whether it follows a linear relationship or another type of relation, remains beyond the scope of this research.

A design's thickness may exhibit slight variations, on the order of a few hundredths of a millimetre, due to the manual pouring of silicone into moulds of specific heights. The viscosity of the silicone can result in one mould being convex while another is concave, even though there was paid attention towards filling these boxes evenly. Additionally, the silicone curing process may introduce further discrepancies. This disparity in thickness can necessitate a slight adjustment of the zero position of the pressure applicator as for the precision of the measurements the procedure had to start at a half-millimetre interval, leading to a potential variance of 0.1N in the measured zero force. Within the scope of this study, such deviations do not significantly impact the results. However, it is imperative to consider these factors in future research.

7.3. Design recommendations

The current design exhibits a thickness range spanning from 4.975mm to 5.55mm, depending on the specific bulge height and the presence of an interlayer. It is advisable to explore opportunities for reducing the overall thickness of the design, such that the

transmission of force onto the skin is almost 1:1, or easier to predict. The blue silicone layer is 2.5mm (exclusive the height of the bulges). One option for reducing the overall thickness could be diminishing the thickness of this specific layer, but increasing the pigment concentration to obviate translucency issues causing the red silicone layer to become visible. These translucency issues could also be adjusted by increasing the height of the bulges a bit. One should optimize these variables against each other to obtain an as thin as possible sheet. Also the red silicone layer, which is now 2mm, could be shortened in height. When the overall thickness is taken into consideration, the logical step would be to choose PP0.075 as top layer. However, it is essential to mention that PP0.075 only works from a specific indentation size on. Paradoxically, up to a certain indent, increasing the indent resulted a reduction in the size of the colour changed area. Therefore, it is recommended to opt for PVC0.20, as it offers greater potential in reducing the overall thickness as the silicone layers' height can be greatly reduced.

Upon understanding variable influences on threshold force and establishing correlations, a modular design can facilitate the need for different threshold pressures at different locations due to varying skin thicknesses. During the MLD massage, the arm or leg will not have to be pressed equally hard on each spot, as the skin thickness changes over the length of the limb. Once this skin thickness, and even more so the depth of the lymph nodes within the skin, has been visualized, a modular design could be offered to the patient. The threshold force for colour change varies at different locations on the colour-changing sheet.

Finally, it is recommended to increase the friction of the silicone red layer by designing a relief that enhances this performance.

7.4. Experimental recommendations

Primarily, it is recommended to conduct separate experiments for each variable to accurately assess the impact of this variable on its relationship with the performance measurements. This is crucial for achieving the ultimate objective, which is the development of a procedural framework that must be followed in the design to attain a specific threshold pressure for colour change. Subsequently, modular designs could be created.

Furthermore, it is advisable to employ an automated vertical stage in all future experiments due to the

potential human errors that can arise during this process. The use of automation enables precise measurement of the indentation depth and the duration of this indentation. If the camera is integrated into this system, there will be no need to align the force data with the video, simplifying the data processing significantly. Multiple codes could be written for the movement of this translation stage versus the time. A rapid removal of the pressure applicator block could be achieved, which could eventually also assess the recovery time of the colour change.

Given the application, it is important that an experiment is performed that simulates the MLD massage onto a limb. Normal- and shear-forces on the colour-changing sheet should be applied, while having a softer base on which the sheet is placed. The experiment was carried out with a PLA pressure applicator. It is advisable to use a silicone pressure applicator in a new experiment to imitate the softness of the hand.

During the experiments of this study, one light source was used in a dark room. Although this setup ensures that the measured colour change is not due to variations in light quantity, this bright light also caused the initial colour to lean more towards red in some samples given the almost transparency of the top layer. In daylight the initial colour is perceived as more bluish compared to the recorded videos. That is why it is recommended to conduct another experiment in a room with constant light, but which more closely imitates daylight.

In addition, it is recommended to gain insight into the durability of the design. A sample should therefore undergo multiple pressure increasing and reducing cycles to be able to say something about this.

Finally, it would be interesting to consider inverting the sample and placing it on a transparent surface, while positioning the camera beneath this surface to analyse colour changes beneath the pressure surface, that are not visible within the current setup. This could also be achieved by employing a transparent pressure applicator. Such an approach may find relevance not only in the context of the PTET but also in various other fields.

7.5. Application fields

Within this study, the focus group comprises lymphedema patients. In the future, this product should also be applicable for therapists to practice strength exercises, or for the general public to safely

perform massages at home while indicating, for instance, when deep tissue is massaged or the superficial muscles. Within the medical field, such a sheet could also provide feedback on the pressure onto the limb when wearing a prosthesis, ensuring the prosthesis is appropriately calibrated. Outside the medical field, for example in the automotive industry, these colour-changing sheet could be integrated into car seat or steering wheels to provide feedback on posture and comfort. The pressure-sensitive colour-changing sheet can also act as a sensor in infrastructure, such as bridges and buildings, to detect structural stress or the load distribution. Another common area for these type of sensors is the robotic industry to mimic skin or to indicated the amount of force applied by a robotic gripper. Beyond these domains, one could contemplate using the colour-changing sheet in the field of artistic designs or in toys. The sheet is interactive, and could act as an element of surprise or be integrated into a design.

8. Conclusion

This study introduced the design and first validations of a bio-inspired flexible colour-changing sheet to be used as a Patient Training Education Tool (PTET) for individuals with lymphedema. Next to this, the study provided information about the impact of the design variables on the threshold force and threshold indent required to attain a colour change characterized by a minimal H-value of 0.851 and an S-value of 0.466, and by an increase in area by 15mm² or a multiplication of 5. The PTET has a layered design and exhibits a thickness range spanning from 4.975mm to 5.55mm. The bottom layer, composed of red silicone, contributes to establishing friction between itself and the underlying surface, facilitating stable placement. Situated above this, the middle layer, comprised of blue silicone, fulfils the main function of colour change. This change occurs through the layer's transition to transparency upon indentation, thereby revealing the layer beneath, while concurrently concealing it in the absence of pressure due to the presence of bulges. Optionally, an interlayer of LDPE0.05 may be introduced between the bottom and middle layer. The top layer not only facilitates smooth sliding movement without slippage but also serves to diffuse the applied pressure across a broader area than the initial point of contact. This diffusion ensures the colour change is visible to the naked eye. The minimum threshold pressure for a slightly visible colour change within this study is 2.0694*10⁻² N/mm², achieved by Sample 2. Within our experiment, sample 7 emerges as the sample

that is most in compliance with the stated requirements for the PTET. The threshold force for this sample is 4.1437*10⁻² N/mm² and the final colour change after 3mm indentation is defined by ΔH of 0.1350.

The envisioned prototype in this study of the colour changing sheet serves as a base platform, paving the way for subsequent experiments and the potential development of a structured framework. This framework would encompass the necessary steps for designing a colour-changing sheet with a predefined pressure threshold and, ultimately, the creation of a modular, pressure-activated, colour-changing flexible sheet.

Appendix

A. Prior experiments

In the final experiment, an S-beam pressure sensor was used to measure the pressure exerted on the colour-changing sheet. Initially, the intention was to concurrently determine the pressure distribution underneath the sheet in order to gain insights into the pressure transmission through this material. The idea was to use FSR sensors for this purpose. However, it was found that these sensors were not sufficiently accurate in measuring the pressure distribution. It became evident that pressure distribution sensors often were inaccurate or were quite expensive. An additional application of the ultimate colour-changing design, and as alternative to the expensive pressure distribution sensors, is its potential use as a pressure sensor to visually show pressure distribution. Moreover, the earlier experiments did not involve components from Thorlabs; instead, a different configuration was utilized, which did not perform optimally. Hence, an alternative setup for the experiment was eventually adopted.

A.1. Use of FSR's

At first instance, there was known that force sensitive resistors (FSRs) are not that accurate. Therefore a method explained by Hrisko [60] has been applied to strive for a consistent and most accurate estimation of the pressure on the FSR. If the FSR were to achieve any degree of accuracy through this method, it could potentially be employed for ascertaining the force distribution between the sheet and the underlying surface using multiple FSRs placed next to each other. This would be of significant value as it would enable the determination of the final pressure exerted on the skin.

We used the RP-S40-ST, which is a thin film FSR of 40x40mm², see [Figure 28](#). There is made use of an Arduino board to read the analog signals which are outputted by the FSR in a voltage divider configuration. Eventually, the force that is applied to the FSR can be estimated using the calibration curve of this sensor. However, we will execute an additional calibration check, which let us compare both graphs and state conclusions about the sensor's behaviour; whether or not it behaves as expected or not, and whether or not modifications are necessary based on drift or hysteresis. Given in the datasheet of the RP-S40-ST, the relationship between mass and resistance is given in [Equation 16](#).



Figure 28. RP-S40-ST

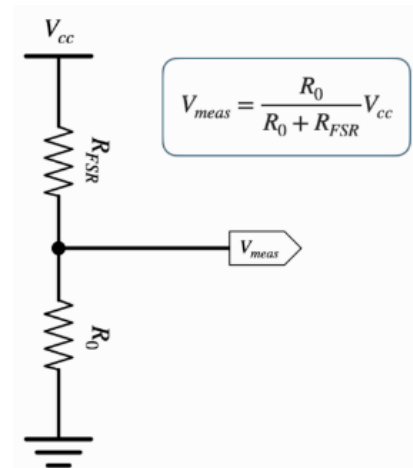


Figure 29. Voltage divider circuit

$$R_{FSR} = 271m_i^{-0.69} \quad (16)$$

- R_{FSR} → the resistance of the FSR
- m_i → the mass applied onto the FSR

To measure the resistance ourselves, we have to wire the FSR in series with a resistor of a known value. Measuring the voltage drop, helps us approximating the resistance of the FSR. The voltage divider circuit is seen in [Figure 29](#). To find V_{meas} theoretically, the following steps are taken:

(1) The equation of the total circuit:

$$R_{total} = \frac{V_{cc}}{I_{total}} \quad (17)$$

(2) I_{total} is equal to I_0 as the current is the same everywhere, as every component within the circuit is in series. The voltage over R_0 is V_{meas} , because this voltage is left after going through the FSR resistor. Therefore:

$$I_{total} = I_0 = \frac{V_{meas}}{R_0} \quad (18)$$

(3) The total resistance of the circuit is the summation of FSR and R_0 , which leaves the following equation:

$$R_{FSR} + R_0 = \frac{V_{cc}}{\frac{V_{meas}}{R_0}} = V_{cc} * \frac{R_0}{V_{meas}} \quad (19)$$

$$V_{meas} = \frac{R_0}{R_0 + R_{FSR}} V_{cc} \quad (20)$$

$$\text{and } R_{FSR} = R_0 \left(\frac{V_{cc}}{V_{meas}} - 1 \right) \quad (21)$$

Here:

- R_{FSR} is the variable resistance, i.e. the sensor
- R_0 is the selected resistor of which the value is known
- V_{cc} is the supply voltage
- V_{meas} is the measured voltage by the analog to digital (ADC) converter of the Arduino

From the mass calibration equation of the graph, we have:

$$m_i = \left(\frac{271.0}{R_{FSR}} \right)^{\frac{1}{0.69}} \quad (22)$$

Filling in this equation with prior found equation for R_{FSR} :

$$m_i = \left(\frac{271.0}{R_0 \left(\frac{V_{cc}}{V_{meas}} - 1 \right)} \right)^{\frac{1}{0.69}} \quad (23)$$

When there is solved for the measured voltage (V_{meas}):

$$m_i^{0.69} = \frac{271.0}{R_0 \left(\frac{V_{cc}}{V_{meas}} - 1 \right)} \quad (24)$$

$$\frac{V_{cc}}{V_{meas}} = \frac{271.0}{m_i^{0.69} * R_0} + 1 \quad (25)$$

$$V_{meas} = \frac{V_{cc}}{\frac{271.0}{m_i^{0.69} * R_0} + 1} = \frac{V_{cc}}{\frac{271.0 * m_i^{-0.69}}{R_0} + 1} * \left(\frac{R_0}{R_0} \right) \quad (26)$$

$$V_{meas} = V_{cc} * \frac{R_0}{271.0 * m_i^{-0.69} + R_0} \quad (27)$$

Plotting voltage as a function of both measured FSR resistance and applied mass, where R_0 is 1 k Ω , and V_{cc} is 5.0V, results in [Figure 30](#).

The RP-S40-ST will thus be wired to an Arduino board in a voltage divider configuration with a 1 kΩ resistor.

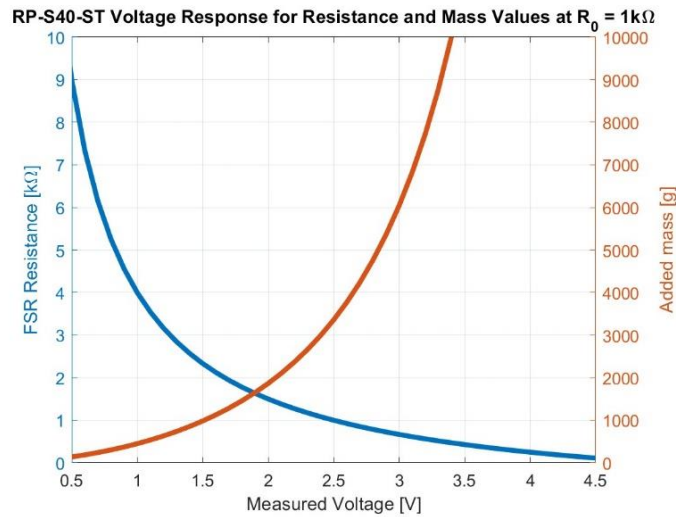


Figure 30. Voltage response

From this plot can be deduced the relations between the measured voltage with the FSR resistance and added mass. The internal resistance of the FSR decreases while applying more mass onto the sensor and therefore the measured voltage increases because much more voltage will pass by this sensor now.

The known resistor can be selected based on the pressure range of interest. The desired sensitivity and used sensor will determine the output range, which can be changed by the known resistor. In [Figure 31](#) the known resistance values are plotted as a function of voltage over a range of mass values.

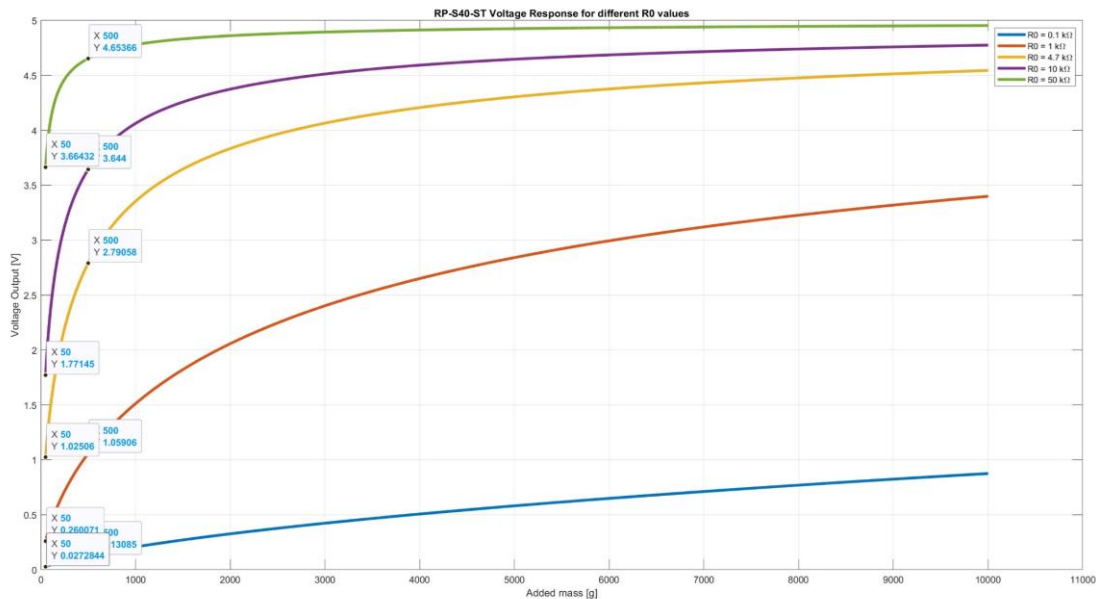


Figure 31. Voltage response for different R0 values

From this plot it can be concluded that if this sensor is applied using higher forces, a better sensitivity is required by choosing a lower known resistance value. The opposite is also true. Measuring forces in the range from approximately 0-500g applied mass, one should to use a 10kΩ known resistor. In [Table V](#) are the rates within this range indicated.

TABLE V. Growth rates within 50-500g range

Known resistance value:	Rate in 50-500g range
50 k Ω	0.0022
10 k Ω	0.0042
4.7 k Ω	0.0039
1 k Ω	0.0018
0.1 k Ω	0.0002

The Matlab code that is used to extract these images is copied below:

```

close all
clear all
clc

V_meas = [0: 0.1: 5];

R_0 = 1;
V_cc = 5;

R_FSR = R_0*((V_cc./V_meas)-1);

m = (271./(R_0*((V_cc./V_meas)-1))).^(1/0.69);

figure
yyaxis left
plot(V_meas, R_FSR, 'LineWidth', 3);
ylim([0 10]);
xlabel('Measured Voltage [V]');
xlim([0.5 4.5])
ylabel('FSR Resistance [k\Omega]');
title('RP-S40-ST Voltage Response for Resistance and Mass Values at R_0 = 1k\Omega');
grid on

yyaxis right
plot(V_meas, m, 'LineWidth', 3);
ylim([0 10000])
ylabel('Added mass [g]');

%%

R_01 = 0.1;
R_02 = 1;
R_03 = 4.7;
R_04 = 10;
R_05 = 50;

mi = 50: 1: 10000;

V_meas1 = (R_01./(R_01+(271*(mi.^(-0.69))))) * V_cc;
V_meas2 = (R_02./(R_02+(271*(mi.^(-0.69))))) * V_cc;
V_meas3 = (R_03./(R_03+(271*(mi.^(-0.69))))) * V_cc;
V_meas4 = (R_04./(R_04+(271*(mi.^(-0.69))))) * V_cc;
V_meas5 = (R_05./(R_05+(271*(mi.^(-0.69))))) * V_cc;

figure
plot(mi, V_meas1, mi, V_meas2, mi, V_meas3, mi, V_meas4, mi, V_meas5, 'LineWidth', 3);
xlabel('Added mass [g]');
ylabel('Voltage Output [V]');
legend('R0 = 0.1 k\Omega', 'R0 = 1 k\Omega', 'R0 = 4.7 k\Omega', 'R0 = 10 k\Omega', 'R0 = 50 k\Omega');
xlim([0 11000]);

```

```
ylim([0 5]);
title('RP-S40-ST Voltage Response for different R0 values');
grid on
```

Eventually, the decision was made not to use FSRs because, despite employing this method, in reality the force measurements remained imprecise. For instance, FSRs show a greater sensitivity at the centre of their surface compared to the edges. Next to this, some presented a higher sensitivity than others, and also the same sensor's sensitivity deviated per use. Furthermore, while they can indicate whether a force is small or large, achieving a truly precise measurement remains unattainable. Therefore, the focus shifted towards achieving the thinnest possible design to ensure that the force transmission onto the skin approximated a 1:1 ratio.

A.2. Experimental trial

A.2.1. Design

The first set up had a similar maximum-minimum approach for the values assigned to variables. However, more variables were chosen to execute these experiments with. See [Table VI](#).

TABLE VI. Variables and their values prior experiment

Variable Test	Bulge size	Groove size	Bulge height	Upper layer	Pigment	Plastic interlayer	Transparent silicone toplayer
1	5mm	2mm	0.4mm	PVC0.30	1 drip	No	No
2	1mm	2mm	0.4mm	PVC0.30	1 drip	No	No
3	5mm	0.4mm	0.4mm	PVC0.30	1 drip	No	No
4	5mm	2mm	1.2mm	PVC0.30	1 drip	No	No
5	5mm	2mm	0.4mm	PVC0.20	1 drip	No	No
6	5mm	2mm	0.4mm	PVC0.30	3 drips	No	No
8	5mm	2mm	0.4mm	PVC0.30	1 drip	Yes	No
9	5mm	2mm	0.4mm	PVC0.30	1 drip	No	Yes
10	1mm	0.4mm	1.2mm	PVC0.20	3 drips	Yes	Yes
11	5mm	0.4mm	1.2mm	PVC0.20	3 drips	Yes	Yes
12	1mm	2mm	1.2mm	PVC0.20	3 drips	Yes	Yes
13	1mm	0.4mm	0.4mm	PVC0.20	3 drips	Yes	Yes
14	1mm	0.4mm	1.2mm	PVC0.30	3 drips	Yes	Yes
15	1mm	0.4mm	1.2mm	PVC0.20	1 drip	Yes	Yes
17	1mm	0.4mm	1.2mm	PVC0.20	3 drips	No	Yes
18	1mm	0.4mm	1.2mm	PVC0.20	3 drips	Yes	No

The experimental setup is shown in [Figure 32](#). A tripod with affixed a translation stage, is strategically positioned adjacent to the platform whereon the sample is placed. The lightbox is situated to the left of the sample. The threading, in conjunction with the pressure sensor and pressure block, remains consistent with the one used in the final experiment. Furthermore, data acquisition procedures remain unchanged, with Labview as software platform. [Figure 33](#) and [34](#) illustrate the specific construction method used for attaching the threaded rod to the translation stage using an L-bracket. Notable, the entire construction is set up in a day light free room to eliminate any potential impact of ambient light on the colour outcomes.

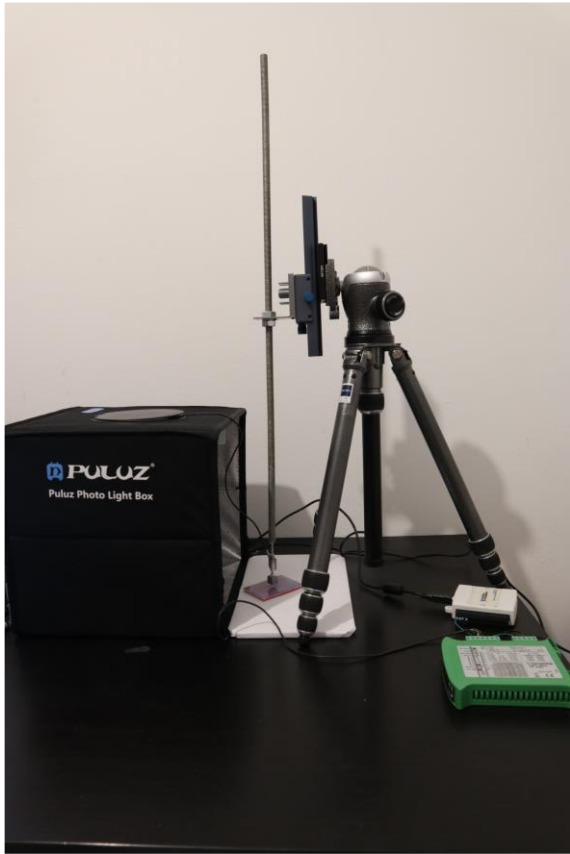


Figure 32. Initial experimental setup



Figure 33. Zoom in picture of threaded rod to translation stage

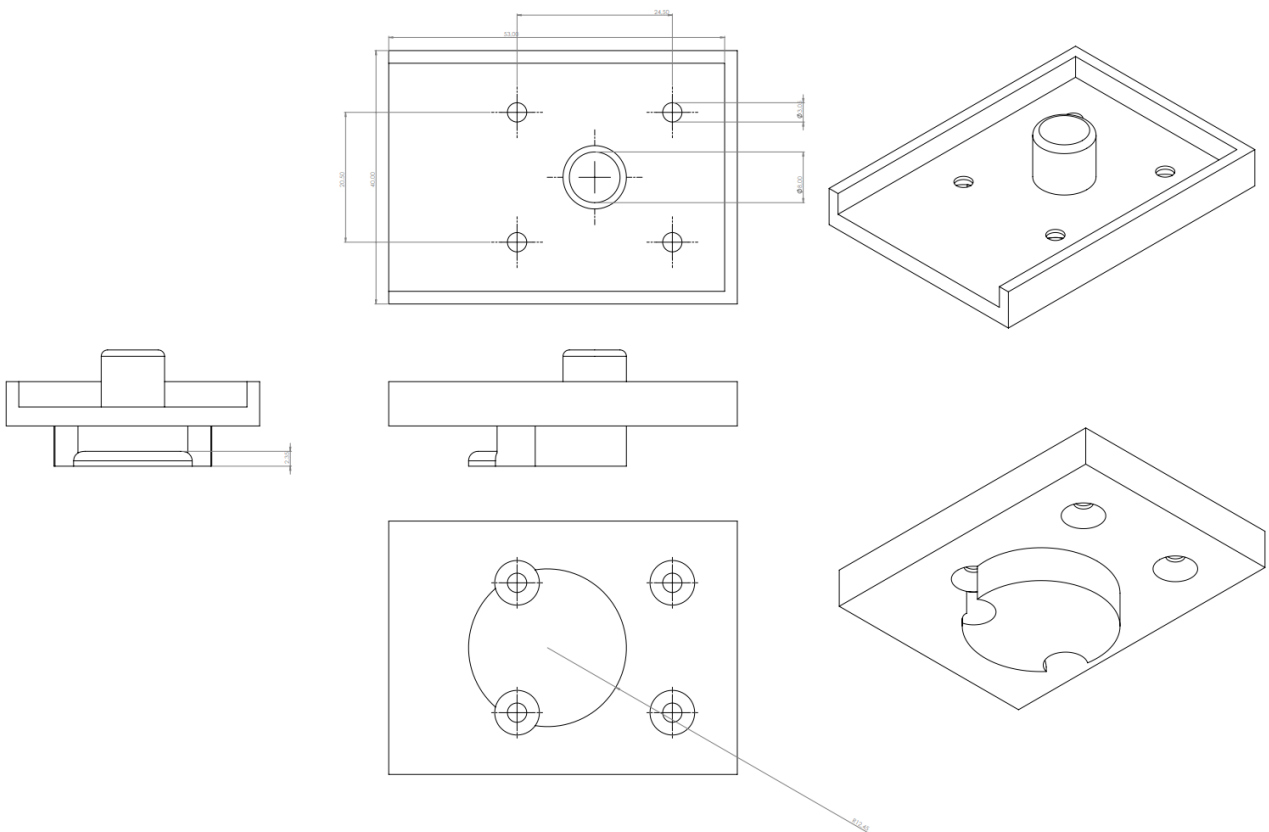


Figure 34. SW drawings of the 3D printed part that is designed to attach the threaded rod to the translation stage

Due to the inherent imbalance that arises when exerting force on the platform via the use of the pressure applicator, there is a risk that one of the legs of the tripod detaches from the table. Therefore the tripod is secured using a wire tightly fastened around the table upon which the tripod is standing. Three other wires are used and secured to each of the legs to eventually come together directly beneath the central point of the tripod, and there suspending a mass of approximately 11kg. See [Figure 35](#).

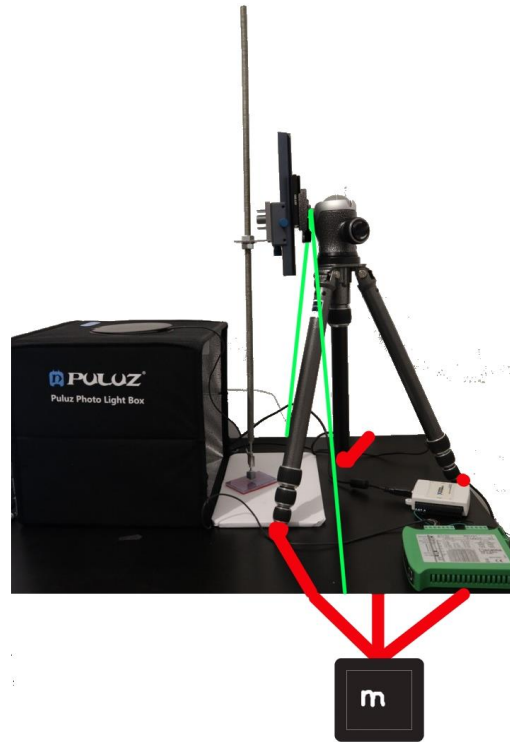


Figure 35. Adapted experimental setup. Masses and strings were placed to prevent motion in the legs of the tripod during pressure application onto a sheet with the pressure block.

The experimental procedure was structured differently, and was as follows:

1. Position the sample # in such a way that the pressure applicator precisely falls within the marked square on top of the PVC layer.
2. Perform a “00” measurement while the block is suspended in the air. Save this data in Labview as “Test # - 00”.
3. Subsequently, lower the stage until the block just makes contact with the surface. This serves as the official zero measurement, saved in Labview as “Test # - 0”.
4. Capture a photo of this moment from a fixed position of the top view of the sheet, and record the associated image number.
5. In Labview, set the data recording to active and lower the stage by 1mm. Allow data recording to continue until the force stabilizes, then stop the data recording after approximately 60 seconds. Save this data in Labview as “Test # - 1”.
6. While the data is being recorded, take a photo of this moment from a fixed position of the top view of the sheet and write down the image number from the camera on a paper.
7. Enable data recording in Labview and lower the stage another 1mm. Record data until the force stabilizes, then halt the data recording after approximately 60 seconds. Save this data in Labview as “Test # - 2”.
8. While the data is running, capture a photo of this moment from a fixed position of the top view of the sheet and document the image.
9. Enable data recording in Labview and lower the stage another 1mm. Record data until the force stabilizes after approximately 60 seconds, then stop the data recording. Save this data in Labview as “Test # - 3”.

10. While the data is being recorded, take a photo of this moment from a fixed position of the top view of the sheet and make a note of the image number.
11. Hereafter, enable Labview data recording again, switch the camera to video mode and start filming from a fixed position of the top view of the sheet and release the pressure block in small incremental steps until the block is removed from the sheet. Note the video number from the camera. Save the Labview data as "Test # - video".
12. Create a directory on the computer labeled "Test #" within the Experiment directory and neatly transfer the data to this location. Ensure that duplicates are saved on a hard drive.
13. Remove the sample from its position.
14. Repeat all steps for each sample.

A.2.2. Improvement points

During the execution of these initial experiments, several areas for improvement emerged for subsequent experiments. Firstly, it is imperative to ensure that the force application system remains stable and is not destabilized by the application of force. Additionally, a camera translation stage was utilized to achieve a 1mm vertical displacement in each trial, with this stage being accurate to within 1mm. However, it proved challenging to discern this precision with the naked eye and manual adjustments. Consequently, more precise measurement equipment will be necessary in the new setup. In these experiments, the sample was assembled layer by layer for each trial without adhesive bonding. However, this approach proved problematic for a PP0.075 top layer, as it tended to curl around the pressure applicator during force application, obstructing the observation of colour changes in the captured photographs. As a result, PVC0.20, a more flexible layer similar to PVC0.30, but with not that much difference, was employed in these experiments to address this issue. Moving forward, prototype samples will need to be constructed by affixing the layers with silicone adhesive, enabling the evaluation of both the colour-changing effect and the pressures exerted on samples with a PP0.075 top layer.

Furthermore, it was crucial during the experiment's preparation to ensure that the pressure applicator precisely aligned with the marked block on the plastic top layer. Achieving this alignment necessitated adjustments to the tripod or the sample, which, in turn, led to changes in the camera's field of view. In the new experimental setup, it is essential to position the sample on a marked piece of paper, which is securely situated within the system, to maintain consistency. The overall setup should be designed for stability, preventing the displacement of individual components.

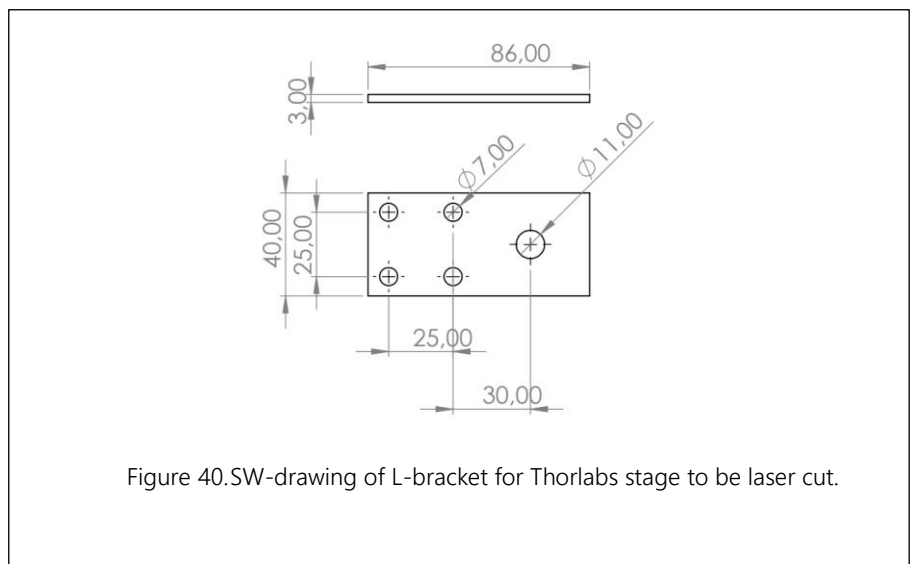
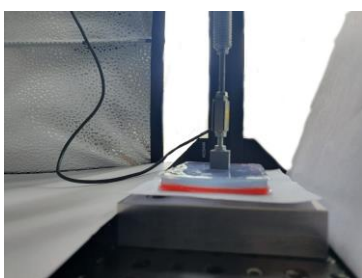
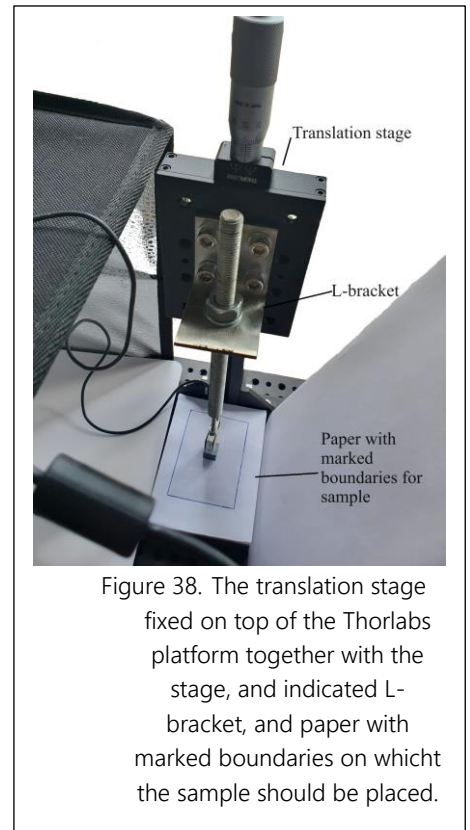
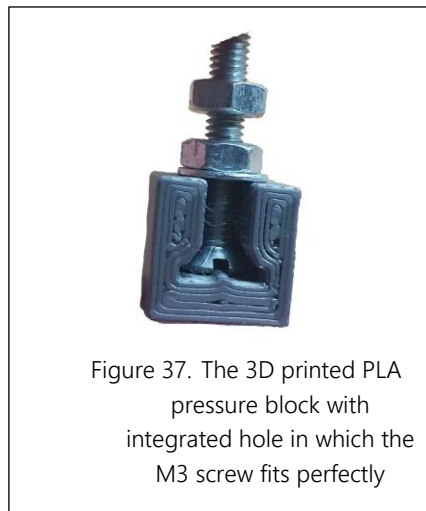
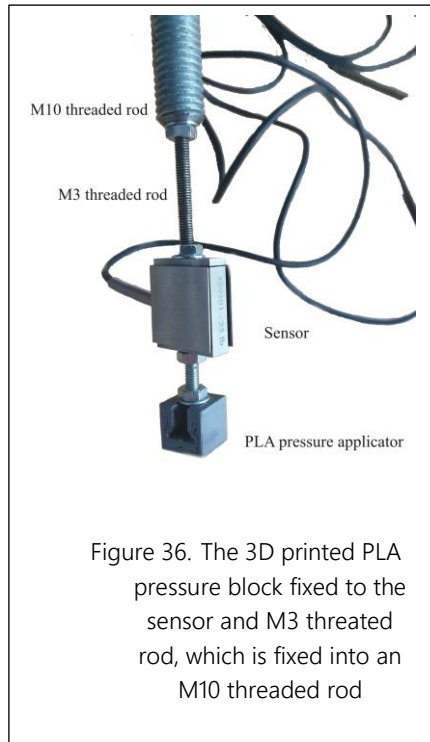
Lastly, it was evident during data processing that only the force measurements obtained during the video recordings, in conjunction with the video footage, yielded valuable insights. More meaningful conclusions could be drawn from this short video regarding the relationship between pressure and colour change, compared to the data obtained from photographs and single one-minute force measurements. Consequently, the future experiment will focus on video recording. In this context, it will be essential to provide information about the indentation and make this information evident in the force data (by waiting for 3 seconds at each incremental step) and the video data (by vocally acknowledging the indentation and physically applying a wooden spatula against the pressure applicator within the frame).

B. Final experiment construction parts

The variables and the experimental setup are outlined in the report. The setup incorporates all the improvements identified during the initial experiments: the entire structure applies force to itself, ensuring stability and preventing imbalance. The layers of the samples are securely affixed together, allowing for testing of the PP0.075 effect. Indentation is accomplished by rotating a Thorlabs translation stage with an accuracy of 0.01mm. A system has been implemented to apply force to the sample at a consistent location, eliminating unnecessary complexity by placing the sample within a marked area on a paper that has a fixed position within the construction. Continuous force measurement is performed without interruption, and during this a video recording is made.

The construction could mostly be assembled using components from Thorlabs. Nevertheless, certain parts necessitated a design process followed by self-fabrication through 3D printing or laser cutting. The L-bracket was custom-designed, laser-cut, and subsequently bent at a 90-degree angle, as the hole spacing did not align with a

European standard L-bracket. Additionally, the pressure applicator was 3D printed to accommodate an M3 screw precisely. Utilizing an M3 bolt allowed for secure fastening. The M3 screw could be rotated within the pressure sensor. On the opposite end, an M3 thread was also inserted, which was subsequently affixed to an M10 threaded rod. This choice was made to eliminate the risk of bending, which might occur with a longer M3 thread. The utilization of an M10 thread ensured the structural integrity. Diagrams illustrating the design of the pressure applicator, the construction between pressure applicator, sensor, and the M3 and M10 threaded rods, the L-bracket and a front view of this system with a sample placed on top of the fixed stage can be found in [Figures 36 until 40](#).





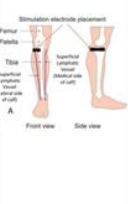





C. Robotic garments

Suarez et al. [15] came up with a prototype of a pneumatic fabric-polymer actuator that is able to exert compression and a lateral force on the human arm by inflating a pre-shaped fabric element. Yoo et al. [6] developed an origami-inspired soft fabric pneumatic actuator that does not only apply a normal force onto the body but also a shear force to replicate the MLD even more. Guan et al. [13] developed a pneumatic soft actuator unit that was able to adapt various design parameters and apply a pressure onto the lower limb to find out which parameters are desired. Rosalia et al. [14] designed a three-layered soft robotic sleeve, which has an expandable component that is made of interconnected pockets of different heights that will create a graduated compression profile when being inflated. Gao et al. [5] developed a proof of concept design of a novel air microfluidics-enabled soft robotic sleeve that is able to execute gradient pressure, but makes the sleeve more wearable by using a very light, and small microfluidic chip. Pawar et al. [2] also focuses more on the portability of the device, and created a design for the lymphatic drainage robot, that is able to climb up to the human limb, while at the same time applying a radial pressure. Pamplin et al. [9] discussed that non-pneumatic compression devices that make use of shape memory actuators is a viable and mobile solution for patients at home.

Further research to alleviate or prevent the symptoms of lymphedema, has been done in electrical stimulation. For example, Wei et al. [61] designed clothing where electrodes and conductive interconnections were integrated to activate lymph nodes. Next to this, research has also been done into pharmacological approaches, and invasive surgical treatments, whereby new imaging techniques to visualize the lymph system is of importance [10, 62].

TABLE VII. Summarizing the robotic sleeves' working principle and pros and cons acquired from literature research

Device:	Professional hands of therapist	Pneumatic fabric-polymer actuator	Air microfluidics-enabled soft robotic sleeve	Wearable compression with shape memory actuators	Wearable electrical stimulation	Lymphatic drainage robot	Origami-inspired soft fabric pneumatic actuators	LymphaTouch
Design by:	Training and practice over the years	Suarez et al. (2018)	Gao et al. (2022)	Pamplin et al. (2022)	Wei et al. (2019)	Pawar et al. (2022)	Yoo et al. (2019)	Kimball (2018)
Working principle:	Rhythmic pressure from distal to proximal to transport the residues of lymph in the interstitial spaces to normal healthy lymphatics and lymph node basins.	The design for the actuator consist out of two mechanical elements: a fabric one, and a hyperelastic polymer, which is connected to the fabric element. The fabric element is longer and has a curved shape. When air is pumped in the fabric element, it bends towards this curved shape, and vice versa. A compression and lateral force is the result.	This device makes use of an innovative, very small, microfluidic chip, which increases the wearability. Each chip has 16 fluidic channels that are able to enable sequential inflation and uniform deflation to 8 air bladders. Such gradient compression is controlled by the fundamentals of microfluidics: air follows the path of least resistance.	Here the opportunity is shown of a shape memory alloy (nitinol) in a novel non-pneumatic compression device. Nitinol is woven through a flexible plastic frame (Flexframe) that transfers the compressive forces onto the limb.	A fabric based wearable electrical stimulation device that consists of electrodes and conductive interconnections. It is able to execute functional electrical stimulation (FES) that stimulates the venous flow, but is also a feasible option for lymphedema.	The lymphatic drainage robot (LDR) climbs up the human limb, while applying radial pressure on the skin. It makes hereby use of only one pneumatic actuator. The roller mechanism also executes a squeezing effect to the skin as the rollers have a concave shape and a spring force.	This device is a soft wearable robot that involves a soft actuators that create besides a normal force, also a shear force. The shear is created by unfolding the Z-shaped fold-lines when the actuator gets inflated.	The LymphaTouch uses negative pressure and high-frequency vibrations to simulate the effect of MLD. The negative pressure will cause the tissue to be pulled up which increases lymph movement and filament movement. A result can be that the endothelial cells open and lymph will be absorbed.
Pros and cons:	<p>Pros</p> <ul style="list-style-type: none"> Performs MLD perfectly Patient is ensured of a good treatment <p>Cons</p> <ul style="list-style-type: none"> Workload on practitioners Patient has to travel a lot from and to the clinic (a lot of dependency) 	<p>Pros</p> <ul style="list-style-type: none"> Robust Lightweight Able to be washed, because it consists only out of soft materials <p>Cons</p> <ul style="list-style-type: none"> This is only a proof-of-concept, and not on the market yet The measured bending force was about 0.35 N, which is too low. Furthermore the pressure are hard to control. 	<p>Pros</p> <ul style="list-style-type: none"> Low cost Simple Scalable Lighter than other wearables <p>Cons</p> <ul style="list-style-type: none"> Pneumatic actuated, thus must be used in combination with an air pump Not on the market Doesn't perform the MLD perfectly 	<p>Pros</p> <ul style="list-style-type: none"> FDA-cleared Non-pneumatic (silent) Minimizes and avoid undesired fluid backflow (through gradient pressure) <p>Cons</p> <ul style="list-style-type: none"> Prescription-only Large in size Open electrical elements (such as wires between the two components) Electrode size 	<p>Pros</p> <ul style="list-style-type: none"> Lightweight Highly flexible Breathable Conformable <p>Cons</p> <ul style="list-style-type: none"> Electrical elements Not yet on the market 	<p>Pros</p> <ul style="list-style-type: none"> Somewhat portable Makes use of only a single pneumatic actuator <p>Cons</p> <ul style="list-style-type: none"> Dependent on electricity Consist of hard robotic hardware Pneumatic Hard to use, as most limbs are non-uniform. This machine seems to work only on non-uniform limbs. 	<p>Pros</p> <ul style="list-style-type: none"> A normal force is combined with a shear force, which is essential in the performance of MLD <p>Cons</p> <ul style="list-style-type: none"> The prototype only consist of a single Z-folded actuator, which isn't probably long enough for the limb Bulky 	<p>Pros</p> <ul style="list-style-type: none"> Pain reduction Can increase movement of fluid Edema decrease Reduced inflammation <p>Cons</p> <ul style="list-style-type: none"> Has to be combined with MLD as MLD does calms down the nervous system, which helps in the treatment Hard to compare to MLD Can only be performed in clinical setting Patients with sensitive skin or the ones that take blood thinners may have "cupping" effect
Appearance:								

Current pressure compression devices (PCDs) make a lot of noise due to the pressurized air and are bulky [9]. And most even fail to execute an effective MLD massage as these systems do not prevent the lymph from flowing back from proximal to distal regions as the shear force is not precise enough during the intermittent compression cycles [15]. Ricci et al. [53] describe that the more pneumatic bags forming the sleeve, the higher the decongestive effect is. Thereby, they say that such a compressor sleeve should also be used next to the MLD. The effective PCDs that do exist are rarely wearable. There is a problematic trade-off between the wearability of the device and its performance [5]. The Z-fold actuator, as described by Yoo et al. [6] does for example apply a normal and shear force that mimic the MLD very well. However, this prototype is still very bulky, and thereby such a device is unable to massage the entire length of the limb. It may work if it isn't a single z-fold actuator, but the sleeve becomes even more bulky, and not even comfortable wearing. Additionally, an obstacle in the design of a robotic sleeve is the non-uniformity of the limb diameter. Such a garment can fit very tightly. Thereby, these garments are susceptible to bacterial growth and should be washed often to prevent skin infections and even worse [2]. See [Table VII](#) for a summary of the robotic sleeves' working principle and pros and cons of these systems.

A device that ensures patients can perform self-MLD, in the most efficient way and with the least adverse effects, will be helpful in alleviating the healthcare system, and in the freedom and health of lymphedema patients. The therapy costs and the bulkiness of devices during the rehabilitation process of patients, opens up many opportunities for a portable, light-weight, self-care, device for at-home use [2].

D. State of the art flexible optical pressure sensors

In this appendix an elaboration is given on the design structures of flexible optical pressure sensors. It is presented that the materials that are used often require extensive knowledge, which makes these products expensive and automatically harder to fabricate.

Photonic crystals are structures that exist out of subwavelength grids from two types of material with different refractive indices, and are periodically arranged as a 1D-, 2D-, or 3D-structure. The colour of a material consisting photonic crystals can be controlled by changing its periodicity, as the reflection peak wavelength is proportionally connected with the periodicity. Temperature, chemicals, mechanical stress, electric field, can all act as control agents when photonic crystals are placed in soft material that is able to change shape to external stimuli. Cholesteric liquid crystals (CLC) is a class of 1D photonic structures, and is similar except for the helical pitch of its molecular orientation [42]. To achieve mechanically responsive CLCs polymeric liquid crystal polymers, elastomers, polymer networks and gels are used. The simplest procedure to acquire such a material is in-situ polymerization of low-molecular weight crystals, where precise alignment is controlled. It is a facile process compared to the process of creating a photonic crystal colour changing material, wherefore it is favoured. However, also mechanochromic systems exists since late 2000s. In mechanochromic materials, the perceived colour changes due to different absorption and/or emission of the molecules as a result of a mechanical stimulus. Already multiple mechanochromic polymers are designed. Even light emissive mechanophores. Although, these are not reversible due to bond scission [34]. A lot of research has been done into creating structural colouration as a result of mechanical stimuli using these described elements [19, 36-41].

Zhang et al. [39] demonstrated that spiropyran (SP) mechanophores can be used to create a colour changing mechanoresponsive material. Their work showed that synthesized dimethylacrylate-functionalized spiropyran mechanophores as crosslinkers and micellar structures will form a tough colour-changing hydrogel. When a mechanical force is applied to SP structural isomerization takes place, which will change its colour from yellow, the closed-ring state, to the ring-opening state of merocyanine (MC), which is purple. This chemical reaction comprises the breaking and forming of a C-O bond. The mechanical properties of their produced smart material are retracted from tensile stress-strain, tearing, and cyclic loading-unloading experiments. Its mechanical properties are: $\sigma_f = 1.1$ MPa, $\epsilon_f = 6$ mm mm⁻¹, $E = 1.1$ MPa, $W = 3.5$ MJ m⁻³. Furthermore, this hydrogel is capable of re-acquiring back its initial stiffness and toughness after being subjected to white light for 10 minutes. Other mechanochromic effects are achieved by using experimental nanostructures. Topcu et al. [38] uses gold nanoparticle-based (Au NP) nanostructures in their design that have plasmonic features, and Quan et al. [37] created a stretchable colour-changing strain sensor based on an array of cone-shaped nanostructures. Both have a cumbersome manufacturing

process. The synthesis of the Au NPs is executed using the so-called Turkevich method, i.e. reduction of HauCl_4 . Multiple solutions are added and the final mixture has to be precisely centrifuged. Other solutions are added to stabilize the colloids, and polyacrylamide to create a homogeneous dispersion. Eventually the mixture needs to be in the oven for 2 hours at 60° , and result in small pieces of 1mm in diameter. Topcu et al. [38] makes use of a focused ion beam (FIB) and modified thermal nanoimprinting processes to create their material.

Although the described mechanoluminescence (ML) is not reversible, this sensing technology is used as sensor to measure stress in the structure of bridges and highways. Next to being irreversible, ML has a faulty sensitivity with a threshold more than 1 MPA. Furthermore, the design of most ML stress sensors consists of an ML film and an image sensor, which are separated due to the inherent structure of a common image sensor with a lens. Because of this space in between the ML film and image sensors, a lot of photons are lost in space, which results in lower sensitivity. Capacitive and piezoresistive sensors are currently filling the gap of sensing technologies in the lower stress range. However, ML does show advantages in stress distribution visualization, remote sensing, dynamic response, and self-powering. The work of Zhuang et al. [41] therefore proposed a near-distance imaging scheme, whereby the ML film and image sensor are closer to each other, increasing the photon harvesting rate up to 80%. Furthermore, Al_2O_3 nanoparticles are added to the ML film, which increased its elastic modulus, and herewith caused a four time magnification of the mechano-to-photon conversion efficiency. All in all, the sensor created can measure stress in the range of kPa, has a pixel size of 100μ (254 dpi) and a response of 3.3ms.

An example of using liquid-crystal hydrogels is presented by Zhang et al. [40]. These researchers present a chameleon-inspired electronic skin that is based on hydroxypropyl cellulose composite hydrogel and still has stable cholesteric liquid-crystal structures, which results in structural colouration in response to pressure, tension or temperature. However, cellulose has a poor conductivity and high transmissivity. To be able to still create a conductive e-skin, this research added carbon nanotubes (CNTs) as conductive agents. These CNTs do create conductive properties, but due to the single electrical output it is hard to locate the stimulation area, and such a device is prone to errors. The researchers solved this problem by adding Poly-Acrylamide-co-Acrylic acid (PACA), which is thermal responsive. Due to PACA, when a stimulus is applied (change in volume or changed internal nanostructures), visible colour switches can be observed. Due to the CNTs there is also an electrical output, which yield quantitative feedback of the external stimulus. Yang et al. [42] created a system where Cholesteric Liquid Crystals (CLCs) are also responsible for the colour change. Difference with Zhang et al. [40] is that this material is 3D printed and is inspired by the octopus.

Huang et al. [19] designed a responsive platform with a dual-channel pressure sensor (DCPS). The DCPS consists of a multilayer that is structured with photonic hydrogel and a flexible piezoresistive pressure sensor to transmit electrical data. The photonic hydrogel provides eye-readable colour changes, which makes the system intuitive for users, and especially useful in point-of-care testing (POCT) scenarios. A mechanical stimulus the photonic hydrogel changes its lattice spacing, which will result in structural colouration, i.e. a visual signal.

Whereas the colour in these sensors described above are mainly for interpretation or aesthetic reasons, these type of measurements can also be quantitative when using the right colour gradient scale. There are two main models for image analysis: the red-green-blue (RGB) colour space, and the CIE $L^*a^*b^*$ colour space. The first model makes use of the additive structure, whereby red (R), green (G), and blue (B) are added in multiple ways to create different array of colours. The second model uses the following dimensions to describe an observed colour: lightness (L), green-red (a), and blue-yellow (b). Check [Equations 28 and 29](#).

$$\Delta E_{RGB} = \sqrt{(\Delta R)^2 + (\Delta G)^2 + (\Delta B)^2} \quad (28)$$

$$\Delta E_{L^*a^*b^*} = \sqrt{(\Delta L^*)^2 + (\Delta a^*)^2 + (\Delta b^*)^2} \quad (29)$$

Although the numerical values may be different for both models, it is proven by Ebralidze et al. [18] that the overall trend of the graph is similar, and thus both models can be used while describing depicted colours. While the first model is widespread in PC monitors, the second model is not device dependent. Eventually there was chosen to use the HSV-colour model, which separates each colour in values for their hue, saturation and brightness (value). This model is a submodel to the RGB model as is seen in its calculations shown in [Equation 30, 31 and 32](#). Each value is

indicated in percentage, or within the range of 0-1. H is actually indicated with a degree between 0-360, but this could be translated to the similar range of 0-1.

$$H = \begin{cases} (0 + ((G-B)/(MAX-MIN))) \times 60, & \text{if } R = \text{MAX} \\ (2 + ((B-R)/(MAX-MIN))) \times 60, & \text{if } G = \text{MAX} \\ (4 + ((R-G)/(MAX-MIN))) \times 60, & \text{if } B = \text{MAX} \end{cases} \quad (30)$$

$$S = (MAX - MIN)/MAX \quad (31)$$

$$V = MAX \quad (32)$$

- The R, G and B values are from the RGB colour model
- The MAX and MIN are respectively the maximum and minimum of these three values

This sensor research has limited itself to sensors that convert mechanical pressure or stress directly to colour change. As discussed, these type of sensors make use of photonic crystals, liquid crystals, or mechanochromics. All make use of the interaction with light and their changing shape while undergoing the mechanical stimulus. A different reflected peak wavelength will result in a different perceived colour. Within this research there is refrained from sensors that indirectly change their colour by for example using carbon dots [48], chemical systems [47], piezoelectric material and QLEDs [13] or with other electronic elements [44]. Only a couple of examples are given in [Section 2.2](#).

E. Matlab codes

E.1. Analysis of a sample

The code for the analysis of sample 1 for each of the three trials is shown. As the analysis is quite long, and some adaptations had to be made per sample, there is chosen to have 12 different codes. An example of an adaptation is that each sample need to be aligned with their video. Another is that to find the mean forces at each incremental step, sometimes the stated requirements such as the length of the flat line, differed per sample. Sometimes point were encountered for, and sometimes it didn't. That is why there is chosen to find the missing indices in the figure that is created in the beginning and add them to the already found ones. This was a procedure that took less time then to find the perfect requirements. For future experiments it was therefore also recommended to use an automatic translation stage, such that the requirements are applicable to all samples.

The code and its explanations as comments:

```
close all
clear all
clc

%% Import data

Force_S1_T1 = readmatrix('23 09 19 10 01 12 Exp1 - Try1.txt');
Force_S1_T2 = readmatrix('23 09 19 10 05 31 Exp1 - Try2.txt');
Force_S1_T3 = readmatrix('23 09 19 10 09 44 Exp1 - Try3.txt');

%% Plot the trials

T1_1 = Force_S1_T1(1:end,3);
T1_1_smooth = sgolayfilt(T1_1,3,41); % 3rd order filter - Savitzky - Golay
T1_2 = Force_S1_T2(1:end,3);
T1_2_smooth = sgolayfilt(T1_2,3,41);
T1_3 = Force_S1_T3(1:end,3);
T1_3_smooth = sgolayfilt(T1_3,3,41);

figure
plot(T1_1, ':')
```

```

hold on
plot(T1_1_smooth, '-');
plot(T1_2, ':');
plot(T1_2_smooth, '-');
plot(T1_3, ':');
plot(T1_3_smooth, '-');
xlabel("Time [steps of 100ms]")
ylabel("Force [N]")
title('Force progression of sample 1')
legend('Raw data try1', 'Data with Savitzky-Golay try1', 'Raw data try2', 'Data with
Savitzky-Golay try2',...
'Raw data try3', 'Data with Savitzky-Golay try3')
set(gca, 'FontName', 'Times New Roman', 'FontSize', 18)

%% Calculate mean at each step

% Calculate differences of each index in the force progression plot
Y1 = diff(T1_1_smooth);
Y2 = diff(T1_2_smooth);
Y3 = diff(T1_3_smooth);

% Find the indices in Y where the step boundaries occur
step_indices1 = find(abs(Y1) < 0.01);          % Threshold = 0.01
step_indices2 = find(abs(Y2) < 0.01);
step_indices3 = find(abs(Y3) < 0.01);

% Find the indices in step_indices where the flat line stops
S1 = diff(step_indices1);
I1 = find(abs(S1) > 20);                      % Threshold = 2 seconds
S2 = diff(step_indices2);
I2 = find(abs(S2) > 20);
S3 = diff(step_indices3);
I3 = find(abs(S3) > 20);

% Find indices in Y where flat line stops
N1 = [];
for i = 1:length(I1);
    Index1 = step_indices1(I1(i));
    N1 = [N1, Index1];
end
N1 = N1';

N2 = [];
for i = 1:length(I2);
    Index2 = step_indices2(I2(i));
    N2 = [N2, Index2];
end
N2 = N2';

N3 = [];
for i = 1:length(I3);
    Index3 = step_indices3(I3(i));
    N3 = [N3, Index3];
end
N3 = N3';

% Initialize variables to store mean values
step_means1 = [];

```

```

% Loop through the identified step indices
for i = 1:length(N1)
    % Extract the data for each step
    step_start = N1(i)-30;      % measure the mean force 3 seconds prior to the steep line
    step_end = N1(i);
    step = T1_1_smooth(step_start:step_end);

    % Calculate the mean for the current step
    step_mean = mean(step);

    % Store the mean value
    step_means1 = [step_means1, step_mean];
end

step_means1 = step_means1';

% Initialize variables to store mean values
step_means2 = [];

% Loop through the identified step indices
for i = 1:length(N2)
    % Extract the data for each step
    step_start = N2(i)-30;
    step_end = N2(i);
    step = T1_2_smooth(step_start:step_end);

    % Calculate the mean for the current step
    step_mean = mean(step);

    % Store the mean value
    step_means2 = [step_means2, step_mean];
end

step_means2 = step_means2';

% Initialize variables to store mean values
step_means3 = [];

% Loop through the identified step indices
for i = 1:length(N3)
    % Extract the data for each step
    step_start = N3(i)-30;
    step_end = N3(i);
    step = T1_3_smooth(step_start:step_end);

    % Calculate the mean for the current step
    step_mean = mean(step);

    % Store the mean value
    step_means3 = [step_means3, step_mean];
end

step_means3 = step_means3';

%% Combine all means in column

step_means = [step_means1, step_means2, step_means3]

MEANS = mean(step_means, 2)

%%
%%

```

```

%% VIDEO COLOUR ANALYSE

% Load videos
video1_1 = VideoReader("EIIS1T1.mp4");
video1_2 = VideoReader("EIIS1T2.mp4");
video1_3 = VideoReader("EIIS1T3.mp4");

% Define time points (in seconds) at which snap shots will be captured

stokvideo1 = 7.5;          % First touch with stick happens at this second in video
stokdata1 = 10.1;         % First touch with stick
stokvideo2 = 4.8;
stokdata2 = 8.6;
stokvideo3 = 4.2;
stokdata3 = 10.9;

% Find timepoints at the start of each step
N1_new = (N1./10) - (stokdata1-stokvideo1) - 3;
N2_new = (N2./10) - (stokdata2-stokvideo2) - 3;
N3_new = (N3./10) - (stokdata3-stokvideo3) - 3;

% Add a startpoint at 1 second, this is zero measurement
timePoints1 = [1; N1_new];
timePoints2 = [1; N2_new];
timePoints3 = [1; N3_new];

% Initialize variables to store the captured frames, Hchannels,
% binaryImages, Hmeans, and redAreas
capturedFrames1 = cell(1, numel(timePoints1));
capturedFrames2 = cell(1, numel(timePoints1));
capturedFrames3 = cell(1, numel(timePoints1));

capturedbinaryImage1 = cell(1, numel(timePoints1));
capturedbinaryImage2 = cell(1, numel(timePoints1));
capturedbinaryImage3 = cell(1, numel(timePoints1));

capturedredArea1 = zeros(1, numel(timePoints1));
capturedredArea2 = zeros(1, numel(timePoints1));
capturedredArea3 = zeros(1, numel(timePoints1));

% Define specific saturation and H-value ranges (for red)
% Found with app color threshold in Matlab
minSaturation = 0.466;    % Can be adjusted
minHvalue = 0.851;      % Can be adjusted

%% Fill in cells and rows

for i = 1:numel(timePoints1)
    % Calculate the frame index corresponding to the desired time point
    desiredTime = timePoints1(i);
    frameIdx = round(desiredTime * video1_1.FrameRate);

    % Read the frame at the specified time point
    currentFrame1 = read(video1_1, frameIdx);

    % Convert the frame to double precision for image processing
    currentFrame1 = double(currentFrame1)/255;

    % Convert the frame to HSV colour space
    currentFrameHSV1 = rgb2hsv(currentFrame1);

    % Create a binary mask for pixels within the specified range

```

```

    redPixels1 = (currentFrameHSV1(:,:,2) >= minSaturation) & (currentFrameHSV1(:,:,1) >=
minHvalue);
    redArea1 = sum(redPixels1(:));

    % Create a binary image where red pixels are black and others are white
    binaryImage1 = zeros(size(currentFrame1, 1), size(currentFrame1, 2));
    binaryImage1(redPixels1) = 1;

    % Store the captured data
    capturedredArea1(i) = redArea1;
    capturedbinaryImage1{i} = binaryImage1;
    capturedFrames1{i} = currentFrame1;
end

for i = 1:numel(timePoints2)
    % Calculate the frame index corresponding to the desired time point
    desiredTime = timePoints2(i);
    frameIdx = round(desiredTime * video1_2.FrameRate);

    % Read the frame at the specified time point
    currentFrame2 = read(video1_2, frameIdx);

    % Convert the frame to double precision for image processing
    currentFrame2 = double(currentFrame2)/255;

    % Convert the frame to HSV colour space
    currentFrameHSV2 = rgb2hsv(currentFrame2);

    % Create a binary mask for pixels within the specified range
    redPixels2 = (currentFrameHSV2(:,:,2) >= minSaturation) & (currentFrameHSV2(:,:,1) >=
minHvalue);
    redArea2 = sum(redPixels2(:));

    % Create a binary image where red pixels are black and others are white
    binaryImage2 = zeros(size(currentFrame2, 1), size(currentFrame2, 2));
    binaryImage2(redPixels2) = 1;

    % Store the captured data
    capturedredArea2(i) = redArea2;
    capturedbinaryImage2{i} = binaryImage2;
    capturedFrames2{i} = currentFrame2;
end

for i = 1:numel(timePoints3)
    % Calculate the frame index corresponding to the desired time point
    desiredTime = timePoints3(i);
    frameIdx = round(desiredTime * video1_3.FrameRate);

    % Read the frame at the specified time point
    currentFrame3 = read(video1_3, frameIdx);

    % Convert the frame to double precision for image processing
    currentFrame3 = double(currentFrame3)/255;

    % Convert the frame to HSV colour space
    currentFrameHSV3 = rgb2hsv(currentFrame3);

    % Create a binary mask for pixels within the specified range
    redPixels3 = (currentFrameHSV3(:,:,2) >= minSaturation) & (currentFrameHSV3(:,:,1) >=
minHvalue);
    redArea3 = sum(redPixels3(:));

    % Create a binary image where red pixels are black and others are white

```

```

binaryImage3 = zeros(size(currentFrame3, 1), size(currentFrame3, 2));
binaryImage3(redPixels3) = 1;

% Store the captured data
capturedredArea3(i) = redArea3;
capturedbinaryImage3{i} = binaryImage3;
capturedFrames3{i} = currentFrame3;
end

%% Create plots for the captured binary images and snapshots 1

figure;

% Get the number of images in this dataset
numImages = numel(capturedbinaryImage1);

% Define the number of rows and columns for subplots
numRows = 4;
numCols = ceil(numImages / numRows);

% A for loop to display the snapshots
for i = 1:numImages
    currentFrame1 = capturedFrames1{i};
    % Create subplots at each incremental step
    subplot(numRows, numCols, i)
    imshow(currentFrame1)
    title(['Original Snapshot at t = ' num2str(timePoints1(i)) ' seconds T1'] )
    set(gca, 'FontName', 'Times New Roman', 'FontSize', 9)
end

% Create new figure for binary
figure;

% A for loop to display the binary images
for i = 1:numImages
    binaryImage1 = capturedbinaryImage1{i};
    % Create subplots at each incremental step
    subplot(numRows, numCols, i)
    imshow(binaryImage1)
    title(['Binary Image at t = ' num2str(timePoints1(i)) ' seconds T1'])
    set(gca, 'FontName', 'Times New Roman', 'FontSize', 9)
end

%% Create plots for the captured binary images and snapshots 2

figure;

% Get the number of images in this dataset
numImages = numel(capturedbinaryImage2);

% Define the number of rows and columns for subplots
numRows = 4;
numCols = ceil(numImages / numRows);

% A for loop to display the snapshots
for i = 1:numImages
    currentFrame2 = capturedFrames2{i};
    % Create subplots at each incremental step
    subplot(numRows, numCols, i)
    imshow(currentFrame2)
    title(['Original Snapshot at t = ' num2str(timePoints2(i)) ' seconds T2'] )
    set(gca, 'FontName', 'Times New Roman', 'FontSize', 9)
end

```



```

% Create new figure for binary
figure;

% A for loop to display the binary images
for i = 1:numImages
    binaryImage2 = capturedbinaryImage2{i};
    % Create subplots at each incremental step
    subplot(numRows, numCols, i)
    imshow(binaryImage2)
    title(['Binary Image at t = ' num2str(timePoints2(i)) ' seconds T2'])
    set(gca, 'FontName', 'Times New Roman', 'FontSize', 9)
end

%% Create plots for the captured binary images and snapshots 3

figure;

% Get the number of images in this dataset
numImages = numel(capturedbinaryImage3);

% Define the number of rows and columns for subplots
numRows = 4;
numCols = ceil(numImages / numRows);

% A for loop to display the snapshots
for i = 1:numImages
    currentFrame3 = capturedFrames3{i};
    % Create subplots at each incremental step
    subplot(numRows, numCols, i)
    imshow(currentFrame3)
    title(['Original Snapshot at t = ' num2str(timePoints3(i)) ' seconds T3'] )
    set(gca, 'FontName', 'Times New Roman', 'FontSize', 9)
end

% Create new figure for binary
figure;

% A for loop to display the binary images
for i = 1:numImages
    binaryImage3 = capturedbinaryImage3{i};
    % Create subplots at each incremental step
    subplot(numRows, numCols, i)
    imshow(binaryImage3)
    title(['Binary Image at t = ' num2str(timePoints3(i)) ' seconds T3'])
    set(gca, 'FontName', 'Times New Roman', 'FontSize', 9)
end

%% Calculate mean colour of initial state after removing pressure applicator from image

frame1 = round(1*video1_1.Framerate);
frame1 = read(video1_1, frame1);
frame1 = double(frame1)/255;
frame1 = rgb2hsv(frame1);

frame2 = round(1*video1_2.Framerate);
frame2 = read(video1_2, frame2);
frame2 = double(frame2)/255;
frame2 = rgb2hsv(frame2);

frame3 = round(1*video1_3.Framerate);
frame3 = read(video1_3, frame3);
frame3 = double(frame3)/255;

```

```

frame3 = rgb2hsv(frame3);

% Create a mask over the images to block out the pressure applicator
% Defining the HSV threshold ranges (picked from color thresholder app)
H_min = 0.549;
H_max = 0.962;
S_min = 0.197;
S_max = 1.000;
V_min = 0.000;
V_max = 0.539;

pixels1 = (frame1(:,:,1) >= H_min) & (frame1(:,:,1) <= H_max) ...
    & (frame1(:,:,2) >= S_min) & (frame1(:,:,2) <= S_max) ...
    & (frame1(:,:,3) >= V_min) & (frame1(:,:,3) <= V_max);
pixels2 = (frame2(:,:,1) >= H_min) & (frame2(:,:,1) <= H_max) ...
    & (frame2(:,:,2) >= S_min) & (frame2(:,:,2) <= S_max) ...
    & (frame2(:,:,3) >= V_min) & (frame2(:,:,3) <= V_max);
pixels3 = (frame3(:,:,1) >= H_min) & (frame3(:,:,1) <= H_max) ...
    & (frame3(:,:,2) >= S_min) & (frame3(:,:,2) <= S_max) ...
    & (frame3(:,:,3) >= V_min) & (frame3(:,:,3) <= V_max);

% Extract pixel values that satisfy the criteria for each frame
H1 = frame1(:,:,1);
H2 = frame2(:,:,1);
H3 = frame3(:,:,1);
S1 = frame1(:,:,2);
S2 = frame2(:,:,2);
S3 = frame3(:,:,2);
V1 = frame1(:,:,3);
V2 = frame2(:,:,3);
V3 = frame3(:,:,3);

% Set the mask values to NaN
H1(~pixels1) = NaN;
H2(~pixels2) = NaN;
H3(~pixels3) = NaN;

S1(~pixels1) = NaN;
S2(~pixels2) = NaN;
S3(~pixels3) = NaN;

V1(~pixels1) = NaN;
V2(~pixels2) = NaN;
V3(~pixels3) = NaN;

% Calculate the mean HSV colour values separately for each frame
MeanH1 = nanmean(H1(:));
MeanH2 = nanmean(H2(:));
MeanH3 = nanmean(H3(:));

MeanS1 = nanmean(S1(:));
MeanS2 = nanmean(S2(:));
MeanS3 = nanmean(S3(:));

MeanV1 = nanmean(V1(:));
MeanV2 = nanmean(V2(:));
MeanV3 = nanmean(V3(:));

% Display the mean HSV colours separately for each frame
fprintf('Try 1 Mean Hue (H): %.4f\n', MeanH1);
fprintf('Try 1 Mean Saturation (S): %.4f\n', MeanS1);
fprintf('Try 1 Mean Value (V): %.4f\n', MeanV1);

```

```

fprintf('Try 2 Mean Hue (H): %.4f\n', MeanH2);
fprintf('Try 2 Mean Saturation (S): %.4f\n', MeanS2);
fprintf('Try 2 Mean Value (V): %.4f\n', MeanV2);

fprintf('Try 3 Mean Hue (H): %.4f\n', MeanH3);
fprintf('Try 3 Mean Saturation (S): %.4f\n', MeanS3);
fprintf('Try 3 Mean Value (V): %.4f\n', MeanV3);

%% Calculate mean colour at maximum state

Time1 = ceil(numel(timePoints1)/2)+1;
Time1 = timePoints1(Time1);
Time2 = ceil(numel(timePoints2)/2)+1;
Time2 = timePoints2(Time2);
Time3 = ceil(numel(timePoints3)/2)+1;
Time3 = timePoints3(Time3);

frame1_top = round(Time1*video1_1.FrameRate);
frame1_top = read(video1_1, frame1_top);
frame1_top = double(frame1_top)/255;
frame1_top = rgb2hsv(frame1_top);

frame2_top = round(Time2*video1_2.FrameRate);
frame2_top = read(video1_2, frame2_top);
frame2_top = double(frame1_top)/255;
frame2_top = rgb2hsv(frame1_top);

frame3_top = round(Time3*video1_3.FrameRate);
frame3_top = read(video1_3, frame3_top);
frame3_top = double(frame3_top)/255;
frame3_top = rgb2hsv(frame3_top);

% Create a mask that is needed at the maximum indent (previous thresholds
% used)
pixels1_top = (frame1_top(:,:,2) >= minSaturation) & (frame1_top(:,:,1) >= minHvalue);
pixels2_top = (frame2_top(:,:,2) >= minSaturation) & (frame2_top(:,:,1) >= minHvalue);
pixels3_top = (frame3_top(:,:,2) >= minSaturation) & (frame3_top(:,:,1) >= minHvalue);

% Extract pixel values that satisfy the criteria for each frame
H1_top = frame1_top(:,:,1);
H2_top = frame2_top(:,:,1);
H3_top = frame3_top(:,:,1);
S1_top = frame1_top(:,:,2);
S2_top = frame2_top(:,:,2);
S3_top = frame3_top(:,:,2);
V1_top = frame1_top(:,:,3);
V2_top = frame2_top(:,:,3);
V3_top = frame3_top(:,:,3);

% Set the mask values to NaN
H1_top(~pixels1_top) = NaN;
H2_top(~pixels2_top) = NaN;
H3_top(~pixels3_top) = NaN;

S1_top(~pixels1_top) = NaN;
S2_top(~pixels2_top) = NaN;
S3_top(~pixels3_top) = NaN;

V1_top(~pixels1_top) = NaN;
V2_top(~pixels2_top) = NaN;
V3_top(~pixels3_top) = NaN;

% Calculate the mean HSV colour values separately for each frame

```

```

MeanH1_top = nanmean(H1_top(:));
MeanH2_top = nanmean(H2_top(:));
MeanH3_top = nanmean(H3_top(:));

MeanS1_top = nanmean(S1_top(:));
MeanS2_top = nanmean(S2_top(:));
MeanS3_top = nanmean(S3_top(:));

MeanV1_top = nanmean(V1_top(:));
MeanV2_top = nanmean(V2_top(:));
MeanV3_top = nanmean(V3_top(:));

% Display the mean HSV colours separately for each frame
fprintf('Try 1 Mean Hue (H) at top: %.4f\n', MeanH1_top);
fprintf('Try 1 Mean Saturation (S) at top: %.4f\n', MeanS1_top);
fprintf('Try 1 Mean Value (V) at top: %.4f\n', MeanV1_top);

fprintf('Try 2 Mean Hue (H) at top: %.4f\n', MeanH2_top);
fprintf('Try 2 Mean Saturation (S) at top: %.4f\n', MeanS2_top);
fprintf('Try 2 Mean Value (V) at top: %.4f\n', MeanV2_top);

fprintf('Try 3 Mean Hue (H) at top: %.4f\n', MeanH3_top);
fprintf('Try 3 Mean Saturation (S) at top: %.4f\n', MeanS3_top);
fprintf('Try 3 Mean Value (V) at top: %.4f\n', MeanV3_top);

%% Calculate mean red area

ra_means = [capturedredArea1; capturedredArea2; capturedredArea3]

RA_MEANS = mean(ra_means, 1) / (485*485) % 485 pixels is 1cm
RA_MEANS = RA_MEANS * 100 % in mm2

%% Plot the mean red area against the mean force

MEANS = MEANS - 0.5953; % account for the force of the pressure sensor untouched

F_MEANS = [0 ; MEANS];

figure
plot(F_MEANS, RA_MEANS, '-c', 'LineWidth', 2, 'Marker', 'o', 'MarkerSize', 3,...
     'MarkerEdgeColor', 'b')
xlabel("Force [N]")
ylabel("Red coloured area [mm^2]")
title('Red coloured area against force of Sample 1')
set(gca, 'FontName', 'Times New Roman')

figure
plot(RA_MEANS, F_MEANS, '-c', 'LineWidth', 2, 'Marker', 'o', 'MarkerSize', 3,...
     'MarkerEdgeColor', 'b')
xlabel("Red coloured area [mm^2]")
ylabel("Force [N]")
title('Force against red coloured area of Sample 1')
set(gca, 'FontName', 'Times New Roman')

```

E.2. Mean forces and mean areas plotted against the indent

In an excel sheet all valuable data from the code from Appendix E.1. is placed. This excelsheet is important and used to plot all the calculated mean forces and mean areas at each incremental step against these indentation steps.

The code in combination with explanation in the comments:

```
clear all
close all
clc

%% Import excel data

dataExcel = 'indent_force_area.xlsx';
dataTable = readtable(dataExcel);
dataTable = dataTable{:,1:25};

indent = dataTable(2:26,1);
F1 = dataTable(2:26,2);
A1 = dataTable(2:26,3);
F2 = dataTable(2:26,4);
A2 = dataTable(2:26,5);
F3 = dataTable(2:26,6);
A3 = dataTable(2:26,7);
F4 = dataTable(2:26,8);
A4 = dataTable(2:26,9);
F5 = dataTable(2:26,10);
A5 = dataTable(2:26,11);
F6 = dataTable(2:26,12);
A6 = dataTable(2:26,13);
F7 = dataTable(2:26,14);
A7 = dataTable(2:26,15);
F8 = dataTable(2:26,16);
A8 = dataTable(2:26,17);
F9 = dataTable(2:26,18);
A9 = dataTable(2:26,19);
F10 = dataTable(2:26,20);
A10 = dataTable(2:26,21);
F11 = dataTable(2:26,22);
A11 = dataTable(2:26,23);
F12 = dataTable(2:26,24);
A12 = dataTable(2:26,25);

%% Create plot indent vs force

figure
plot(indent(~isnan(F1)), F1(~isnan(F1)), '-c', 'LineWidth', 2, 'Marker', 'o', 'MarkerSize',
3, ...
'MarkerEdgeColor', 'b');
xlabel('Indentation [mm]')
ylabel('Force [N]')
title('The mean forces of sample 1 versus the indentation')
set(gca, 'FontName', 'Times New Roman')

figure
hold on
plot(indent(~isnan(F1)), F1(~isnan(F1)), 'o-', 'DisplayName', 'F1');
plot(indent(~isnan(F2)), F2(~isnan(F2)), 'o-', 'DisplayName', 'F2');
plot(indent(~isnan(F3)), F3(~isnan(F3)), 'o-', 'DisplayName', 'F3');
plot(indent(~isnan(F4)), F4(~isnan(F4)), 'o-', 'DisplayName', 'F4');
plot(indent(~isnan(F5)), F5(~isnan(F5)), 'o-', 'DisplayName', 'F5');
plot(indent(~isnan(F6)), F6(~isnan(F6)), 'o-', 'DisplayName', 'F6');
```

```

legend('F1', 'F2', 'F3', 'F4', 'F5', 'F6')
xlabel('Indent [mm]')
ylabel('Force [N]')
title('The mean forces of the samples versus the indent')
set(gca, 'FontName', 'Times New Roman')
hold off

figure
hold on
plot(indent(~isnan(F7)), F7(~isnan(F7)), 'o-', 'DisplayName', 'F7');
plot(indent(~isnan(F8)), F8(~isnan(F8)), 'o-', 'DisplayName', 'F8');
plot(indent(~isnan(F9)), F9(~isnan(F9)), 'o-', 'DisplayName', 'F9');
plot(indent(~isnan(F10)), F10(~isnan(F10)), 'o-', 'DisplayName', 'F10');
plot(indent(~isnan(F11)), F11(~isnan(F11)), 'o-', 'DisplayName', 'F11');
plot(indent(~isnan(F12)), F12(~isnan(F12)), 'o-', 'DisplayName', 'F12');
legend('F7', 'F8', 'F9', 'F10', 'F11', 'F12')
xlabel('Indent [mm]')
ylabel('Force [N]')
title('The mean forces of the samples versus the indent')
set(gca, 'FontName', 'Times New Roman')
hold off

%% Create plot indent vs area
figure
plot(indent(~isnan(A1)), A1(~isnan(A1)), '-c', 'LineWidth', 2, 'Marker', 'o', 'MarkerSize',
3, ...
'MarkerEdgeColor', 'b');
xlabel('Indentation [mm]')
ylabel('Area [mm^2]')
title('The mean areas of sample 1 versus the indentation')
set(gca, 'FontName', 'Times New Roman')

figure
hold on
plot(indent(~isnan(A1)), A1(~isnan(A1)), 'o-', 'DisplayName', 'A1');
plot(indent(~isnan(A2)), A2(~isnan(A2)), 'o-', 'DisplayName', 'A2');
plot(indent(~isnan(A3)), A3(~isnan(A3)), 'o-', 'DisplayName', 'A3');
plot(indent(~isnan(A4)), A4(~isnan(A4)), 'o-', 'DisplayName', 'A4');
plot(indent(~isnan(A5)), A5(~isnan(A5)), 'o-', 'DisplayName', 'A5');
plot(indent(~isnan(A6)), A6(~isnan(A6)), 'o-', 'DisplayName', 'A6');
legend('A1', 'A2', 'A3', 'A4', 'A5', 'A6')
xlabel('Indent [mm]')
ylabel('Area [mm^2]')
title('The mean areas of the samples versus the indent')
set(gca, 'FontName', 'Times New Roman')
hold off

figure
hold on
plot(indent(~isnan(A7)), A7(~isnan(A7)), 'o-', 'DisplayName', 'A7');
plot(indent(~isnan(A8)), A8(~isnan(A8)), 'o-', 'DisplayName', 'A8');
plot(indent(~isnan(A9)), A9(~isnan(A9)), 'o-', 'DisplayName', 'A9');
plot(indent(~isnan(A10)), A10(~isnan(A10)), 'o-', 'DisplayName', 'A10');
plot(indent(~isnan(A11)), A11(~isnan(A11)), 'o-', 'DisplayName', 'A11');
plot(indent(~isnan(A12)), A12(~isnan(A12)), 'o-', 'DisplayName', 'A12');
legend('A7', 'A8', 'A9', 'A10', 'A11', 'A12')
xlabel('Indent [mm]')
ylabel('Area [mm^2]')
title('The mean areas of the samples versus the indent')
set(gca, 'FontName', 'Times New Roman')
hold off

```


E.3. Coloured area size means and force means

In the code from Appendix E.1. the coloured area size means and force means per incremental step are already plotted against each other, but this is done separately for each sample. These codes combines these graphs into one graphs. The first code does this for sample 1-6, and the second code for the samples 7-12.

First code:

```
close all
clear all
clc
```

```
%% DATA IMPORT
```

```
ALLMEANS = 'ALLEMEANS.xlsx';
dataTable = readtable(ALLMEANS);
```

```
F_MEANS1 = dataTable.F_MEANS1;
F_MEANS2 = dataTable.F_MEANS2;
F_MEANS3 = dataTable.F_MEANS3;
F_MEANS4 = dataTable.F_MEANS4;
F_MEANS5 = dataTable.F_MEANS5;
F_MEANS6 = dataTable.F_MEANS6;
```

```
F_MEANS1 = double(F_MEANS1);
F_MEANS2 = double(F_MEANS2);
F_MEANS3 = double(F_MEANS3);
F_MEANS4 = double(F_MEANS4);
F_MEANS5 = double(F_MEANS5);
F_MEANS6 = double(F_MEANS6);
```

```
F_MEANS1 = F_MEANS1(1:17);
F_MEANS2 = F_MEANS2(1:16);
F_MEANS3 = F_MEANS3(1:19);
F_MEANS4 = F_MEANS4(1:20);
F_MEANS5 = F_MEANS5(1:22);
F_MEANS6 = F_MEANS6(1:16);
```

```
RA_MEANS1 = dataTable.RA_MEANS1;
RA_MEANS2 = dataTable.RA_MEANS2;
RA_MEANS3 = dataTable.RA_MEANS3;
RA_MEANS4 = dataTable.RA_MEANS4;
RA_MEANS5 = dataTable.RA_MEANS5;
RA_MEANS6 = dataTable.RA_MEANS6;
```

```
RA_MEANS1 = double(RA_MEANS1);
RA_MEANS2 = double(RA_MEANS2);
RA_MEANS3 = double(RA_MEANS3);
RA_MEANS4 = double(RA_MEANS4);
RA_MEANS5 = double(RA_MEANS5);
RA_MEANS6 = double(RA_MEANS6);
```

```
RA_MEANS1 = RA_MEANS1(1:17);
RA_MEANS2 = RA_MEANS2(1:16);
RA_MEANS3 = RA_MEANS3(1:19);
RA_MEANS4 = RA_MEANS4(1:20);
RA_MEANS5 = RA_MEANS5(1:22);
RA_MEANS6 = RA_MEANS6(1:16)
```

```
%% PLOT
```

```

figure
hold on
grid on
plot(F_MEANS1, RA_MEANS1, 'LineWidth', 1, 'Marker', 'o', 'MarkerSize', 3)
plot(F_MEANS2, RA_MEANS2, 'LineWidth', 1, 'Marker', 'o', 'MarkerSize', 3)
plot(F_MEANS3, RA_MEANS3, 'LineWidth', 1, 'Marker', 'o', 'MarkerSize', 3)
plot(F_MEANS4, RA_MEANS4, 'LineWidth', 1, 'Marker', 'o', 'MarkerSize', 3)
plot(F_MEANS5, RA_MEANS5, 'LineWidth', 1, 'Marker', 'o', 'MarkerSize', 3)
plot(F_MEANS6, RA_MEANS6, 'LineWidth', 1, 'Marker', 'o', 'MarkerSize', 3)
xlabel("Force [N]")
ylabel("Red coloured area [mm^2]")
title('Red coloured area against force of all samples')
set(gca, 'FontName', 'Times New Roman')
legend('Sample 1', 'Sample 2', 'Sample 3', 'Sample 4', 'Sample 5', 'Sample 6')
hold off

```

```

figure
hold on
grid on

plot(RA_MEANS1, F_MEANS1, 'LineWidth', 1, 'Marker', 'o', 'MarkerSize', 3)
plot(RA_MEANS2, F_MEANS2, 'LineWidth', 1, 'Marker', 'o', 'MarkerSize', 3)
plot(RA_MEANS3, F_MEANS3, 'LineWidth', 1, 'Marker', 'o', 'MarkerSize', 3)
plot(RA_MEANS4, F_MEANS4, 'LineWidth', 1, 'Marker', 'o', 'MarkerSize', 3)
plot(RA_MEANS5, F_MEANS5, 'LineWidth', 1, 'Marker', 'o', 'MarkerSize', 3)
plot(RA_MEANS6, F_MEANS6, 'LineWidth', 1, 'Marker', 'o', 'MarkerSize', 3)

xlabel("Red coloured area [mm^2]")
ylabel("Force [N]")
title('Force against Red coloured area of all samples')
set(gca, 'FontName', 'Times New Roman')
legend('Sample 1', 'Sample 2', 'Sample 3', 'Sample 4', 'Sample 5', 'Sample 6')

hold off

```

Second code:

```

clear all
close all
clc

%% Excel data ophalen

dataExcel = 'F_and_RA_Means_S7tS12.xlsx';
dataTable = readtable(dataExcel);
dataTable = dataTable{:,1:12};

F7 = dataTable(1:22,1);
A7 = dataTable(1:22,2);
F8 = dataTable(1:23,3);
A8 = dataTable(1:23,4);
F9 = dataTable(1:20,5);
A9 = dataTable(1:20,6);
F10 = dataTable(1:20,7);
A10 = dataTable(1:20,8);
F11 = dataTable(1:17,9);
A11 = dataTable(1:17,10);
F12 = dataTable(1:24,11);
A12 = dataTable(1:24,12);

```

%% PLOT

```

figure
hold on
grid on
plot(F7, A7, 'LineWidth', 1, 'Marker', 'o', 'MarkerSize', 3)
plot(F8, A8, 'LineWidth', 1, 'Marker', 'o', 'MarkerSize', 3)
plot(F9, A9, 'LineWidth', 1, 'Marker', 'o', 'MarkerSize', 3)
plot(F10, A10, 'LineWidth', 1, 'Marker', 'o', 'MarkerSize', 3)
plot(F11, A11, 'LineWidth', 1, 'Marker', 'o', 'MarkerSize', 3)
plot(F12, A12, 'LineWidth', 1, 'Marker', 'o', 'MarkerSize', 3)
xlabel("Force [N]")
ylabel("Red coloured area [mm^2]")
title('Red coloured area against force of all samples')
set(gca, 'FontName', 'Times New Roman')
legend('Sample 7', 'Sample 8', 'Sample 9', 'Sample 10', 'Sample 11', 'Sample 12')
hold off

```

```

figure
hold on
grid on

plot(A7, F7, 'LineWidth', 1, 'Marker', 'o', 'MarkerSize', 3)
plot(A8, F8, 'LineWidth', 1, 'Marker', 'o', 'MarkerSize', 3)
plot(A9, F9, 'LineWidth', 1, 'Marker', 'o', 'MarkerSize', 3)
plot(A10, F10, 'LineWidth', 1, 'Marker', 'o', 'MarkerSize', 3)
plot(A11, F11, 'LineWidth', 1, 'Marker', 'o', 'MarkerSize', 3)
plot(A12, F12, 'LineWidth', 1, 'Marker', 'o', 'MarkerSize', 3)

xlabel("Red coloured area [mm^2]")
ylabel("Force [N]")
title('Force against Red coloured area of all samples')
set(gca, 'FontName', 'Times New Roman')
legend('Sample 7', 'Sample 8', 'Sample 9', 'Sample 10', 'Sample 11', 'Sample 12')

hold off

```

E.4. Calculating the deviation of the sensor

Force measurements are executed while the pressure applicator block was hanging in the air to calculate its deviation. The resulted deviation calculated from this code was 0.5953N. This value is retracted from all the measured mean force values.

Matlab code:

```

close all
clear all
clc

%% Import data

Force_T1 = readmatrix('23 09 19 11 13 04 Block in the air 1.txt');
Force_T2 = readmatrix('23 09 19 11 14 03 Block in the air 2.txt');
Force_T3 = readmatrix('23 09 19 11 15 29 Block in the air 3.txt');

F1 = Force_T1(1:end,3);
F2 = Force_T2(1:end,3);
F3 = Force_T3(1:end,3);

F1_mean = mean(F1);
F2_mean = mean(F2);
F3_mean = mean(F3);

F_mean = (F1_mean+F2_mean+F3_mean)/3

```

```

F1_smooth = sgolayfilt(F1,3,41);
F2_smooth = sgolayfilt(F2,3,41);
F3_smooth = sgolayfilt(F3,3,41);

F1_smooth_mean = mean(F1_smooth);
F2_smooth_mean = mean(F2_smooth);
F3_smooth_mean = mean(F3_smooth);

F_smooth_mean = (F1_smooth_mean+F2_smooth_mean+F3_smooth_mean)/3

figure
plot(F1, '-');
hold on
plot(F2, '-');
plot(F3, '-');
xlabel("Time [steps of 100ms]")
ylabel("Force [N]")
title('Force when block is in the air', 'FontName', 'Times New Roman')
legend('F1', 'F2', 'F3')

figure
plot(F1_smooth, '-')
hold on
plot(F2_smooth, '-');
plot(F3_smooth, '-');
xlabel("Time [steps of 100ms]")
ylabel("Force [N]")
title('Force when block is in the air', 'FontName', 'Times New Roman')
legend('F1 filtered', 'F2 filtered', 'F3 filtered')

```

E.5. Measurement pixel

A pixel was measured to calculate the colour changed area in mm^2 . This was possible as we knew that the pressure applicator block was exact 10mm. In one of the snapshots two points could be appointed that would represent this 10mm. After a couple times measuring these distance in pixels, the mean amount of pixels within 10mm was 485.

The code:

```

close all
clear all
clc

% Load the image
image = imread('snapshot.jpg');

% Display the image and use a tool
imshow(image);
d = imdistline; % Click on two points on the reference object separated by 1 cm in real life
pixelDistance = d.getDistance(485); % write down the amount of pixels equals to 1cm

knownLengthInMM = 10; % 1 cm is 10 mm
pixelSizeInMM = knownLengthInMM / pixelDistance;

```

E.6. Creating colour change visualisation

To actually indicate the amount of colour change a figure was created where colours of the HSV colour model were presented, and the initial mean colour of a sample and the final colouration at maximum were plotted over the HSV colours.

The code:

```
close all
clear all
clc

%% Mean HSV-values extracted from initial measurements in matlab

HSV1_1 = [0.8591    0.3355    0.4053];
HSV1_2 = [0.8639    0.3418    0.3963];
HSV1_3 = [0.8656    0.3412    0.3954];

HSV1 = (HSV1_1 + HSV1_2 + HSV1_3)/3;

HSV1_1_max = [0.9221    0.5446    0.3097];
HSV1_2_max = [0.9558    0.6679    0.8217];
HSV1_3_max = [0.9233    0.5444    0.3103];

HSV1_max = (HSV1_1_max + HSV1_2_max + HSV1_3_max)/3;

HSV2_1 = [0.8374    0.3139    0.4462];
HSV2_2 = [0.8395    0.3108    0.4461];
HSV2_3 = [0.8387    0.3214    0.4339];

HSV2 = (HSV2_1 + HSV2_2 + HSV2_3)/3;

HSV2_1_max = [0.9279    0.5459    0.3228];
HSV2_2_max = [0.9285    0.5439    0.3186];
HSV2_3_max = [0.9264    0.5419    0.3392];

HSV2_max = (HSV2_1_max + HSV2_2_max + HSV2_3_max)/3;

HSV3_1 = [0.8060    0.2882    0.4208];
HSV3_2 = [0.8173    0.2914    0.4162];
HSV3_3 = [0.8185    0.2804    0.3973];

HSV3 = (HSV3_1 + HSV3_2 + HSV3_3)/3;

HSV3_1_max = [0.9253    0.5447    0.3276];
HSV3_2_max = [0.9273    0.5476    0.3168];
HSV3_3_max = [0.9264    0.5480    0.3110];

HSV3_max = (HSV3_1_max + HSV3_2_max + HSV3_3_max)/3;

HSV4_1 = [0.7296    0.2602    0.4258];
HSV4_2 = [0.7266    0.2519    0.4254];
HSV4_3 = [0.7337    0.2584    0.4269];

HSV4 = (HSV4_1 + HSV4_2 + HSV4_3)/3;

HSV4_1_max = [0.9095    0.5338    0.2514];
HSV4_2_max = [0.9260    0.6957    0.7322];
HSV4_3_max = [0.9118    0.5246    0.2455];

HSV4_max = (HSV4_1_max + HSV4_2_max + HSV4_3_max)/3;
```

```

HSV5_1 = [0.9268    0.4319    0.4395];
HSV5_2 = [0.9259    0.4435    0.4411];
HSV5_3 = [0.9297    0.4269    0.4337];

HSV5 = (HSV5_1 + HSV5_2 + HSV5_3)/3;

HSV5_1_max = [0.9514    0.5503    0.4495];
HSV5_2_max = [0.9512    0.6230    0.8861];
HSV5_3_max = [0.9528    0.5496    0.4430];

HSV5_max = (HSV5_1_max + HSV5_2_max + HSV5_3_max)/3;

HSV6_1 = [0.9216    0.4241    0.4319];
HSV6_2 = [0.9233    0.4282    0.4346];
HSV6_3 = [0.9232    0.4317    0.4352];

HSV6 = (HSV6_1 + HSV6_2 + HSV6_3)/3;

HSV6_1_max = [0.9466    0.5619    0.4075];
HSV6_2_max = [0.9487    0.6087    0.8933];
HSV6_3_max = [0.9467    0.5538    0.4195];

HSV6_max = (HSV6_1_max + HSV6_2_max + HSV6_3_max)/3;

HSV7_1 = [0.7892    0.2614    0.4272];
HSV7_2 = [0.7946    0.2615    0.4311];
HSV7_3 = [0.7891    0.2595    0.4260];

HSV7 = (HSV7_1 + HSV7_2 + HSV7_3)/3;

HSV7_1_max = [0.9189    0.5705    0.2260];
HSV7_2_max = [0.9386    0.6992    0.7792];
HSV7_3_max = [0.9203    0.5742    0.2201];

HSV7_max = (HSV7_1_max + HSV7_2_max + HSV7_3_max)/3;

HSV8_1 = [0.7916    0.2583    0.4143];
HSV8_2 = [0.7882    0.2559    0.4106];
HSV8_3 = [0.7883    0.2555    0.4097];

HSV8 = (HSV8_1 + HSV8_2 + HSV8_3)/3;

HSV8_1_max = [0.9066    0.5262    0.2300];
HSV8_2_max = [0.9302    0.7319    0.7617];
HSV8_3_max = [0.9036    0.5308    0.1766];

HSV8_max = (HSV8_1_max + HSV8_2_max + HSV8_3_max)/3;

HSV9_1 = [0.8968    0.3826    0.4227];
HSV9_2 = [0.8974    0.3788    0.4209];
HSV9_3 = [0.8979    0.3811    0.4195];

HSV9 = (HSV9_1 + HSV9_2 + HSV9_3)/3;

HSV9_1_max = [0.9382    0.5571    0.3896];
HSV9_2_max = [0.9446    0.6390    0.8755];
HSV9_3_max = [0.9398    0.5567    0.3937];

HSV9_max = (HSV9_1_max + HSV9_2_max + HSV9_3_max)/3;

HSV10_1 = [0.8884    0.3210    0.4302];
HSV10_2 = [0.8781    0.3017    0.4338];

```



```

HSV10_3 = [0.8745    0.2892    0.4324];

HSV10 = (HSV10_1 + HSV10_2 + HSV10_3)/3;

HSV10_1_max = [0.9419    0.5566    0.3728];
HSV10_2_max = [0.9424    0.6879    0.8543];
HSV10_3_max = [0.9437    0.5617    0.3528];

HSV10_max = (HSV10_1_max + HSV10_2_max + HSV10_3_max)/3;

HSV11_1 = [0.9444    0.4596    0.4417];
HSV11_2 = [0.9435    0.4607    0.4431];
HSV11_3 = [0.9443    0.4626    0.4433];

HSV11 = (HSV11_1 + HSV11_2 + HSV11_3)/3;

HSV11_1_max = [0.9592    0.5685    0.4463];
HSV11_2_max = [0.9430    0.6116    0.8973];
HSV11_3_max = [0.9577    0.5663    0.4481];

HSV11_max = (HSV11_1_max + HSV11_2_max + HSV11_3_max)/3;

HSV12_1 = [0.9509    0.4530    0.4600];
HSV12_2 = [0.9531    0.4571    0.4670];
HSV12_3 = [0.9529    0.4528    0.4663];

HSV12 = (HSV12_1 + HSV12_2 + HSV12_3)/3;

HSV12_1_max = [0.9626    0.5784    0.4604];
HSV12_2_max = [0.9333    0.6321    0.9026];
HSV12_3_max = [0.9639    0.5804    0.4347];

HSV12_max = (HSV12_1_max + HSV12_2_max + HSV12_3_max)/3;

%% Create a colour change plot

% Set the initial colour for each sheet
initial_colors = [HSV1; HSV2; HSV3; HSV4; HSV5; HSV6; HSV7; HSV8; HSV9; HSV10; HSV11; HSV12];

% Set the final colour for each sheet
final_colors = [HSV1_max; HSV2_max; HSV3_max; HSV4_max; HSV5_max; HSV6_max; ...
    HSV7_max; HSV8_max; HSV9_max; HSV10_max; HSV11_max; HSV12_max];

figure;
hold on;

% Define the Hue and Saturation values for the 2D map
num_points = 360; % Number of points on the map
H_values = linspace(0, 1, num_points);
S_values = linspace(0, 1, num_points);

% Create a grid of HSV values for the 2D map
[H, S] = meshgrid(H_values, S_values);
V = ones(size(H)); % Set Value to 1 for all colours

% Combine the HSV channels
hsv_map = cat(3, H, S, V);

% Convert the 2D HSV map to RGB for display
rgb_map = hsv2rgb(hsv_map);

% Display the 2D HSV map
imshow(rgb_map);

```

```

% Set axis limits and labels for the HSV diagram
xlim([0 num_points]);
ylim([0 num_points]);

xlabel('Hue', 'FontSize', 40);           % (0-1)
ylabel('Saturation', 'FontSize', 40);    % (0-1)
title('2D HSV Colour Map with Colour Changes', 'FontSize', 12);
set(gca, 'FontName', 'Times New Roman')

% Hold on to add colour change arrows
hold on;

% Plot initial colours as points on the 2D HSV map
initial_hue_indices = round(initial_colors(:, 1) * (num_points - 1)) + 1;
initial_saturation_indices = round(initial_colors(:, 2) * (num_points - 1)) + 1;

scatter(initial_hue_indices, initial_saturation_indices, 10, 'cyan', 'o', 'filled');

% Plot lines to represent colour changes and add sheet numbers to initial points
for sheet = 1:12
    final_hue_index = round(final_colors(sheet, 1) * (num_points - 1)) + 1;
    final_saturation_index = round(final_colors(sheet, 2) * (num_points - 1)) + 1;

    % Plot a line from the initial point to the final point
    line([initial_hue_indices(sheet), final_hue_index], [initial_saturation_indices(sheet),
final_saturation_index], 'LineWidth', 1, 'Color', 'k');

    % Add sheet number to the initial point
    text(initial_hue_indices(sheet), initial_saturation_indices(sheet), num2str(sheet),
'FontSize', 24, 'FontWeight', 'normal', 'FontName', 'Times New Roman', 'Color', 'k');

    % Add a red dot at the final point
    plot(final_hue_index, final_saturation_index, 'ko', 'MarkerSize', 3, 'MarkerFaceColor',
'r');

    % Add sheet number next to the final point
    text(final_hue_index, final_saturation_index, num2str(sheet), 'FontSize', 9,
'FontWeight', 'normal', 'FontName', 'Times New Roman', 'Color', 'k', 'HorizontalAlignment',
'left', 'VerticalAlignment', 'middle');
end

% Specify the starting and ending points for the vertical line
vertical_hue = 0.851;           % Hue value
vertical_start_saturation = 0.466; % Starting Saturation value
vertical_end_saturation = 1.0;   % Ending Saturation value

% Convert the specified values to grid indices
vertical_hue_index = round(vertical_hue * (num_points - 1)) + 1;
vertical_start_saturation_index = round(vertical_start_saturation * (num_points - 1)) + 1;
vertical_end_saturation_index = num_points; % To the edge of the plot

% Draw the vertical line
line([vertical_hue_index, vertical_hue_index], [vertical_start_saturation_index,
vertical_end_saturation_index], 'Color', 'k', 'LineWidth', 1);

% Specify the starting and ending points for the horizontal line
horizontal_saturation = 0.466; % Saturation value
horizontal_start_hue = 0.851;  % Starting Hue value
horizontal_end_hue = 1.0;      % Ending Hue value

% Convert the specified values to grid indices
horizontal_saturation_index = round(horizontal_saturation * (num_points - 1)) + 1;

```

```
horizontal_start_hue_index = round(horizontal_start_hue * (num_points - 1)) + 1;
horizontal_end_hue_index = num_points; % To the edge of the plot
```

```
% Draw the horizontal line
line([horizontal_start_hue_index, horizontal_end_hue_index], [horizontal_saturation_index,
horizontal_saturation_index], 'Color', 'k', 'LineWidth', 1);
```

```
% Hold off to finish plotting
hold off;
```

E.7. Stiffness hypotheses

```
clear all
close all
clc
```

```
%% stiffness coefficient Design a from an area of 5x5mm2 to 30x30mm2
```

```
% Constants
G_a = 0.4;           % groove size is 0.4mm
B_a = 1;            % bulge size is 5mm
```

```
% Define pressure area
```

```
for n_a = 5:1:25;
```

```
    x = n_a/2 - 0.2;
    count_a = 0;
```

```
    while x > 1
        l = x-1;
        x = l - 0.4;
        count_a = count_a+1;
        x;
    end
```

```
    A_a(n_a) = (count_a*2)^2 * B_a^2 + (((count_a*2)*4)*x.*B_a) + (4*x.^2);
```

```
    numberofislands_a(n_a) = (count_a*2)^2 + (count_a*2)*4 + 4;
```

```
end
```

```
%% stiffness coefficient Design b from an area of 5x5mm2 to 25x25mm2
```

```
% Constants
G_b = 0.4;           % groove size is 0.4mm
B_b = 5;            % bulge size is 5mm
```

```
% Define pressure area
```

```
for n_b = 5:1:25;
```

```
    y = n_b/2 - 2.5 - 0.4;
    count_b = 0;
```

```
    while y > 5
        y = y - 5;
        y = y - 0.4;
        count_b = count_b + 1;
        y;
    end
```

```
    A_b(n_b) = ((count_b*2)+1)^2 * B_b^2 + ((count_b*2)+1)*4*y*B_b + 4*y^2;
```

```

    if n_b == 5;
        numberofislands_b(5) = 1;
    else
        numberofislands_b(n_b) = ((count_b*2)+1)^2 + ((count_b*2)+1)*4 + 4;
    end

end

A_b = [A_b(1:4), 25, A_b(6:25)];

%% Plot figure

p = linspace(1,25,25);

figure
%plot (x,A)
%hold on
plot (p,A_a, "r")
hold on
plot (p, A_b, "c")
xlabel('Length and width of pressure area in mm')
ylabel('k-factor  $((Y/L_0))$ ')
title('Pressure width versus stiffness')

legend('Design a', 'Design b')
set(gca, 'FontName', 'Times New Roman')

figure
plot(p, numberofislands_a, "r")
hold on
plot(p, numberofislands_b, "c")
xlabel('Length and width of pressure area in mm')
ylabel('Number of bulges')
title('Pressure width versus amount of bulges')

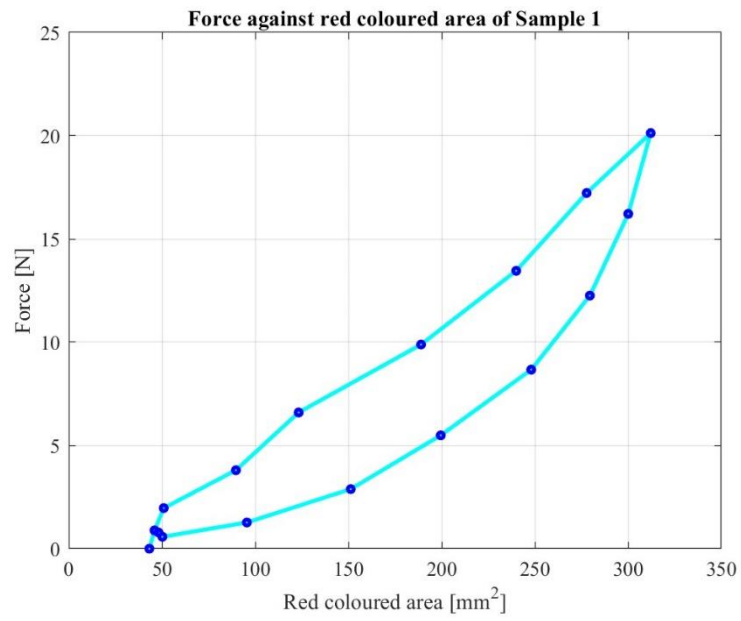
legend('Design a', 'Design b')
set(gca, 'FontName', 'Times New Roman')

```

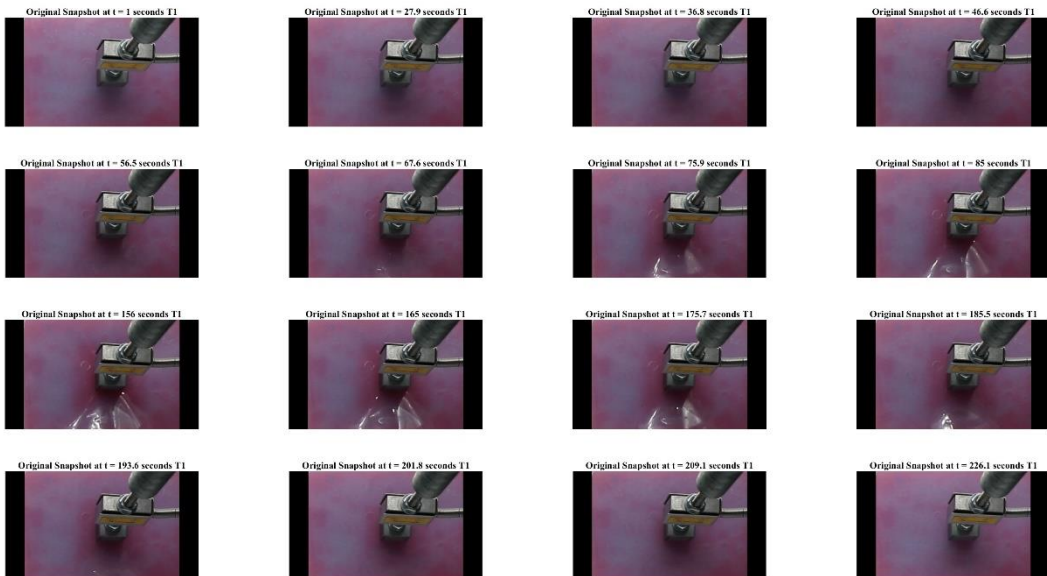
F. Figures, snapshots and binary images for each first trial of a sample

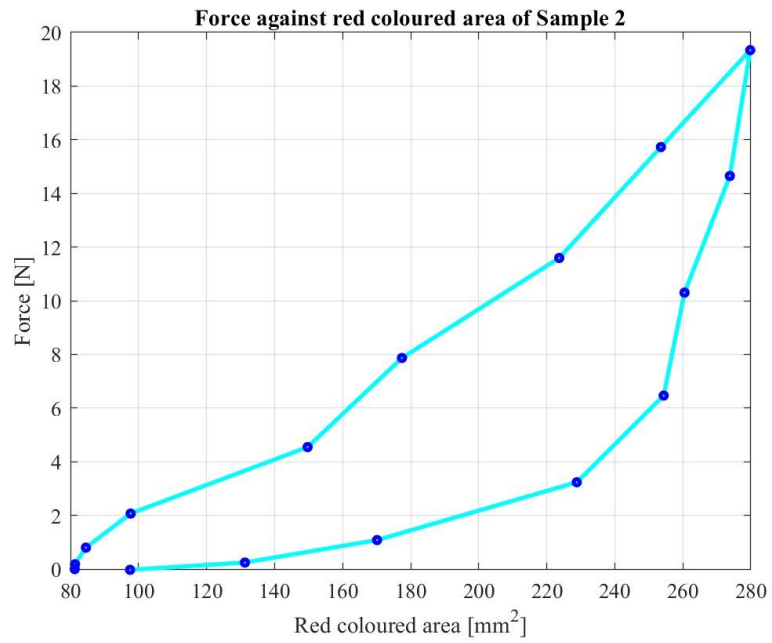
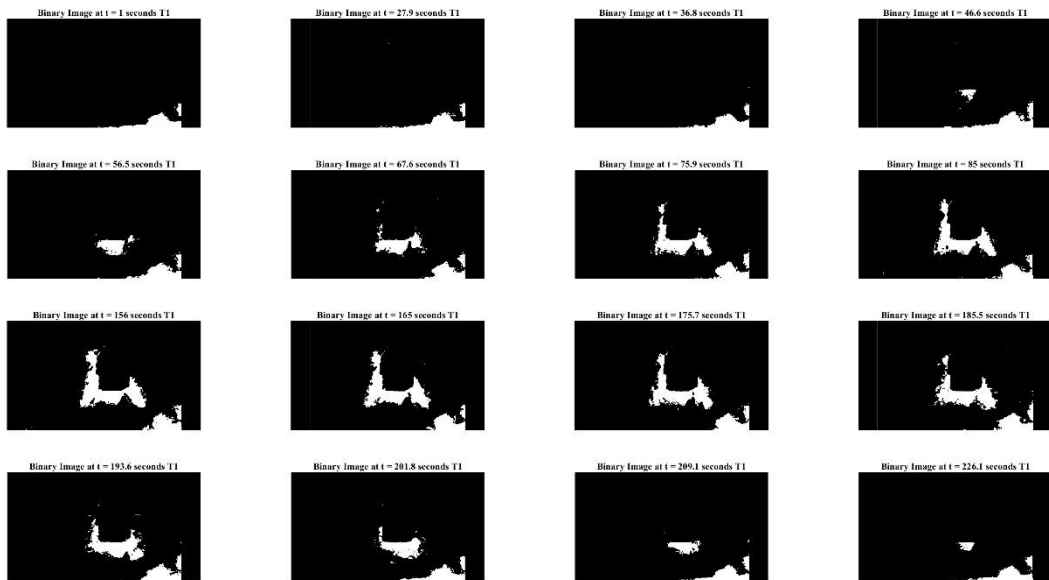
F.1. Sample 1



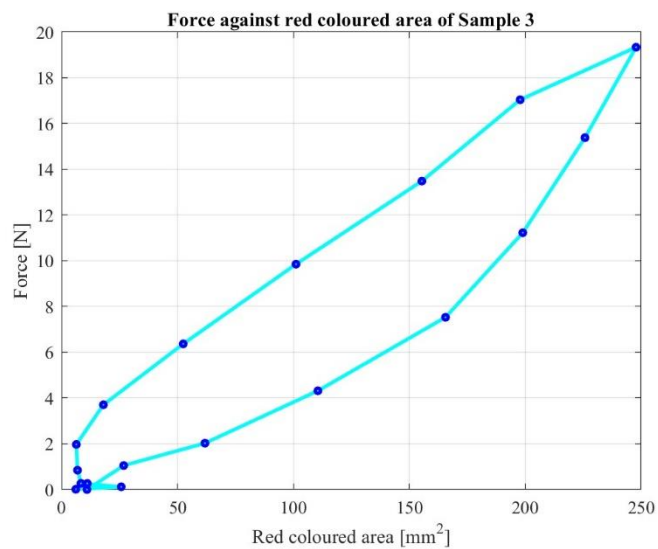


F.2. Sample 2

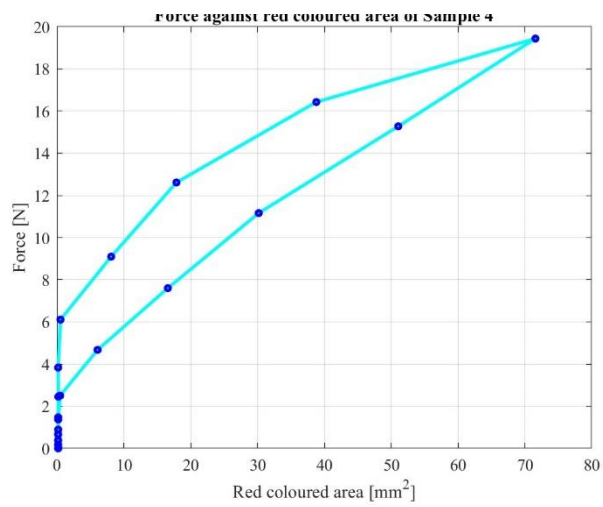




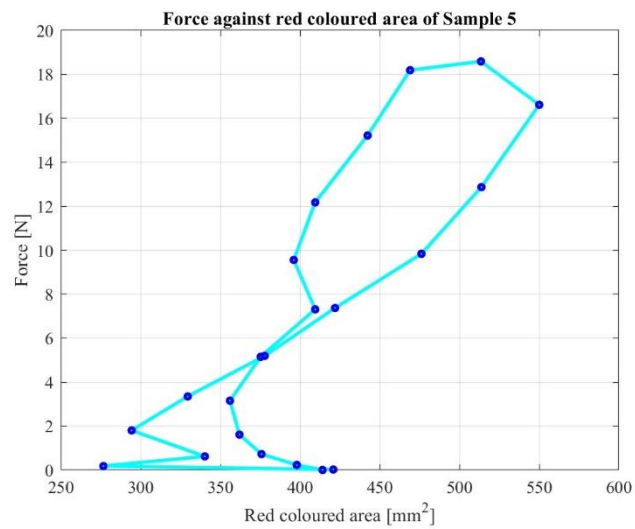
F.3. Sample 3



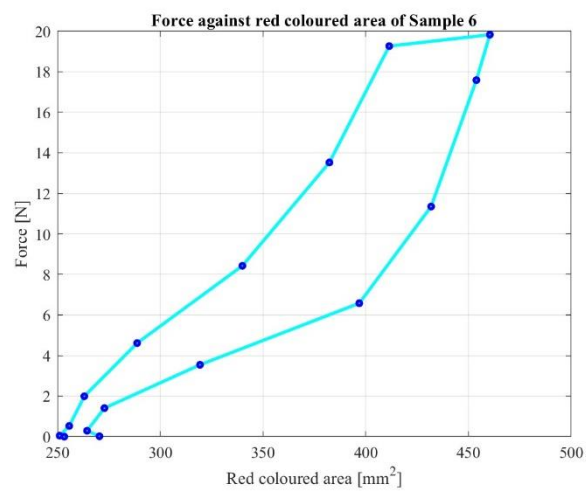
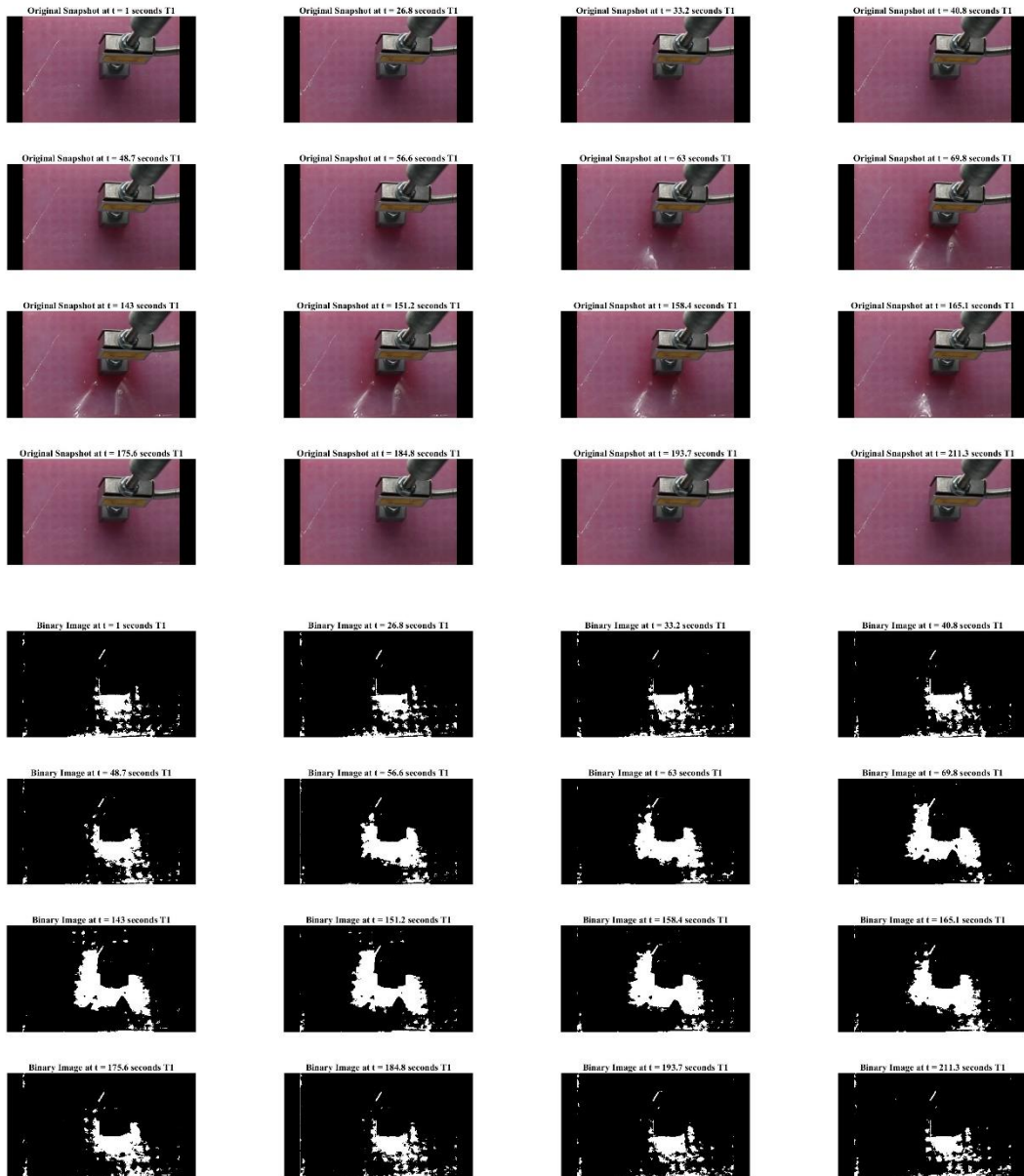
F.4. Sample 4



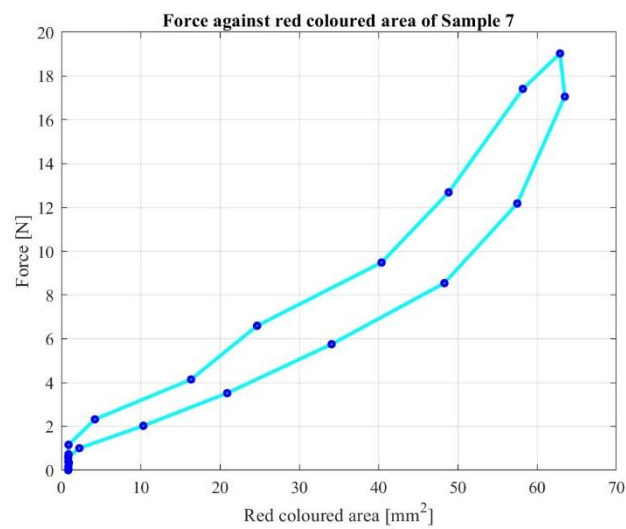
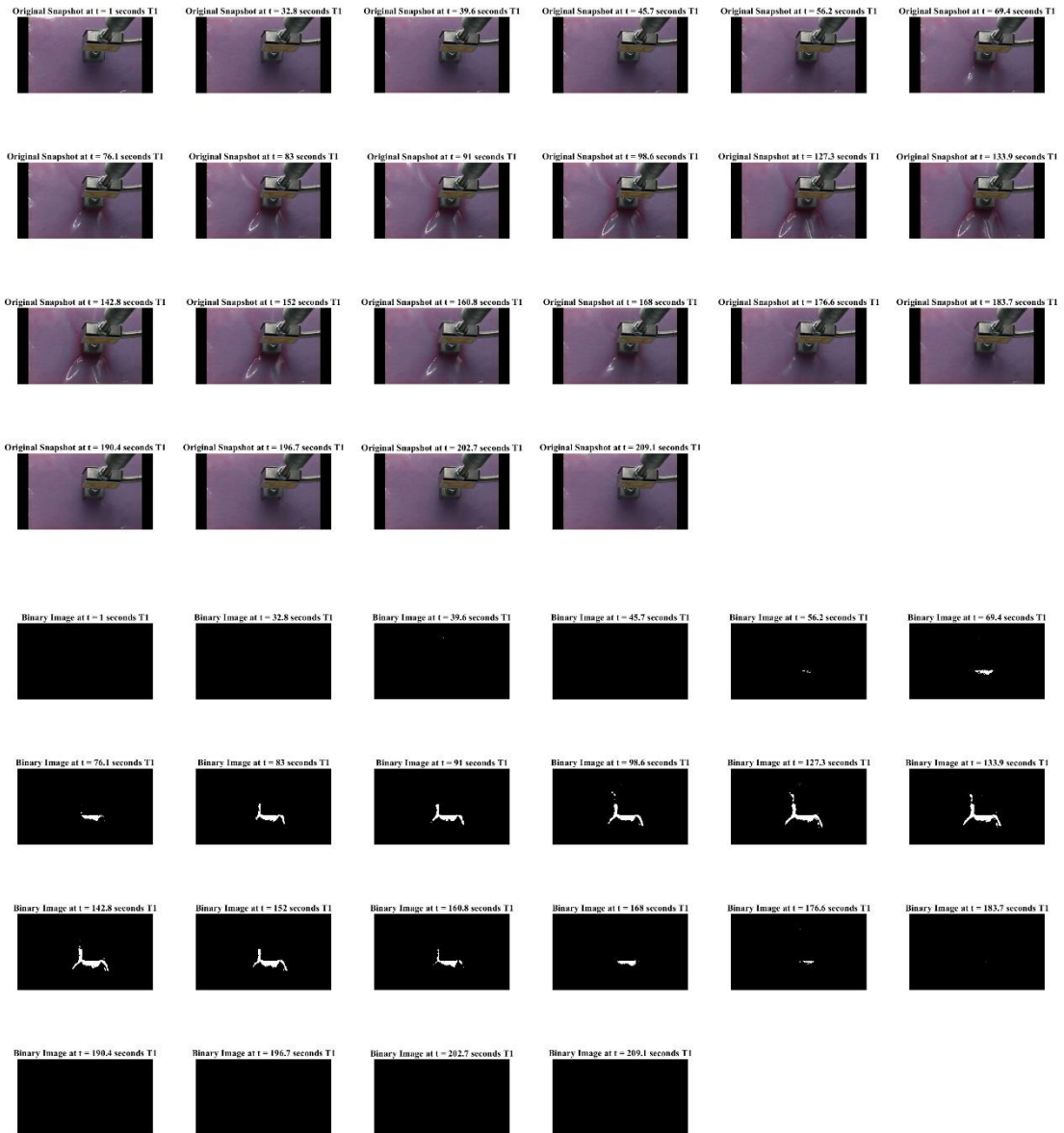
F.5. Sample 5



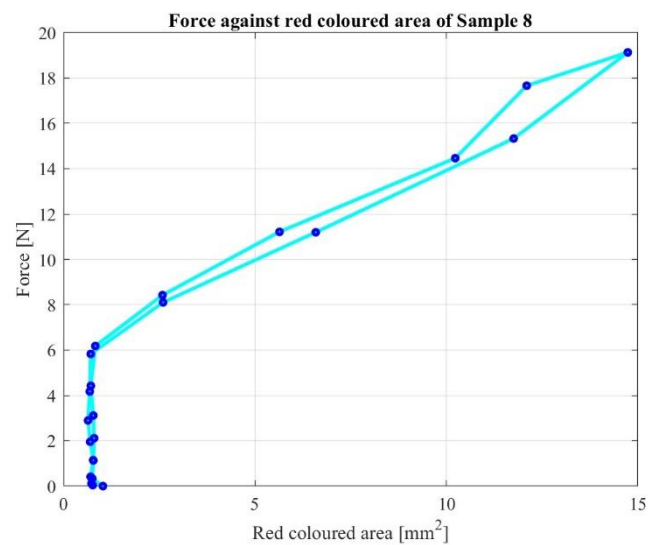
F.6. Sample 6



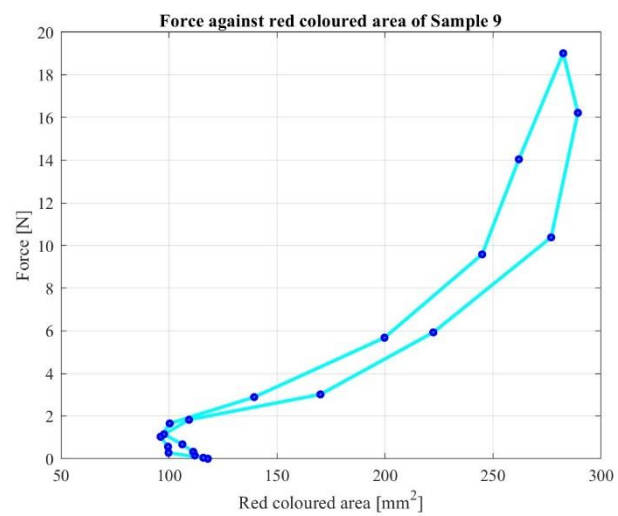
F.7. Sample 7



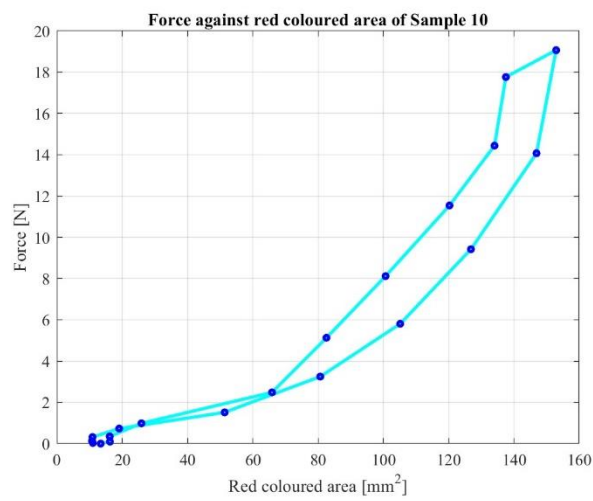
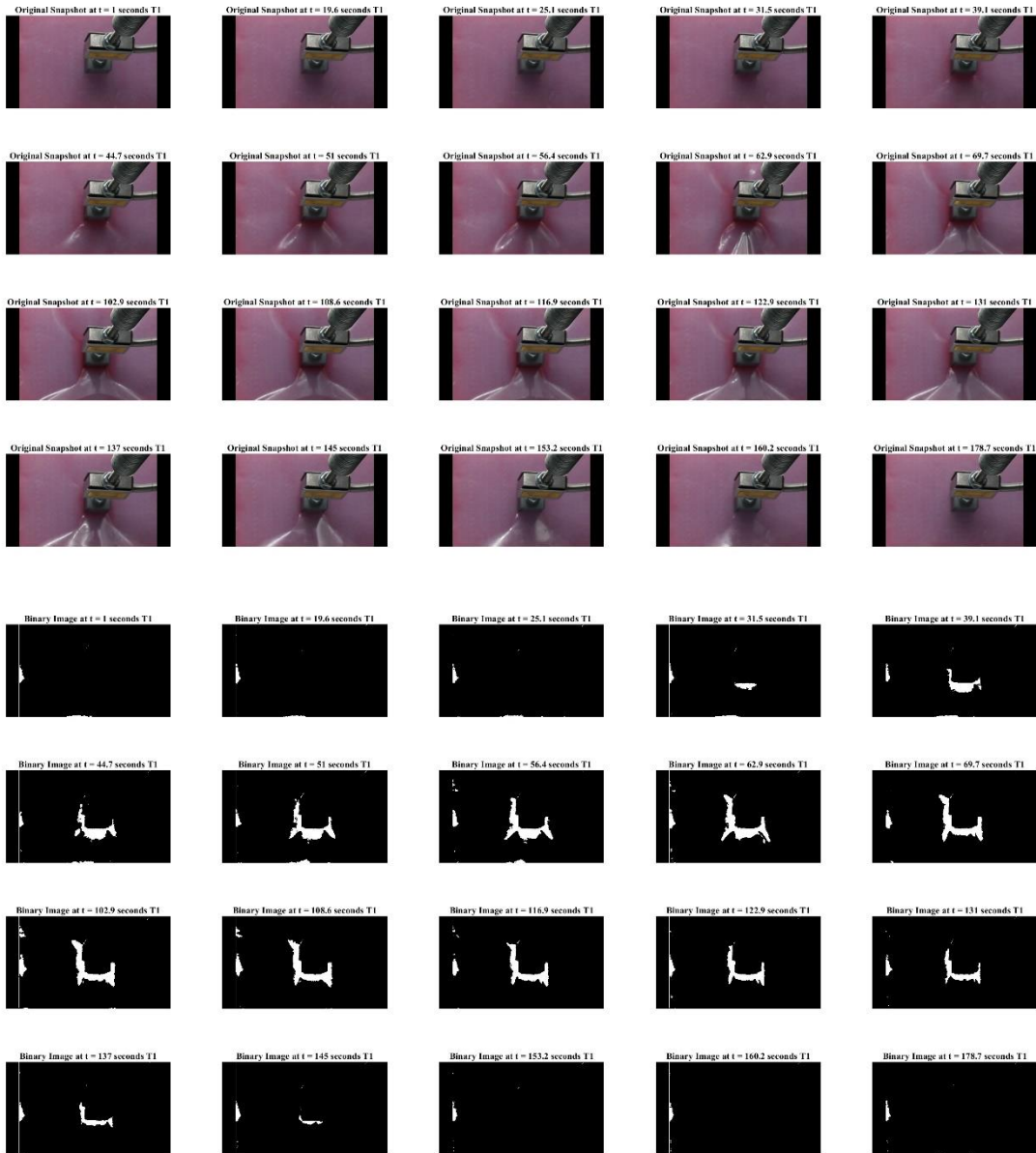
F.8. Sample 8



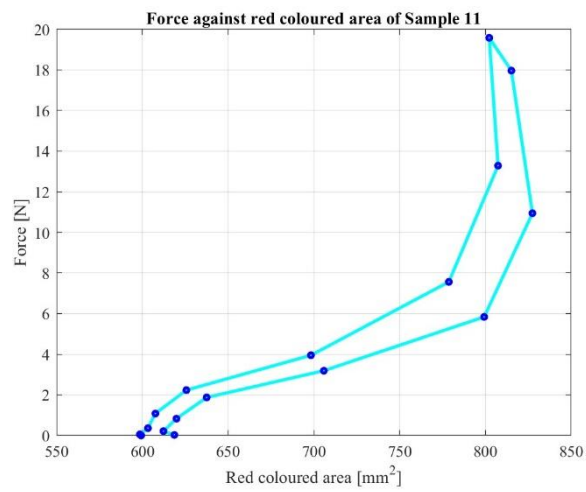
F.9. Sample 9



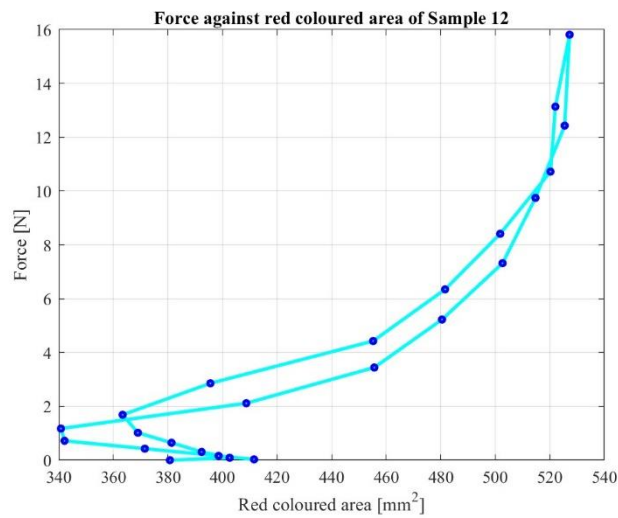
F.10. Sample 10



F.11. Sample 11

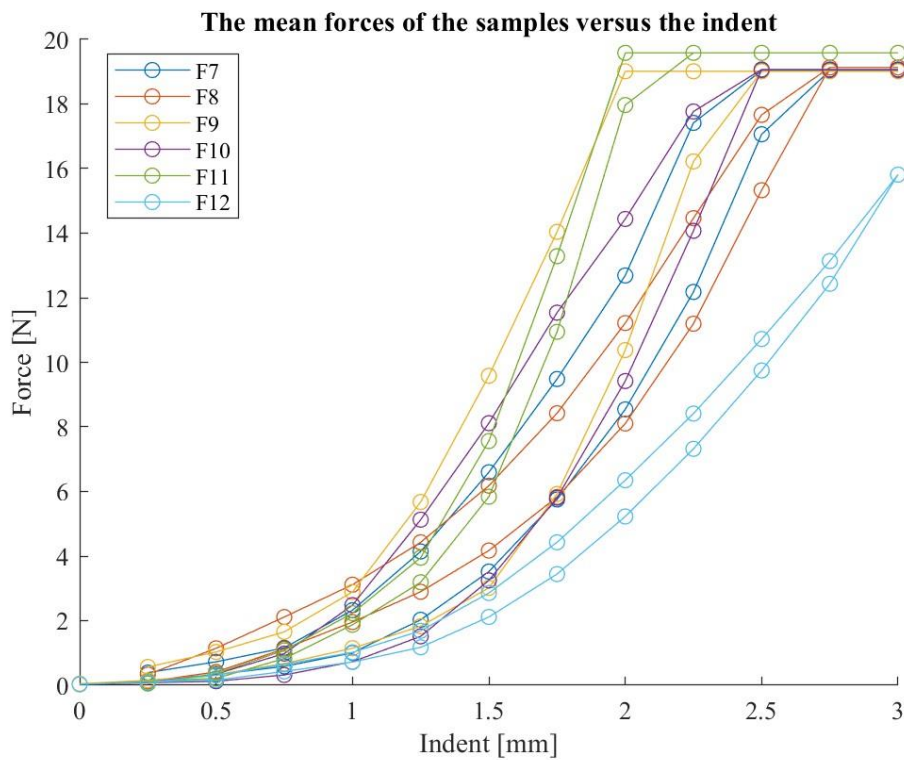
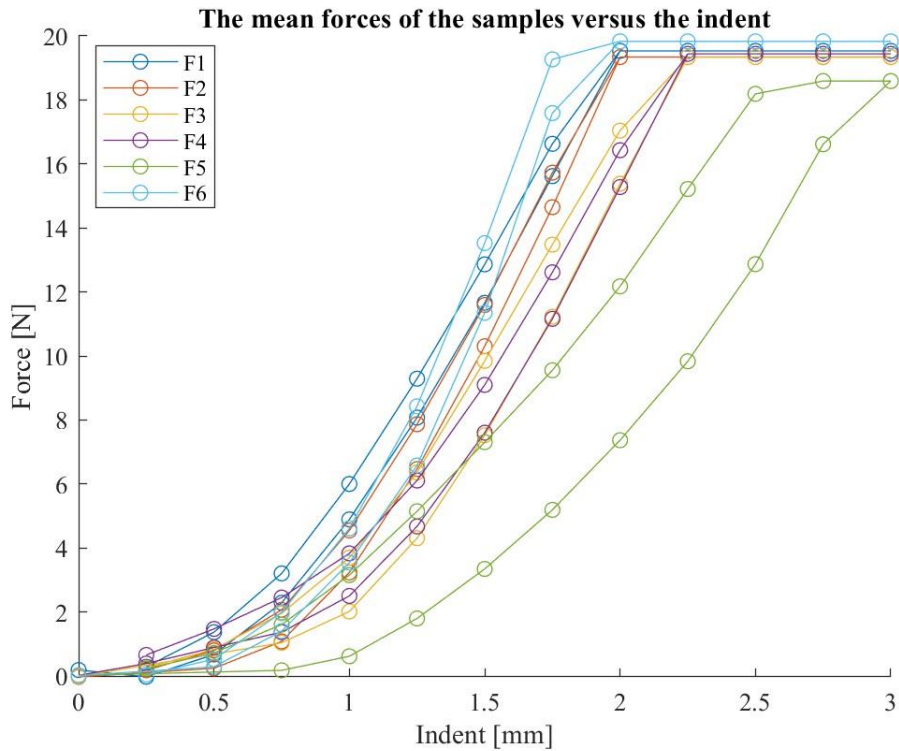


F.12. Sample 12

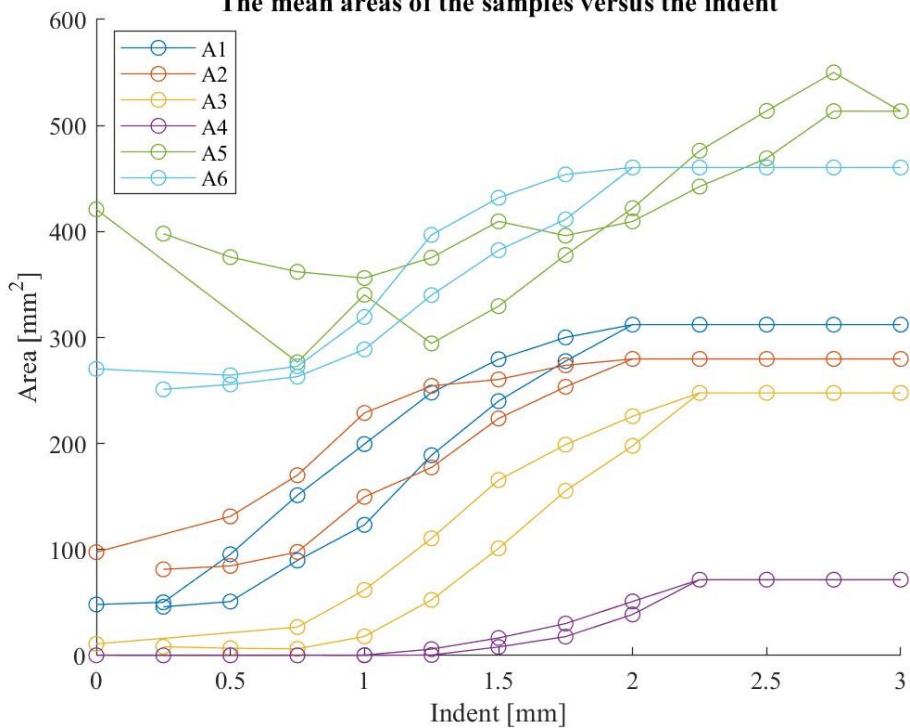


G. Summarizing images

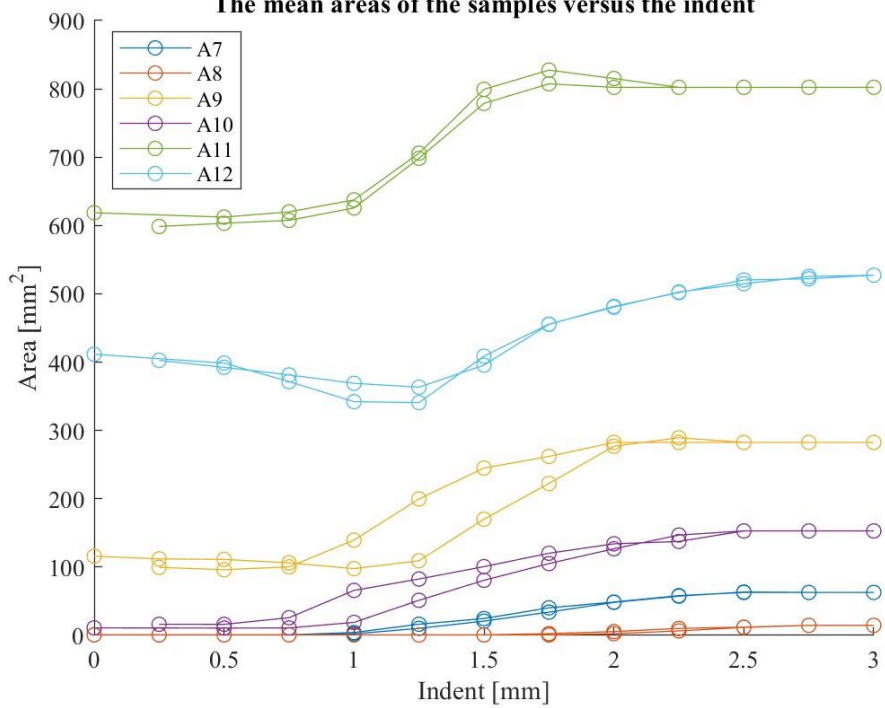
Several figures were generated to provide a concise overview of the distinctions between the samples. It was decided to plot the mean forces and mean areas against the indentation depth. To maintain clarity, the samples were divided into two subsets, namely samples 1-6 and samples 1-12. Finally, the complete 2D HSV colour plot was displayed, with an enlarged screenshot included in the report.



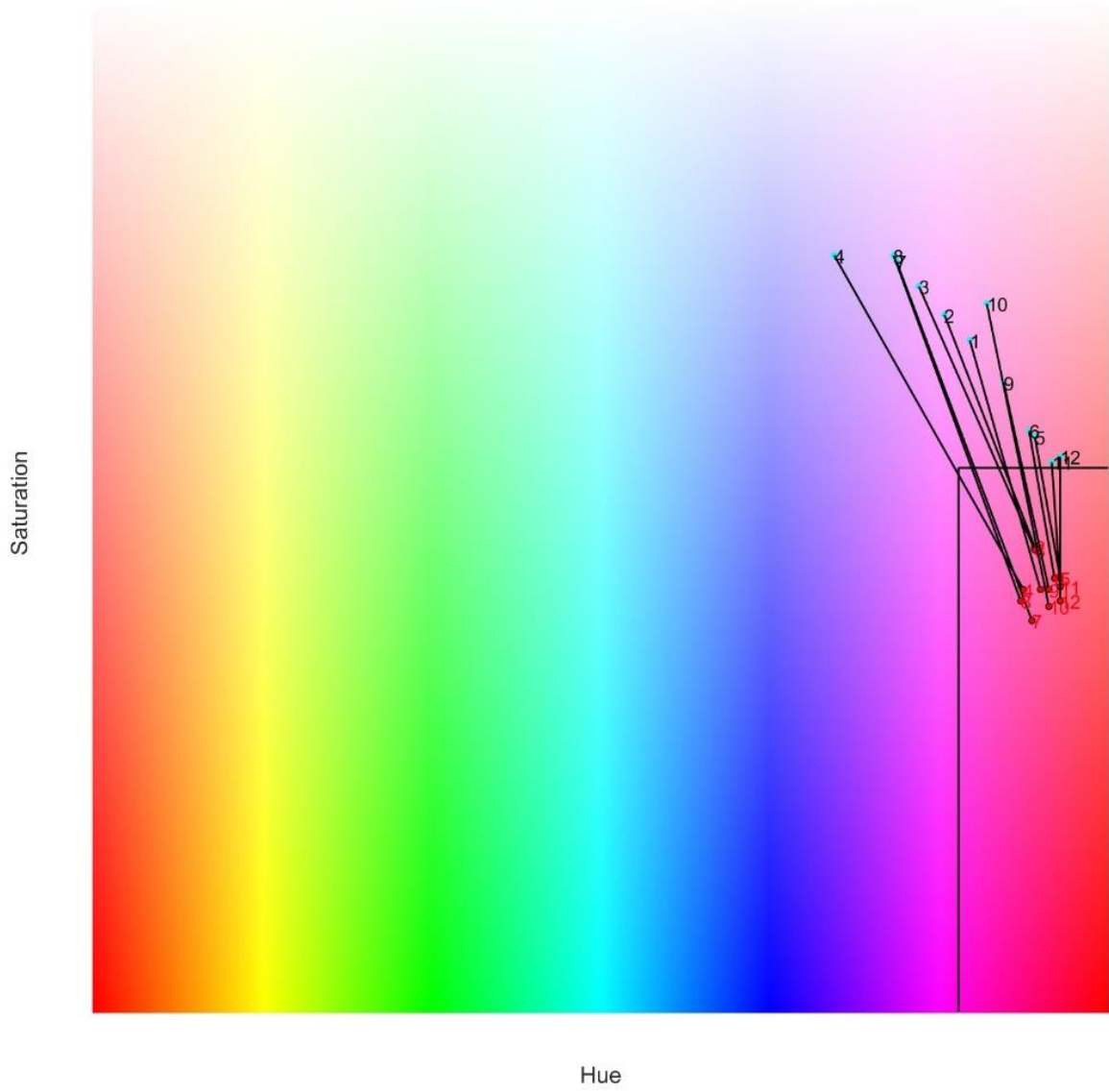
The mean areas of the samples versus the indent



The mean areas of the samples versus the indent



2D HSV Colour Map with Colour Changes



H. Tables

Certain values in the force progression graph were indiscernible, denoted by being rendered in black. Meanwhile, the values exceeding specified thresholds are delineated in red.

Indent [mm]	F1 [N]	A1 [mm ²]	F2 [N]	A2 [mm ²]	F3 [N]	A3 [mm ²]	F4 [N]	A4 [mm ²]	F5 [N]	A5 [mm ²]	F6 [N]	A6 [mm ²]
0	0	43,2088	0	81,2555	0	6,1609	0	0,1712	0	414,1443	0	253,3265
0,25	0,2888	46,0079	0,1797	81,3423	0,2578	8,3898	0,6595	0,1778	0,2278	397,9856	0,0423	251,1085
0,5	1,37	50,9536	0,7997	84,5439	0,835	6,9093	1,4721	0,1931	0,723	375,8654	0,5253	255,7609
0,75	3,2059	89,6627	2,0694	97,6968	1,9603	6,3756	2,4521	0,2111	1,6081	362,0239	1,9905	263,0846
1	6,0009	123,2995	4,5461	149,7057	3,698	18,0842	3,8333	0,1837	3,1533	356,087	4,6141	288,8067
1,25	9,2917	188,9499	7,8674	177,4324	6,3618	52,5035	6,1082	0,5362	5,1478	375,3447	8,4279	339,9892
1,5	12,8631	239,996	11,5943	223,6651	9,8479	101,1386	9,0964	8,1142	7,3077	409,5565	13,5274	382,3291
1,75	16,6297	277,7593	15,7278	253,5528	13,4806	155,4037	12,6135	17,8754	9,554	396,0935	19,2682	411,4308
2	19,5325	312,1498	19,3393	279,8073	17,041	197,8054	16,43	38,804	12,1761	409,5356	19,8311	460,3964
2,25	19,5325	312,1498	19,3393	279,8073	19,337	247,7847	19,4406	71,5817	15,2181	442,3942	19,8311	460,3964
2,5	19,5325	312,1498	19,3393	279,8073	19,337	247,7847	19,4406	71,5817	18,1902	469,0706	19,8311	460,3964
2,75	19,5325	312,1498	19,3393	279,8073	19,337	247,7847	19,4406	71,5817	18,591	513,5011	19,8311	460,3964
3	19,5325	312,1498	19,3393	279,8073	19,337	247,7847	19,4406	71,5817	18,591	513,5011	19,8311	460,3964
2,75	19,5325	312,1498	19,3393	279,8073	19,337	247,7847	19,4406	71,5817	16,6171	550,0763	19,8311	460,3964
2,5	19,5325	312,1498	19,3393	279,8073	19,337	247,7847	19,4406	71,5817	12,87	513,7926	19,8311	460,3964
2,25	19,5325	312,1498	19,3393	279,8073	19,337	247,7847	19,4406	71,5817	9,8341	476,177	19,8311	460,3964
2	19,5325	312,1498	19,3393	279,8073	15,3824	225,7612	15,278	51,0616	7,3688	422,0047	19,8311	460,3964
1,75	15,6218	300,1039	14,6496	273,8188	11,224	198,94	11,1611	30,1881	5,1919	377,8571	17,5906	453,8428
1,5	11,6613	279,5175	10,3033	260,4978	7,523	165,6017	7,6034	16,593	3,3469	329,6003	11,3496	431,8049
1,25	8,0753	248,0507	6,4675	254,3688	4,3071	110,559	4,6732	6,0821	1,7994	294,4231	6,5796	396,8593
1	4,8935	199,5131	3,2359	228,8239	2,0162	61,8725	2,5034	0,4747	0,617	340,3088	3,5417	319,3769
0,75	2,2895	151,2361	1,0818	170,1154	1,0393	26,8252	1,3712	0,1912	0,1778	276,7016	1,4025	272,8753
0,5	0,6736	95,5301	0,2437	131,2818			0,8908	0,1895			0,2891	264,4165
0,25	-0,022	50,2309					0,3908	0,1784				
0	0,1886	48,1661	-0,0275	97,5231	-0,0125	10,994	0,0233	0,2116	0,0199	420,8831	0,0167	270,4283

Indent [mm]	F7 [N]	A7 [mm ²]	F8 [N]	A8 [mm ²]	F9 [N]	A9 [mm ²]	F10 [N]	A10 [mm ²]	F11 [N]	A11 [mm ²]	F12 [N]	A12 [mm ²]
0	0	0,8724	0	1,0274	0	118,0184	0	13,4242	0	599,3056	0	380,7308
0,25	0,3925	0,8904	0,3329	0,7509	0,567	99,6029	0,0943	16,2729	0,0521	598,5584	0,0898	402,6441
0,5	0,7263	0,9106	1,1444	0,7739	1,0308	96,1647	0,3471	16,2106	0,3613	603,2865	0,3067	392,3666
0,75	1,1588	0,9086	2,1129	0,7961	1,6542	100,3945	0,9815	25,9145	1,0802	607,6086	0,6467	381,3328
1	2,3238	4,2426	3,1143	0,7761	2,8887	139,4823	2,4811	65,9067	2,2321	625,6815	1,0185	369,0016
1,25	4,1437	16,3665	4,4269	0,7118	5,6748	199,7728	5,1273	82,5719	3,9489	698,3045	1,6873	363,4067
1,5	6,5958	24,6989	6,1802	0,8291	9,5828	244,9595	8,1161	100,6877	7,563	778,6875	2,8571	395,5849
1,75	9,4832	40,3952	8,4234	2,5852	14,0408	261,9832	11,5386	120,2666	13,287	807,3919	4,4274	455,2315
2	12,689	48,8555	11,2165	5,6414	19,0122	282,496	14,4391	134,049	19,5834	802,2466	6,3485	481,6281
2,25	17,415	58,2294	14,4644	10,2306	19,0122	282,496	17,7669	137,5392	19,5834	802,2466	8,413	501,8166
2,5	19,0334	62,9067	17,663	12,0975	19,0122	282,496	19,0689	152,9303	19,5834	802,2466	10,7229	520,2542
2,75	19,0334	62,9067	19,1315	14,737	19,0122	282,496	19,0689	152,9303	19,5834	802,2466	13,1366	522,04
3	19,0334	62,9067	19,1315	14,737	19,0122	282,496	19,0689	152,9303	19,5834	802,2466	15,8134	527,239
2,75	19,0334	62,9067	19,1315	14,737	19,0122	282,496	19,0689	152,9303	19,5834	802,2466	12,4316	525,4476
2,5	17,0631	63,5103	15,3303	11,7556	19,0122	282,496	19,0689	152,9303	19,5834	802,2466	9,7468	514,7426
2,25	12,1796	57,5095	11,1961	6,5867	16,2203	289,2962	14,0733	146,9232	19,5834	802,2466	7,3205	502,6728
2	8,5432	48,3213	8,1045	2,5996	10,3795	276,9041	9,4206	126,8428	17,9674	815,1575	5,2264	480,481
1,75	5,7532	34,0967	5,8301	0,7107	5,9247	222,3813	5,8053	105,1792	10,9448	827,4329	3,4434	455,665
1,5	3,5195	20,9252	4,1716	0,685	3,0155	170,1235	3,2468	80,6728	5,8381	799,282	2,1149	408,7416
1,25	2,027	10,344	2,8945	0,6374	1,8282	109,3005	1,5139	51,3935	3,1891	705,8251	1,1751	340,7938
1	1,0037	2,267	1,9577	0,6959	1,147	97,7712	0,7269	19,0799	1,8712	637,5028	0,7197	342,1146
0,75	0,5849	0,8707	1,1286	0,7768	0,6739	106,217	0,3183	10,9348	0,828	619,9114	0,4273	371,5392
0,5	0,3291	0,9472	0,4119	0,7049	0,3253	111,2427	0,1245	10,7789	0,2125	612,3028	0,1594	398,5785
0,25	0,1531	0,8837	0,1157	0,7272	0,1519	112,0077						
0	0,0297	0,904	0,0415	0,7613	0,0467	115,947	0,0297	11,033	0,0256	618,6831	0,0293	411,5898

References

- [1] R. G. Budynas and A. M. Sadegh, *Roark's formulas for stress and strain*. McGraw-Hill Education, 2020.
- [2] M. Pawar, H. K. Wazir, and V. Kapila, "A Lymphatic Drainage Robot for Lymphedema Rehabilitation," in *2022 44th Annual International Conference of the IEEE Engineering in Medicine & Biology Society (EMBC)*, 2022: IEEE, pp. 2598-2601.
- [3] F. Figon and J. Casas, "Morphological and physiological colour changes in the animal kingdom," *eLS*, pp. 1-11, 2018.
- [4] A. Coccarelli and M. D. Nelson, "Modeling Reactive Hyperemia to better understand and assess Microvascular Function: a review of techniques," *Annals of Biomedical Engineering*, vol. 51, no. 3, pp. 479-492, 2023.
- [5] R. Z. Gao *et al.*, "A novel air microfluidics-enabled soft robotic sleeve: Toward realizing innovative lymphedema treatment," *Biomicrofluidics*, vol. 16, no. 3, p. 034101, 2022.
- [6] H. J. Yoo *et al.*, "Wearable lymphedema massaging modules: Proof of concept using origami-inspired soft fabric pneumatic actuators," in *2019 IEEE 16th International Conference on Rehabilitation Robotics (ICORR)*, 2019: IEEE, pp. 950-956.
- [7] L. Nazarko, "Identification and treatment of chronic oedema and lymphoedema," *Independent Nurse*, vol. 2022, no. 2, pp. 14-18, 2022.
- [8] K. Wang and A. Kopsini, "Design of an Innovative Medical Device to Improve Quality of Life in Lymphedema Patients," in *BIODEVICES*, 2020, pp. 323-328.
- [9] J. Pamplin, J. Baldwin, J. Rodrick, C.-L. OTR/L, WCC, and A. Doraiswamy, "Active Wearable Compression with Shape Memory Actuators for Treating Chronic Edema," *Shape Memory and Superelasticity*, vol. 8, no. 2, pp. 142-149, 2022.
- [10] L. M. G. Bianchi *et al.*, "Diagnosis and Treatment of Post-Prostatectomy Lymphedema: What's New?," *Current Oncology*, vol. 30, no. 5, pp. 4512-4526, 2023.
- [11] K. D. Kimball, "LymphaTouch as a Tool for Manual Lymph Drainage: A Therapist's Perspective," 2018.
- [12] P. A. Morgan, S. Murray, C. J. Moffatt, and A. Honnor, "The challenges of managing complex lymphoedema/chronic oedema in the UK and Canada," *International wound journal*, vol. 9, no. 1, pp. 54-69, 2012.
- [13] D. Guan, R. Liu, C. Fei, S. Zhao, and L. Jing, "Fluid-structure coupling model and experimental validation of interaction between pneumatic soft actuator and lower limb," *Soft robotics*, vol. 7, no. 5, pp. 627-638, 2020.
- [14] L. Rosalia *et al.*, "A Soft Robotic Sleeve for Compression Therapy of the Lower Limb," in *2021 43rd Annual International Conference of the IEEE Engineering in Medicine & Biology Society (EMBC)*, 2021: IEEE, pp. 1280-1283.
- [15] E. Suarez, J. J. Huaroto, A. A. Reymundo, D. Holland, C. Walsh, and E. Vela, "A soft pneumatic fabric-polymer actuator for wearable biomedical devices: Proof of concept for lymphedema treatment," in *2018 IEEE International Conference on Robotics and Automation (ICRA)*, 2018: IEEE, pp. 5452-5458.
- [16] J. Green. "Should I Use Compression Garments for Lymphedema?" <https://tactilemedical.com/resource-hub/lymphedema/compression-garments-for-lymphedema/> (accessed August 26, 2022).
- [17] Y. Luo *et al.*, "Technology roadmap for flexible sensors," *ACS nano*, vol. 17, no. 6, pp. 5211-5295, 2023.
- [18] I. I. Ebralidze, N. O. Laschuk, J. Poisson, and O. V. Zenkina, "Colorimetric sensors and sensor arrays," in *Nanomaterials design for sensing applications*: Elsevier, 2019, pp. 1-39.
- [19] L. Huang, R. Zeng, J. Xu, and D. Tang, "Point-of-care immunoassay based on a multipixel dual-channel pressure sensor array with visual sensing capability of full-color switching and reliable electrical signals," *Analytical Chemistry*, vol. 94, no. 38, pp. 13278-13286, 2022.
- [20] A. Cannavale, "Chromogenic technologies for energy saving," *Clean Technologies*, vol. 2, no. 4, pp. 462-475, 2020.
- [21] C. Woodford. "Thermochromic color-changing materials." <https://www.explainthatstuff.com/thermochromic-materials.html> (accessed May 23, 2022).
- [22] Q. Guo and X. Zhang, "A review of mechanochromic polymers and composites: From material design strategy to advanced electronics application," *Composites Part B: Engineering*, vol. 227, p. 109434, 2021.
- [23] C. M. Lampert, "Chromogenic smart materials," *Materials today*, vol. 7, no. 3, pp. 28-35, 2004.
- [24] L. M. Mäthger and R. T. Hanlon, "Malleable skin coloration in cephalopods: selective reflectance, transmission and absorbance of

- light by chromatophores and iridophores," *Cell and tissue research*, vol. 329, no. 1, pp. 179-186, 2007.
- [25] S. V. Saenko, J. Teyssier, D. Van Der Marel, and M. C. Milinkovitch, "Precise colocalization of interacting structural and pigmentary elements generates extensive color pattern variation in Phelsumalizards," *BMC biology*, vol. 11, no. 1, pp. 1-13, 2013.
- [26] J. Teyssier, S. V. Saenko, D. Van Der Marel, and M. C. Milinkovitch, "Photonic crystals cause active colour change in chameleons," *Nature communications*, vol. 6, no. 1, p. 6368, 2015.
- [27] T. L. Williams *et al.*, "Dynamic pigmentary and structural coloration within cephalopod chromatophore organs," *Nature communications*, vol. 10, no. 1, p. 1004, 2019.
- [28] N. Green *et al.*, "Documentary: Life in Colour with David Attenborough," in *Hiding in Colour* vol. 1, A. Geiger and N. Green, Eds., ed: Humble Bee Films and Sealight Pictures, 2021.
- [29] B. B. Mahapatra, S. A. Marathe, V. B. Meyer-Rochow, and M. Mishra, "A closer look at the feather coloration in the male purple sunbird, *Nectarinia asiatica*," *Micron*, vol. 85, pp. 44-50, 2016.
- [30] D. G. Stavenga, H. L. Leertouwer, N. J. Marshall, and D. Osorio, "Dramatic colour changes in a bird of paradise caused by uniquely structured breast feather barbules," *Proceedings of the Royal Society B: Biological Sciences*, vol. 278, no. 1715, pp. 2098-2104, 2011.
- [31] C. A. Thorstenson, A. D. Pazda, and E. G. Krumhuber, "The influence of facial blushing and paling on emotion perception and memory," *Motivation and Emotion*, vol. 45, pp. 818-830, 2021.
- [32] M. Ferrara and M. Bengisu, "Intelligent design with chromogenic materials," *JAIC- Journal of the International Colour Association*, vol. 13, 2014.
- [33] A. Behera, *Advanced Materials: An Introduction to Modern Materials Science*. Springer Nature, 2021.
- [34] M. Xie *et al.*, "Flexible multifunctional sensors for wearable and robotic applications," *Advanced Materials Technologies*, vol. 4, no. 3, p. 1800626, 2019.
- [35] J. Xu *et al.*, "Multimode visualization of electronic skin from bioinspired colorimetric sensor," *ACS Applied Materials & Interfaces*, vol. 13, no. 25, pp. 30205-30212, 2021.
- [36] B. H. Miller, H. Liu, and M. Kolle, "Scalable optical manufacture of dynamic structural colour in stretchable materials," *Nature Materials*, vol. 21, no. 9, pp. 1014-1018, 2022.
- [37] Y.-J. Quan, Y.-G. Kim, M.-S. Kim, S.-H. Min, and S.-H. Ahn, "Stretchable biaxial and shear strain sensors using diffractive structural colors," *ACS nano*, vol. 14, no. 5, pp. 5392-5399, 2020.
- [38] G. Topcu, T. Guner, E. Inci, and M. M. Demir, "Colorimetric and plasmonic pressure sensors based on polyacrylamide/Au nanoparticles," *Sensors and Actuators A: Physical*, vol. 295, pp. 503-511, 2019.
- [39] Y. Zhang *et al.*, "Micellar-incorporated hydrogels with highly tough, mechanoresponsive, and self-recovery properties for strain-induced color sensors," *Journal of Materials Chemistry C*, vol. 6, no. 43, pp. 11536-11551, 2018.
- [40] Z. Zhang, Z. Chen, Y. Wang, and Y. Zhao, "Bioinspired conductive cellulose liquid-crystal hydrogels as multifunctional electrical skins," *Proceedings of the National Academy of Sciences*, vol. 117, no. 31, pp. 18310-18316, 2020.
- [41] Y. Zhuang *et al.*, "Visualizing Dynamic Mechanical Actions with High Sensitivity and High Resolution by Near-Distance Mechanoluminescence Imaging," *Advanced Materials*, vol. 34, no. 36, p. 2202864, 2022.
- [42] C. Yang *et al.*, "3D-Printed Biomimetic Systems with Synergetic Color and Shape Responses Based on Oblate Cholesteric Liquid Crystal Droplets," *Advanced Materials*, vol. 33, no. 10, p. 2006361, 2021.
- [43] T. Yokota, K. Fukuda, and T. Someya, "Recent progress of flexible image sensors for biomedical applications," *Advanced materials*, vol. 33, no. 19, p. 2004416, 2021.
- [44] H.-H. Chou *et al.*, "A chameleon-inspired stretchable electronic skin with interactive colour changing controlled by tactile sensing," *Nature communications*, vol. 6, no. 1, p. 8011, 2015.
- [45] X. Li, J. Liu, D. Li, S. Huang, K. Huang, and X. Zhang, "Bioinspired Multi-Stimuli Responsive Actuators with Synergistic Color- and Morphing-Change Abilities," *Advanced Science*, vol. 8, no. 16, p. 2101295, 2021.
- [46] S. A. Morin, R. F. Shepherd, S. W. Kwok, A. A. Stokes, A. Nemiroski, and G. M. Whitesides, "Camouflage and display for soft machines," *Science*, vol. 337, no. 6096, pp. 828-832, 2012.
- [47] M. Si *et al.*, "Optimizing supramolecular fluorescent materials with responsive multi-color tunability toward soft biomimetic skins," *Materials Chemistry Frontiers*, vol. 5, no. 13, pp. 5130-5141, 2021.

- [48] S. Wu *et al.*, "Aggregation-Induced Emissive Carbon Dots Gels for Octopus-Inspired Shape/Color Synergistically Adjustable Actuators," *Angewandte Chemie International Edition*, vol. 60, no. 40, pp. 21890-21898, 2021.
- [49] Y. Zhu *et al.*, "Intelligent, biomimetic, color-tunable, light-emitting artificial skin with memory function," *Nano Energy*, vol. 90, p. 106569, 2021.
- [50] F. Ikomi, Y. Kawai, and T. Ohhashi, "Recent advance in lymph dynamic analysis in lymphatics and lymph nodes," *Annals of vascular diseases*, vol. 5, no. 3, pp. 258-268, 2012.
- [51] J. R. Casley-Smith, "Modern treatment of lymphoedema," *Modern Medicine*, vol. 17, no. 9, pp. 49-65, 1992.
- [52] N. Maesele, "De preventieve rol van manuele lymfedrainage na axillaire ontruiming."
- [53] M. Ricci, F. Federighi, and P. Capodaglio, "Lower Limb Lymphedema," *Rehabilitation interventions in the patient with obesity*, pp. 143-155, 2020.
- [54] B. Thompson, K. Gaitatzis, X. Janse de Jonge, R. Blackwell, and L. A. Koelmeyer, "Manual lymphatic drainage treatment for lymphedema: a systematic review of the literature," *Journal of Cancer Survivorship*, vol. 15, pp. 244-258, 2021.
- [55] M. Rosser, G. Couldridge, and S. Rosser, *Body Massage*. Hachette UK, 2013.
- [56] K. J. D. C. C. Larson, "Can you estimate modulus from durometer hardness for silicones," pp. 1-6, 2016.
- [57] S. Winczewski and J. Rybicki, "Negative Poisson's ratio from pentagons: A new auxetic structure combining three different auxetic mechanisms," *Computational Materials Science*, vol. 201, p. 110914, 2022.
- [58] W. Wu *et al.*, "Mechanical design and multifunctional applications of chiral mechanical metamaterials: A review," vol. 180, p. 107950, 2019.
- [59] Z. Liao, J. Yang, M. Hossain, G. Chagnon, L. Jing, and X. J. I. J. o. M. S. Yao, "On the stress recovery behaviour of Ecoflex silicone rubbers," vol. 206, p. 106624, 2021.
- [60] J. Hrisko. "Force Sensitive Resistors (FSRs) with Arduino." <https://makersportal.com/blog/2020/5/24/force-sensitive-resistors-fsrs-arduino> (accessed April, 2023).
- [61] Y. Wei, K. Yang, M. Browne, L. Bostan, and P. Worsley, "Wearable electrical stimulation to improve lymphatic function," *IEEE Sensors Letters*, vol. 3, no. 2, pp. 1-4, 2019.
- [62] S. van Heumen, J. J. Riksen, W. M. Bramer, G. van Soest, and D. Vasilic, "Imaging of the lymphatic vessels for surgical planning: a systematic review," *Annals of surgical oncology*, vol. 30, no. 1, pp. 462-479, 2023.